University of Calabria

Department of Pharmacy and Health and Nutrition Sciences (DFSSN)

Research Doctorate in Translational Medicine

CYCLE XXXII

EVALUATION OF A PH-SENSITIVE MESOPOROUS SILICA-BASED NANOSYSTEM AS A VEHICLE FOR TARGETED CANCER THERAPY

S.S.D. MED / 04 General Pathology

PhD student: Alessandra Nigro

ABSTRACT

Introduction: One of the main challenges in cancer treatment is to develop a therapeutic strategy able to selectively target tumor cells preserving normal tissues from unwanted side effects. Localized drug delivery should cope this aim. A patented mesoporous silica-based nanodevice (EP 3 288 955 B1), bearing the antineoplastic drug bortezomib (BTZ), whose release is triggered by the acidic tumor environment, and grafted with the targeting function folic acid (FOL) on the external surface, was developed (FOL-MSN-BTZ) and tested in vitro and in vivo against multiple myeloma (MM) cells and in xenograft models, respectively.

Methods: FOL-MSN-BTZ efficacy studies were conducted by means of growth experiments, TEM, TUNEL assay and Western Blotting (WB). Metabolic investigations, performed through Seahorse analysis and intracellular Reactive Oxygen Species (ROS) production detection, have had the purpose to assess which different metabolic pathways are involved in response to MSNs treatment. Finally, in vivo studies were carried out on mice models bearing RPMI 8226 (RPMI) MM cells derived tumors.

Results: FOL-MSN-BTZ was able to kill folate receptor overexpressing (FR+) cancer cells, but not FR- normal cells, while free BTZ was toxic for all cell lines tested, regardless of FR expression. MSNs uptake occurred exclusively in FR+ RPMI cells, through FR-mediated endocytosis, while no uptake was observed in FR- cells. Both FOL-MSN-BTZ and free BTZ led to comparable apoptotic rates in RPMI cells, but only BTZ, and not the FOL-MSN-BTZ device, caused also death in FR- normal cells. The impairment in glycolysis and the OXPHOS-driven respiratory deficit, fit well with the apoptotic phenotype triggered by MSN-loaded BTZ and BTZ in FR+ RPMI cancer cells, supported by a consistent intracellular ROS production. In FR- normal cells only the free

drug was able to significantly inhibit mitochondrial respiration and promote a significant ROS production, tendentially shifting the cell to a more glycolytic phenotype. Noteworthy, in both cell lines, MSN-FOL alone did not show any significant effect on both processes, confirming that the vehicle itself does not affect cell metabolism.

In mice bearing RPMI-derived tumors, the FOL-MSN-BTZ nanosystem resulted significantly more efficacious than the free drug, as soon as after the first administration.

Conclusions: These data show the outstanding specificity of FOL-MSN-BTZ toward FR+ tumor cells, and together with the highly promising in vivo studies, pave the way for a future exploitation of our MSNs technology for drug targeting applications, particularly in cancer therapy.

1. INTRODUCTION

1.1 Mesoporous Silica Nanoparticles (MSNs): new frontiers in modern medicine.

The engineering of nano drug delivery systems (DDS) has received great attention in the past two decades owing to the potential that biocompatible nanomaterials can theoretically act as "magic bullets" and selectively deliver therapeutic agents to cancer cells while sparing normal tissues. The ultimate goal is to enable more effective treatment regimens by reducing drug concentration and dosing frequency, thus offering easier administrations and improving safety [1, 2].

Many of the conventional organic-based DDS (liposomes, micelles, dendrimers, and polymers) have reached the latest stages of development, but only few have received FDA approval, since their intrinsic instability and low drug-loading capacity/efficiency inhibit their further clinical translation [1, 3, 4].

This has led to the emergence of developing the newest inorganic or organic/inorganic hybrid DDS (carbon nanotubes, quantum dots, iron oxide, gold and mesoporous silica nanoparticles), most of which are still in their pre-clinical stages of development [5, 6].

In particular, mesoporous silica nanoparticles (MSNs) offer a solid framework with regularly-sized pores, in the range of 15-100 Å, which allows to encapsulate a variety of hydrophobic and hydrophilic therapeutic agents and a high surface area that is able to host targeting groups. These properties endow the MSNs with the unique advantage of directly delivering therapeutic/diagnostic (theranostic) agents (e.g., drug, siRNA, miRNA, enzymes, proteins, DNA, as well as probes for imaging applications) to the desired location (e.g. tumors) [3, 7-9].

Since MCM (Mobil Crystalline Materials)-41-type ordered mesoporous silica (MCM-41), belonging to the wider family of MSU-type mesoporous materials (Michigan State University), was first discovered in the early 1990s [10], MSNs have brought new possibilities and found widespread applications because of their beneficial physical and chemical characteristics, becoming a new generation of inorganic framework to use as clinical tool for various biomedical applications [11]. Several materials fall within this family and the choice of the starting precursors and reaction conditions may tune the structural arrangement of the pores (Fig.1), adapting them to the different applications [11, 12].

In particular, the MCM-41 is characterized by an ordered hexagonal texture and an ordered arrangement of pores with pore size in the range of 2–50 nm (mesopores).

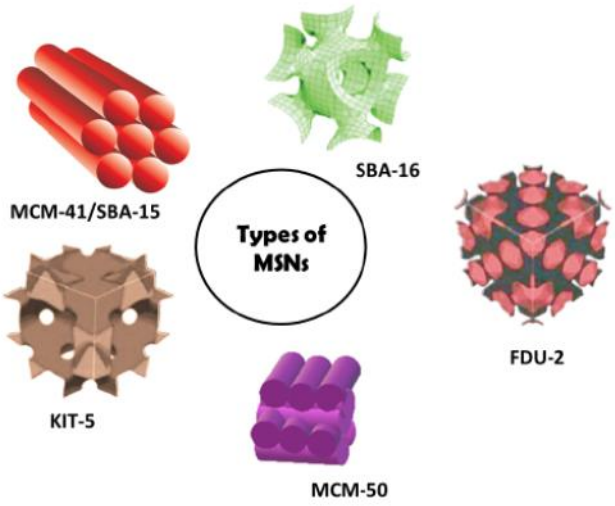

Figure 1*: Different types of mesoporous silica nanoparticles (MSN): the hexagonal shape of MCM-41 and SBA-15, the cage structure of SBA-16, the lamellar arrangement of MCM-50, the cubic pore symmetry of KIT-5 and the three-dimensional ordered mesoporous silica of FDU-2 [12].*

MCM-41 was patented by Mobil corporation scientists in 1992 and represented an important breakthrough in the material science [12]. Great strides have been made during the last decades in the control of particle and pore size, morphology, structure and surface

functionalization, to make MSNs a multifunctional platform in the fields of biomedicine [10], catalysis [13], environmental protection [14], optics [15] or as potential alternatives for gene transfection [16], given their ability to transfer DNA both *in vitro* and in animal models [17].

Vallet-Regí *et al.* were the first, in 2001, to develop ordered mesoporous materials carrying the drug ibuprofen as DDS [18]. Since then, MSNs have been tested for the delivery of a variety of drugs including nonsteroidal anti-inflammatories (e.g., aspirin), antibiotics (e.g., vancomycin), and chemotherapeutics (e.g., doxorubicin and methotrexate) [19].

In particular, MSNs have found potential application in targeted therapy [20]. Indeed, Durfee et al. [21] developed a drug nanocarrier named "protocell" which consists of a MSN core for drug loading and a lipid bilayer as gatekeeper and platform for surface modifications. They availed an epithelial growth factor receptor (EGFR)-antibody to efficiently target leukemic cells *in vitro* and *in vivo*. Moreover, Zhou and coworkers [22] conjugated rituximab to MSNs [23]. Rituximab is a chimeric monoclonal antibody targeting the CD20 antigen on B cells and approved for B-cell non-Hodgkin lymphoma therapy. A pronounced reduction of tumor volume was observed in rituximab-targeted and doxorubicin-loaded MSNs treated mice, bearing a lymphoma-derived xenograft. Moreover, mice general health status of the MSNs treated group was much better in comparison to that of mice treated with free doxorubicin.

More recently, Sanchez-Salcedo et al [24] proposed new multifunctional polyethylenimine (PEI) coated core-shell Fe3O4@SiO2 MSNs, with a zwitterionic 2-methacryloyloxyethyl phosphorylcholine (MPC) surface, aimed at reducing unwanted protein (corona proteins) adsorption on the MSNs surface once entered the bloodstream,

thus minimizing opsonization and prolonging MSNs blood circulation time. The device also carries an anti-TWIST siRNA, which, knocking down TWIST expression, sensitizes ovarian cancer cells to the action of the other cargo molecule, daunorubicin, whose release is triggered by externally applied oscillating magnetic fields (OMF). Particularly fascinating is also the totally innovative approach of using human Decidua Mesenchymal Stem Cells (DMSCs) as carriers for doxorubicin (DOXO) loaded MSNs to direct the delivery system exclusively to the tumor site, exploiting DMSCs migratory attitude towards tumors [25].

Moreover, multifunctional MSNs are currently being applied in the bio-sensing field and as ideal cell tracing in the detection of analytes within individual cells both *in vitro* and *in vivo*. Since nanoparticles, they do not suffer from fluorescent self-quenching and other diffusion-related problems [26], thus they can be functionalized with large quantities of cell-recognition or other site-directing compounds. Therefore, fluorescence-traceable MSNs are useful tools for cell tracking via fluorescence microscopy. Likewise, magnetic resonance imaging (MRI)-traceable MSNs are employed in both clinical- and research-based fields, due to their deep tissue imaging capabilities [8]. To date, MSNs have also been explored for simultaneous imaging and therapy, making them a biomedical platform for theranostic applications driving the biomedical field towards personalized medicine [7]. MSNs have emerged as suitable for long-term quantitative imaging at low doses, since they are safely cleared from the body after imaging is complete. It is also noteworthy that MSNs exhibit low hemolytic activity [27], confirming their suitability for systemic delivery through the bloodstream. Not so long ago, dye-doped silica NPs, called Cornell dots (C dots), have been approved from the FDA for the first Investigational New Drug (IND) application for targeted molecular imaging in the oncology field [28, 29].

Finally, as we recently reviewed, MSNs proved to be suitable and advantageous platforms in delivering drugs even across the very low permeable biological barriers such as the skin and the blood brain barrier (BBB) [11, 30].

Last but not the least, we cannot fail to mention the MSNs employment in tissue engineering where they represent an ideal scaffold that confers mechanical and biological support, by controlled release of morphogenic signals that guide cellular differentiation [31].

1.2 Synthetic approaches of MSNs.

Ordered silica-based mesoporous materials are produced through a sol-gel synthesis process. The silica precursors polymerize on the surface of a liquid crystal phase that acts as a cast. The liquid crystal phase is obtained dissolving several kinds of surfactants in water. The resulting material is a composite one in which a regularly structured organic phase is included in a rigid silica framework. The chemico-physical properties of the obtained material, the pore diameters and the packing of the pores can be tuned using different surfactants or synthesis parameters. In most reported syntheses for MSNs production, tetraethoxysilane (TEOS) has been used as precursor of silica, and cationic quaternary ammonium salts, the most common being cetyltrimethyl ammonium bromide (CTAB), have been used as structure directing agents under alkaline conditions. This mixture typically leads to materials with cylindrical mesopores and hexagonal arrangement in the range of 3–4 nm, as in the case of MCM-41 type materials. In 1998, a new family of highly ordered mesoporous silica materials (SBA-15) has been synthesized in an acid medium by using commercially available non-ionic triblock copolymers (EOnPOmEOn) with large polyethyleneoxide (EO)n and

polypropyleneoxide (PO)m blocks. MSU materials are prepared with non-ionic polyethylene glycol polymers (not necessarily triblock copolymers) in neutral environment, in contrast to SBA-15, PHTS (Plugged hexagonal templated silica) and MCF (Mesostructured Cellular Foam), which are made in acidic media. A large number of different synthesis approaches to mesoporous silica materials have been reviewed in ref. [32]. For targeted intracellular drug delivery applications, MSNs with particle size at the nanometer scale need to be employed [33]. In addition, functional silanes can be used to obtain more complex functional hybrid mesoporous materials resulting by the covalent anchoring of organic molecules to the silica framework, potentially useful also in medicine and biotechnology [3, 11]. Preferential functionalization of the external surface of the particles can be achieved before removal of the structure-directing agent, leading to the opening of the pores volume [12]. MSNs typically have a high specific surface area (600–1000 m2/g) and a high pore volume (0.6–1.0 ml/g), which allow high levels of drug loadings to be achieved [34]. Currently, much effort has been made in the attempt of increasing the MSNs pore sizes. In fact, since smaller mesopores are sufficient to host small-molecule drugs, larger pores are needed in order to efficiently encapsulate most macromolecular substances such as proteins (enzymes, antibodies) and nucleic acids (DNA, RNA) [35]. Pore size-engineering can be achieved by addition of auxiliary organics such as trimethylbenzene (TMB) as pore swelling agents (being enclosed in the inner hydrophobic core of the micelles) or co-solvents to the synthesis. In Table 1 several example of mesoporous silica-based drug targeting devices are reported.

MSNs Type	Features	Loaded drug	Performance
MCM-41	Nanovalves functionalized with K8 peptide and a peptide containing two Arg–Gly–Asp (RGD) sequences for pH-induced drug release	Doxorubicin	*In vitro* enhanced cellular uptake of nanoparticles by cancerous cells, through the interaction of RGD ligands and the $\alpha_v\beta_3$ and $\alpha_v\beta_5$ integrins overexpressed on cancer cells, with consequent cell growth inhibition due to the pH dependent release of the loaded drug.
MCM-41 type	Octyl derivatization interacting with amphiphilic peptide molecules through hydrophobic Interactions	-	Good cyto-compatibility with vascular smooth muscle and vascular endothelial cells. The peptide coating improves the cellular uptake of particles up to 6.3 fold
Rattle-Type MSNs	Magnetic Core, and poly(ethylene glycol) (PEG) and folic acid on the surface	Docetaxel	Low *in vitro* toxicity and negligible hemolytic activity; increased uptake by cancer cells that over-express FRs
SBA-15	MSNs labeled with fluorescent aptamer specific for the tumor marker MUC-1 and the radionuclide Tc-99m	-	Aptamer – impregnated MSNs are internalize by cancer cells and do not show any evident cytotoxicity.
MCM-41	Fluorescein on the surface	Cisplatin	Prodrug-conjugated nanoparticles showing high cellular uptake and an IC50 value about 63 times lower than that of free cisplatin in HeLa cells, with consequent potential reduction of the drug associated side effects.
MCM-41	A layer of PEG-galactose is grafted onto the external surface MSNs, while the internal surface of MSNs is preserved for the encapsulation of doxorubicin (DOX)	Doxorubicin	Higher cellular uptake of MSNs-P/G than that of the pristine MSNs due to the galactose-receptor-mediated endocytosis process. Higher cytotoxicity of the DOX@MSNs-P/G on the HepG2 cell line, compared to the free drug
Hollow Mesoporous Silica NPs	A pH-sensitive amphiphilic diblock polymer grafted to the surface of hollow mesoporous silica NPs	Doxorubicin	Less than 10 % of DOX is released in neutral condition and the 80% at acidic pH. The nanocomposites are internalized by human hepatoma 7402 cells and L02 lung cancer cells
MCM-41	Fluorescein and anti-HER2/neu monoclonal antibody (mAb) on the outer surface	-	Nanoparticles with high amounts of Herceptin have greater selectivity and higher targeting efficiency towards BT-474 (more than 90% of cells targeted within 6 h from exposure)
MCM-41	Fluoresceine, phosphonate (to increase dispersibility of the NPs) and folic acid on the surface	Camptothecin	Folate conjugation dramatically increases the tumor-suppressing effects of CPT-loaded MSNs; TEM images of MSN in the urin confirm excretion of the particles
MCM-41	MSNs covalently encapsulating fluoresceine or a photosensitizer, functionalized with galactose on the surface	Camptothecin	MSN combining drug delivery and photodynamic therapy showing a dramatic increase of cancer cell death compared to separate treatments

MSU	Folic acid on the surface	Cisplatin	Highly selective receptor-mediated uptake and cell kill in FR expressing cells and no uptake in FR negative cells

Table 1. *Examples of mesoporous silica-based drug targeting devices. [4]*

1.3 Targeting functions

To satisfy the various application requirements of cancer diagnosis and therapy, MSNs integrated with multiple functionalities (Generation III), such as small molecules, antibodies, aptamers, peptides and glycoproteins, have been generated in these last years [36, 37]. Selective targeting strategies employ ligands that specifically interact with receptors highly overexpressed by cancer cells relative to normal cells, thus promoting nanocarrier binding and internalization.

Among the targeting functions that can be anchored on the external surface of MSNs, the use of folic acid (FOL) has been widespread recognized [38, 39]. FOL is a low molecular weight essential vitamin compound, with a high affinity for the folate receptor (FR), a membrane protein which can actively internalize bound folates and folate conjugated compounds via receptor-mediated endocytosis. FR constitutes a useful target for tumor-specific drug delivery since it is up-regulated in many human cancers (including ovary [40], colorectal tract [41], brain [42], kidney [43], breast [44], myeloid cells [45] and lung [46]) and its density on cell membrane appears to increase as the stage/grade of the cancer worsens [47, 48] (Tab 2). Thus, it has been hypothesized that folate conjugation to anti-cancer drugs will improve drug selectivity and decrease negative side effects [4]. Indeed, folate based active targeting has been used to deliver nanoparticles to ovarian and other types of cancer that overexpress folate receptors [19, 49].

Qi et al. reported a greater reduction in laryngeal tumor size in a mouse model by using cisplatin-loaded and folate-conjugated MSNs, compared to free cisplatin [50]. Zhang and colleagues [51] also used folate as targeting ligand on MSNs to improve the radio-enhancer effect of valproic acid in glioblastoma cells.

These features make FRs interesting Tumor Associated Antigens (TAAs) to be exploited to target imaging molecules and therapeutic compounds directly to cancerous tissues [52].

In humans, three FR isoforms have been described, referred as isoform α, β and γ, each with tumor-specific distribution (Table 2).

***Table 2**: Expression of Folate Receptor Isoform (FRα, FRβ and γ) malignant human tissues. Adapted from Kelemen. et al. (2006) [48].*

Malignant tissues	FRα	FR β	FR γ
• High expression	Cervical carcinoma Uterine carcinoma Bladder carcinoma Metastatic endometrial carcinoma Non-mucinous ovarian carcinoma Metastatic pancreatic carcinoma Primary renal cell carcinoma Nasopharyngeal carcinoma Lung carcinoma	Leukemia Lymphoma Multiple Myeloma Lung carcinoma Pancreatic carcinoma	Leukemia
• Low or negligible expression	Mucinous ovarian carcinoma Primary endometrial carcinoma Metastatic renal cell carcinoma Lung carcinoma and adenocarcinoma Primary breast carcinoma Primary bladder carcinoma Primary pancreatic carcinoma Colorectal carcinoma Primary prostate carcinoma Primary brain carcinoma Primary liver carcinoma Primary head and neck carcinoma		

Folate receptors α and β are glycosylphosphatidylinositol (GPI)-anchored membrane protein which can internalize folates and folate conjugated compounds via a receptor-mediated endocytosis following the CLIC (clathrin-independent carrier)/GEEC (GPI-anchored protein-enriched early endocytic compartment) endocytic pathway. Unlike

the other members, FRγ is a secretory protein that lacks an efficient signal for GPI anchor attachment [53, 54].

Nevertheless, the advent of personalized medicine demands that additional moieties targeting different molecular markers that are overexpressed in cancer cells, other than FR, are anchored to the surface of MSNs and used to deliver drugs to a broader range of tumors (Fig. 2). In this regard, the transferrin peptide or anti-transferrin receptor antibodies have been employed as targeting moieties of nano-based drug delivery systems against a wide variety of cancers over-expressing the transferrin receptor, even glioma, since drug loaded/transferrin-conjugated nanocarriers have been reported to cross the blood brain barrier [55]. Additionally, transferrin-targeted nanoparticles may be used in selective diagnostic applications with enhanced selectivity and sensitivity [56].

Other adopted targeting moieties are the epidermal growth factor receptor (EGFR) targeting peptide for active targeting of EGFR overexpressing cancers [57, 58], the arginine–glycine–aspartic acid (RGD) tripeptide to target the integrin receptors expressing tumors (the α5β5 or α5β3 integrin receptors are overexpressed on vascular endothelial cells of angiogenic blood vessels of proliferating tumors) [59, 60], nucleic acid constructs, such as aptamers, used to selectively bind to prostate-specific membrane antigen (PSMA) or the tumor marker MUC-1 in other types of cancers [61-63], hyaluronic acid (HA) to target CD44 antigen [64, 65], trastuzumab (Her2/neu antibody, Herceptin®) for Her2/neu-positive breast cancers [66], TRC105 antibody, specific for the tumor vasculature marker CD105/endoglin [67]. MSNs conjugated with galactose and fluorescent dyes, for cell targeting and imaging, respectively, have also been described and the authors demonstrated that the uptake by cancer cells was

mediated by galactose receptors leading to the accumulation of the nanoparticles in the endosomal and lysosomal compartments [68], or into the cytoplasm following release from the lysosomes [4]. Finally, luteinizing hormone-releasing hormone (LHRH) has been used as a targeting moiety (ligand) to LHRH receptors that are overexpressed in breast [69], ovarian [70], endometrial [71], prostate [72] and lung [73] cancers, while being not expressed, or expressed at a low level, in most visceral organs. Particularly, a tumor targeted MSN-based system for complex delivery of drugs and siRNA, where the targeting was achieved by the conjugation of LHRH peptide on the surface of MSNs, was developed and seems to be highly promising for inhalation treatment of non-small cell lung carcinoma [74].

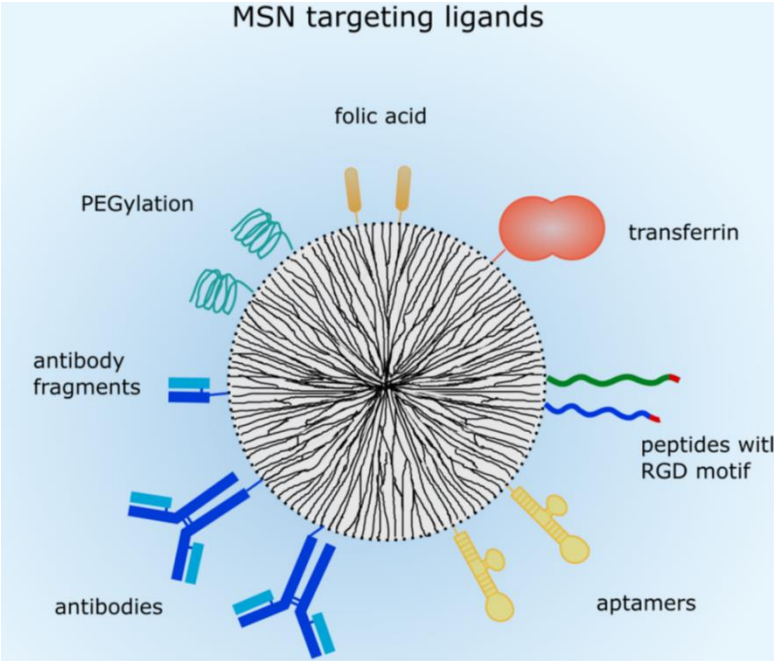

***Figure 2**: Multiple functionalities used for active targeting of MSNs [37].*

1.4 Mesoporous silica stimuli-responsive nanosystems.

Recent breakthroughs have been made in the design, synthesis and applications of stimuli responsive nanosystems which are able to change their properties upon external stimuli (e.g. temperature, light, ultrasounds, heat, magnetic field) and/or internal stimuli (e.g. pH, enzymes, macromolecules, reducing agents) [75, 76], achieving concentrated dosage release to targeted sites preventing premature cargo leakage [77].

Among all the materials dedicated to this application, multifunctional MSNs are gaining great attention owing to their unique features (good biocompatibility, tunable pore size, etc), multiple functionality for targeting different types of cells and ability to efficiently entrap cargo molecules inside the pores [4, 19, 75, 76]. Functionalization of silica surface with stimuli-responsive molecules (macrocycles molecules, linear molecules, polymers, proteins, magnetic nanoparticles, etc.), Functionalization of silica surface with stimuli-responsive molecules (macrocycles molecules, linear molecules, polymers, proteins, magnetic nanoparticles, etc.), usually termed capping agents (CAs), or "gating agents" or "gatekeepers", allow to control drug release since they prevent drug leakage until particular conditions occur [78].

In the last decade a large variety of MSN-based stimuli-responsive systems have been developed [4, 76, 78]. Here we focused on the more recent progresses in the field of stimuli-responsive MSNs. The systems are summarized in Table 3 and grouped on the base of the gating agents and the release stimuli.

***Tab. 3**: Stimuli-responsive mesoporous silica based systems. Adapted from Pasqua et al. (2016) [4].*

STIMULI	*GATING AGENT*
pH	TSP-DATA ligand (N-(3-trimethoxysilylpropyl) ethylenediamine triacetate)
	polyelectrolyte multilayers (PEMs)
	protein-gated carbohydrate
	NIPAM-co-MAA polymer (N-isopropylacrylamide-co-methacrylic acid polymer)
	poly(l-glutamic acid) (PLGA)
	poly (methacrylic acid) (PMAA)
Enzymes	Azopyridine derivatives
	hyaluronic acid (HA)
Nucleic acids	ATP aptamer
Reducing agents	peptides
	β-Cyclodextrin
Temperature	polymer
	AuNP–DNA conjugates
Light	supported lipid bilayer (SLB) and photosensitizer molecule (PS)
	thymine derivatives
	cyclodextrin-modified gold nanoparticle (CD-Au)
Magnetic field	monodispersed Fe_3O_4 nanoparticles
	superparamagnetic iron oxide nanocrystals (SPION) capped with lipid bilayer

Table 1Stimuli-responsive mesoporous silica based systems. Adapted from Pasqua et al. (2016) [4].

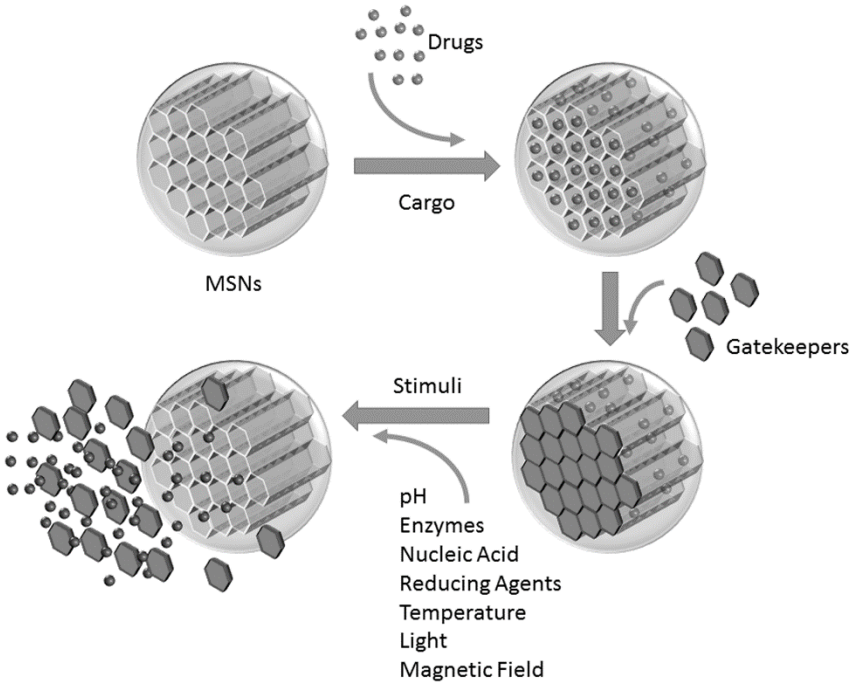

Various gatekeepers at the MSNs surface have been reported and can be classified in three different groups: 1) pore gating systems, consisting of macromolecules (proteins, polymers, etc.) or nanoparticles (magnetic or gold nanoperticles) which block the pore entrance, entrapping the drug; 2) surface coating systems, such as oligonucleotides or lipid bilayers which prevent premature drug release; 3) internal pore modified systems which consist of cargo molecules attached to the mesopores through coordinative or covalent bonds [78, 79].

When internal or external stimuli do occur, these gatekeepers are triggered to release the guest molecules. Some of these systems can release the cargo in response to more than one stimulus, improving the efficiency and reducing side effects to even greater extent.

1.4.1 pH

pH sensitive systems have been extensively developed in cancer therapy. In fact, it is well known that neoplastic cells have a more acidic environment compared to normal cells and an even lower pH is found in endosomes and lysosomes (pH 4.5-5.5). Thus, once the pH-sensitive MSNs are internalized by cells, the low pH of lysosomes triggers the release of the anticancer drug, achieving the desired therapeutic efficacy. Different as conceived systems have been developed incorporating molecules linked to the MSN surface through electrostatic interactions or acid-labile covalent bonds [80]. For example, Chan et al. have developed pH–dependent MSN-based carriers coated with poly-N-isopropylacrylamide-co-methacrylic acid (P NIPAM-co-MAA) for doxorubicin (DOX) delivery (P-MSN-DOX). P-MSN-DOX with pH-triggered

drug release showed greater cytotoxicity in vitro and therapeutic efficacy in vivo compared with traditional MSN-DOX [81].

1.4.2 Biomolecules

Biomolecules such as enzymes, antibodies and nucleotides, due to their biocompatibility and interesting biological activities, have been employed as stimuli to trigger drug release. Various enzyme-responsive MSN-based systems have been developed to release the guest molecules in cancer tissues or into the cytosol of cells overexpressing the specific enzyme [65, 82]. Among them, a simple azopyridine (Azo) derivative was used as a gatekeeper to prepare enzyme-responsive silica nanoparticles loaded with Rhodamine B (Rh-Azo-S) or camptothecin (CPT-Azo-S). The developed systems are able to release the entrapped cargo in the presence of reductases or esterases through the enzyme-induced rupture of the anchored azo gatekeeper [83].

Another very interesting strategy to design MSN controlled drug release triggered by biological stimuli consists in the employment of nucleic acids aptamers, mainly DNA aptamers, to functionalize silica nanoparticles [84]. In these systems using aptamers as nanovalves, the so called “aptavalves”, MSNs are modified with adenosine triphosphate (ATP)-binding DNA aptamers which allow the loading and release of drugs under the ATP control [4]. These aptavalve–nanoparticle systems have the advantage of protecting the cargo molecules until their delivery and release to the site of interest occur.

1.4.3 Reducing agents

Gatekeepers linked to MSNs through chemically labile disulphide bonds, have been used to develop redox potential-responsive release systems [85]. The design of these systems is based on the knowledge that the concentration of the reducing agent glutathione (GSH, reduces disulfide bonds formed within cytoplasmic proteins to cysteines by serving as an electron donor) in tumor cells (2−8 mM) is much higher than that in blood plasma (1−2μM) [86]. Moreover, tumor tissues are highly reducing compared to normal tissues, with several times higher concentrations of GSH in the tumor cytosol compared to that in normal cells [87]. The unique intracellular redox potential has provided an inbuilt different release mechanism for controlled drug delivery [88].

1.4.4 Temperature

Temperature is another stimulus that has been studied to trigger the cargo release from MSNs. Thermo-responsive release systems have been developed by attaching thermo-sensitive molecules on the surface of MSN [76, 89]. Vallet-Regí *et al.* reported the synthesis of MSNs coated with a thermoresponsive copolymer of poly(ethyleneimine)-*b*-poly(N-isopropylacrylamide) (PEI/ NIPAM) which acts as temperature-responsive gatekeeper for proteins and small molecules loaded inside the silica matrix. The developed nanodevices trap the guest molecules at low temperatures (20 °C) and release the retained molecules when the temperature exceeds 35−40 °C [4].

1.4.5 Light

Light-responsive release systems have received increased interest due to the advantages in spatial and temporal control of cargo release. In fact, the processes involving external light activation are rapid and directional. The release of guest molecules included in the pores of mesoporous silica is promoted by irradiation with UV and/or visible light [90]. As an example, thymine-modified mesoporous silica nanoparticles (TA-MSN) were synthesized as reversible light-responsive molecule-gated systems. The release of the entrapped molecules is related to a photodimerization-cleavage cycle of thymine by different irradiation. The irradiation with 240 nm wavelength UV light of TA-MSN loaded with the dye $Ru(bipy)_3^{2+}$ (bipy = 2,2′-bipyridine) leads to the opening of pores allowing the diffusion of the guest molecule. Instead the irradiation with 365 nm UV light causes the blockage of pores inhibiting the release of the cargo [91]. In addition, a versatile trigged release system has recently been developed by capping cyclodextrin-modified gold nanoparticle (CD-Au) onto the mesoporous silica (CD-Au-MS). The silica nanopores and the CD cavity of this MS-based system can be loaded with different cargoes to realize multiple molecules loading and sequential release by light initiation [92].

1.4.6 Magnetic fields

Also magnetic field has been used as an external stimulus to realize various stimuli-responsive MSN systems [93]. Magnetic-responsive materials utilize alternating external magnetic field as a trigger to switch drug release. These systems usually include magnetic nanoparticles inside or on the surface of MS particles. Recently the capping of MSNs with superparamagnetic iron oxide (Fe_3O_4) nanoparticles has been reported. Superparamagnetic iron oxide nanocrystals have been trapped inside the

mesoporous silica matrix, in order to provide the heating capability under alternating magnetic fields, which is also suitable for hyperthermia treatment of cancer [8, 94].

1.4.7 Dual or multi-stimuli responsive MSNs

Also dual or multi-responsive controlled release systems have been reported. They respond to two or more stimuli either in an independent or in a synergistic way [95]. A MSN drug controlled-release system has been developed by using L-cysteine derivatized gold nanoparticles (AuNPs), bound to the MSNs using Cu^{2+} as a bridging ion. Both pH and ATP concentration can trigger the release of the caps and hence the delivery of the drug. These stimuli are either: low pH (pH < 5) or elevated levels of adenosine triphosphate (ATP) (concentration > 4 mM) [4]. Also DNA-gated mesoporous silica nanoparticles with Ti^{IV} chelating phosphonate have been developed for simultaneous and cascade release of two drugs in response to a single stimulus (endonuclease degradation or heat dehybridization) or dual stimuli (first basic pH and subsequent heating), respectively [96].

1.5 Target specificity, cellular uptake, intracellular fate and exocytosis of MSNs.

Although the direct accumulation of MSNs at the tumor site can passively occur through tumor vascular leakage (the so-called enhanced permeability and retention (EPR) effect) [19], the lack of cell-specific interactions needed to induce MSNs internalization decreases therapeutic efficacy and can result in drug expulsion from the carrier outside the target tissue, leading to drug resistance. Therefore, as above reported, great efforts are being devoted to the development of MSNs functionalized

with opportune targeting functions, so to deliver and release the antineoplastic drug directly to the tumor site. All the DDSs described by the numerous research groups working on this matter, are promptly internalized by cells through an active endocytosis pathway, as their uptake is inhibited by decrease in temperature to 4°C, by incubation with metabolic inhibitors, as well as by the disruption of microtubules [4]. Cellular uptake, compartmentalization, and intracellular retention of MSNs seem to be dependent on their physiochemical and morphological characteristics, as well as on their size, surface charge functionalization and on the nature of the target cancer cells [35]. Although the presence of a ligand grafted to the MSNs surface do always improve the uptake respect to control carriers (devoid of the targeting moiety) [19] , the lack of tumor specificity hampers their potential implementation as targeting devices.

This might be, at least in part, also ascribed to the fact that the MSNs employed in the various studies have been, in most cases, labelled with a fluorescent tracer (e.g. fluorescein isothiocyanate, FITC), which allows the MSNs to enter the cells regardless of the presence of a targeting function, either on account of the EPR effect or for an unspecific, caveolae-mediated, uptake [4, 37]. For this reason, it would be advisable to track MSN-ligand route in the cells by means of colloidal-gold immunocytochemistry (immunogold, IG) and transmission electron microscopy (TEM), since the electron density properties of MSNs allow their clear identification within cells and tissues. Indeed, by means of this technical approach, we were able to demonstrate how a highly specific, receptor mediated, cellular internalization of multifunctional MSNs, covalently conjugated to the ligand folic acid (MSN-FOL), occurs exclusively in FR expressing cells, as demonstrated by colloidal-gold labelling

for FR (see *Results and discussion in vitro* section) while non-functionalized MSNs are not able to enter cells [4]. It is worth mentioning that, to our knowledge, this feature is unique for our MSNs.

Once inside the cells, different routes have been proposed for MSNs, which have been described to colocalize with lysosomes, but also with not-specific endosomal cavities, or even with mitochondria [97] or secretory granules of mastocyte-like rat basophilic leukemia (RBL) [98]. Recently Yan *et al*. published a fascinating work describing how fluorescent disulfide-bonded poly(methacrylic acid) (PMASH) nanoporous polymer particles (NPPs), prepared by mesoporous silica templating, migrate from the early endosomes to the lysosomes within a few minutes and how, upon cell division, the lysosome-enclosed PMASH NPPs are distributed asymmetrically between two daughter cells [99]. However, DDSs based on MSNs have also been reported to easily escape from endosomes and protect the loaded drugs from bioerosion, assuring an efficient intracellular delivery of therapeutics, and consequently kill cancer cells at enhanced efficacy [97, 100]. Again, all the reported studies do not take into account that the endocytotic route undertaken by MSNs could very easily be influenced by the fluorescent tracer, thus, a more accurate investigation of the mechanisms involved in non-fluorescent MSNs endocytosis and intra-cellular trafficking is still needed.

Less confusing seems to be the data regarding the exit of nanoparticles from the cells. It has been exhaustively demonstrated that non fluorescent particles are expulsed from the cells starting from 48 h and are almost completely exocytosed within 96 h [19]. Moreover, Slowing *et al.* reported that fluorescent MSNs can undergo cell-to-cell transfer and when exiting the cells they are coated by proteins on their surface [101],

while Yanes *et al* identified the lysosomal route as the mechanism responsible for the exocytosis of phosphonate modified fluorescent mesoporous silica nanoparticles (P-MSNs) [102]. However, due to the presence of the fluorescent tracer employed in these studies, the cellular mechanism for MSNs exocytosis should still be deeper investigated.

1.6 MSNs biocompatibility

The *in vivo* behavior of MSN-based nano-DDSs is drawing increasing attention for MSNs clinical application perspectives and has become a current hot topic in MSNs biosafety research. In fact, even though our understanding on biocompatibility (blood compatibility, biodegradability, biodistribution, cell and tissue toxicity and excretion) of MSNs and their interaction with the immune system has significantly improved, to date, the available literature on the specific issue is still quite conflicting, thus the adjuvant effect of MSNs still requires deeper investigation and understanding before their use in a clinical setting [103].

It is well established that, due to wide range of synthesis procedures and the resulting physical characteristics, general assumptions about MSNs potential toxicity and organ accumulation cannot be drawn [104]. In fact, MSNs degradability and toxicity is affected by different parameters such as size, morphology, porosity, surface charge (e.g., anionic surfaces are generally less toxic than cationic NPs, which can cause hemolysis) and functionalization, but also by the cell type employed and by the dosage [11, 20]. Therefore, in order to develop safe silica nanoparticles carriers, a fine-tuning of these structural characteristics is mandatory.

1.7 Multiple Myeloma: pathogenesis and management

Multiple myeloma (MM) is a B-cell neoplasm characterized by uncontrolled growth of malignant plasma cells that secrete monoclonal immunoglobulins within the bone marrow (BM) [105].

MM accounts for 15% of hematopoietic cancers and 1% of cancers worldwide. It is the second most common hematological malignancy, with an incidence of 6/100,000 in Europe and its incidence increase with age (median age of patients at diagnosis is approximately 67 years) [106].

MM is characterized by dissemination of multiple tumor cells throughout the BM and results from a series of heterogeneous chromosomal aberrations and numerous mutation in a range of genes that accumulate during B cell maturation, making the treatment of this pathology problematic [107]. A mnemonic sometimes used for the common MM pathologies is CRAB: C (calcium, elevated), R (renal failure), A (anemia), B (bone lesions) [108].

MM begins as monoclonal gammopathy of undetermined significance (MGUS), progresses to smoldering (asymptomatic) myeloma and finally becomes overt (symptomatic) myeloma, resulting in BM infiltration and osteolytic lesions. During MM progression the normal equilibrium between osteoblastic (bone building) and osteoclastic (bone breakdown and resorption) activity is skewed toward net bone loss. MM-induced osteolysis releases growth factors embedded inside the bone matrix, fueling MM progression and expansion in the BM niche and resulting in greater osteoclastic activity in a process known as the “vicious cycle” [109].

During this MM-induced cycle, osteoclastic bone breakdown releases bone-embedded growth factors to promote tumor growth, which, in turn, stimulates greater

osteoclast activity. In addition to osteoblasts and osteoclasts, other BM niche cells, including mesenchymal stem cells (MSCs), BM adipocytes, immune cells, and osteocytes also likely affect MM progression [110].

It is established that the majority of MM cases are associated with an initiating somatic mutation and are frequently accompanied by additional oncogenic mutations [111, 112]. Thus far, MM treatments primarily rely on chemotherapies in conjunction with proteasome inhibitors (PI) [113], anti-resorptive agents such as bisphosphonates [114], corticosteroids and bone marrow transplantation [115].

Over the last years, many agents and therapeutic combinations have been approved with the aim of reaching new possible treatment options in the management of MM [116]. The most widely used molecules include proteasome inhibitors, monoclonal antibodies, immunomodulatory agents (IMiDs), alkylators and histone deacetylase inhibitors (DACIs) that can be combined in doublet, triplet or even quadruplet regimens, and used together with or without high-dose therapy and autologous stem cell transplantation (ASCT), or in some cases as continuous treatment [117]. These drugs work through a variety of mechanisms, some of which are not fully understood.

1.7.1 *Proteasome inhibitors (PI)*

Currently, PI as *bortezomib* (Velcade, Millenium), *carfilzomib* (Kyprolis, Amgen) and *ixazomib* (Ninlaro, Takeda) are considered a cornerstone in the treatment of this malignancy since the massive antibody production leads to high accumulation of misfolded or unfolded proteins in the endoplasmic reticulum (ER) of plasma cells, causing the so called “ER stress”. In this context, ubiquitin–proteasome inhibition

contributes to the dangerous accumulation of these proteins, activating apoptotic pathways and, consequently, inducing cell death [108, 113].

1.7.1.2. Bortezomib (PS-341, Velcade ®)

Bortezomib (BTZ) is the first proteasome inhibitor approved by US FDA for the treatment of multiple myeloma patients [113, 118]. BTZ is a dipeptide boronic acid that reversibly inhibits the chymotrypsin-like activity (subunits β5) of the 20S proteasome core in the 26S proteasome complex and consequently degrading cell proteins (Fig. 2). The proteins accumulation induces overproduction of Reactive Oxygen Species (ROS) in the ER, resulting in fatal cell stress which, in turn, leads to cell cycle arrest and caspase-dependent apoptosis [106]. Therefore, ROS production, in addition to mitochondrial-mediated intracellular Ca2+ dysregulation [119], represent the main mechanisms of BTZ-induced cytotoxicity in MM cells.

It is also reported that the anti-myeloma activity of BTZ is supported by the suppression of NK-kB signaling pathway that leads to the down-regulation of its anti-apoptotic target genes and to the simultaneous induction of NOXA, a pro-apoptotic member of the Bcl-2 protein family [120].

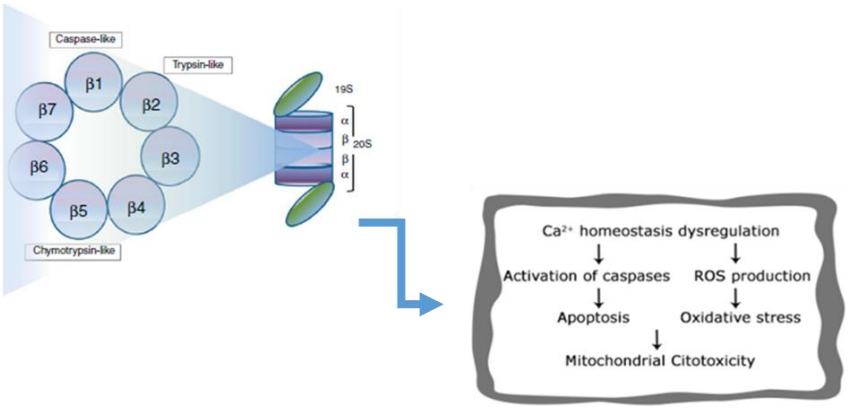

Figure 3: *Structure of 26S proteasome: four heptameric rings of α and β subunits shape the 20S core in which the proteolytic sites with caspase-like, trypsin-like and chymotrypsin-like activity are located in the subunits β1, β2 and β5, respectively (left). Target mechanisms of BTZ toxicity in multiple myeloma cells (right).*

Patients often discontinue BTZ treatment because of peripheral neuropathy BTZ-induced (BIPN) that occurs typically by the end of cycle 5 of chemotherapy treatment, with an estimated incidence of up to 40% of patients [120]. The peripheral neuropathy is predominantly sensory, with symptoms including burning, paresthesia, hyperesthesia–hypoesthesia, neuropathic pain and weakness. Still elusive are the knowledge concerning the mechanism of BIPN, although a multifactorial cause seems likely, due to the amount of sites involved in BTZ-damage, from the level of the sensory cell bodies in the dorsal root ganglion (DRG) to the distal terminal axon [106].

Cavaletti and colleagues, miming the BiNP in a rat model, suggested that BTZ causes a dying-back degeneration of sensory nerves with pathological changes to both Schwann and Satellite cells, representative of a toxic axonopathy [121]. In the same work, the authors also indicated that DRG of BTZ-treated animals show intracytoplasmic vacuolization which can be attributed to mitochondrial and endoplasmic reticulum enlargement [121, 122]. Moreover, a later study performed by Meregalli and co-workers reported that nerve terminals are involved in the genesis of BTZ neurotoxicity, that leads

to unmyelinated fiber axonopathy, especially with large and C-fiber damage [123]. Conversely, other studies suggested that BIPN was mainly due to dysfunction at the neuronal level, with a secondary alteration in axon and myelin structures [124]. Furthermore, the proteasome inhibition by BTZ results in accumulation of cytoplasmic aggregates in neuronal cells, reduction of extranucleolar transcription and nuclear retention of polyadenylated RNAs in nuclear bodies [124].

Moreover, Alè *et al.* proposed that BTZ mainly affected DRG neurons and induced neurite dysfunction altering the axonal transport, due to more marked susceptibility of sensory neurons to BTZ compared with Schwann cells [125]. Several preclinical studies suggest that the disruption of axonal transport processes by microtubule dynamics alteration is another possible neurotoxicity mechanism. Further preclinical data also demonstrated that BTZ toxicity is correlated by tubulin polymerization to microtubule dynamics in both cancer cells and neurons, interfering with the normal axonal transport and showing an accumulation of neurofilaments in the soma [126]. Subsequent i*n vivo* studies by Staff *et al.* and Meregalli *et al.* both reported that BTZ is a drug that increases the polymerized tubulin in microtubules, thus affecting microtubule function and stabilization, altering axonal transport in rat DRG neurons [127].

Patients prevalently describe numbness/tingling in hands and feet, burning pain, altered sensitivity to touch and heat, muscle weakness, skin or nail changes, and/or lack of coordination. In fact, sensory neuropathy and neuropathic pain are more common; therefore, hyperesthesia, hypoesthesia, and paresthesia are very often referred, usually in a distal stocking-and-glove distribution over the hands and feet, frequently associated with altered heat and cold sensation. Additionally, sensory PN can lead to areflexia and loss of proprioception. Symptoms or signs of motor and/or autonomic nervous system

damage can also emerge, even if less frequently. Motor symptoms prevalently occur in the case of a severe sensory PN causing muscle cramps, muscle atrophy, or loss of strength in distal muscles. Rarely, orthostatic hypotension, bradycardia, constipation, or impotence can occur as signs of autonomic damage [124].

Moreover, the axonal transport degeneration may be induced by a deficit in mitochondrial energy metabolism and by an impairment of mitochondrial respiratory chain due to damage to DRG neurons. In addition, the neurotoxic action of BTZ is through transient release of intracellular calcium store, leading to mitochondrial calcium influx and apoptosis induced by caspase activation, as demonstrated in the study of Landowski and co-worker in BTZ-treated myeloma cells in which mitochondrial dysfunction leads to a decrease of ATP levels [119].

In neurons, the calcium homeostasis disruption, promoting bioenergetics deficits that induced depolarization and spontaneous discharge, is probably responsible of the typical degeneration in primary sensory neurons and intraepidermal nerve fibers observed in BTZ-treated patients [124]. Moreover, it is acknowledged that mitochondrial dysfunctions and oxidative stress, as a biochemical process resulting from the generation of reactive oxygen species (ROS) in electron transport chain, occur in BTZ-induced chronic painful peripheral neuropathy [119]. Therefore, the generation of oxidative stress may represent a relevant step in BTZ-induced neuronal cell death.

Furthermore, thrombocytopenia, gastrointestinal disorders and the development of resistance to treatment, strongly limit BTZ clinical use, since these debilitating effects have a great impact on MM patients' quality of life [106, 128, 129].

1.7.1.2. Carfilzomib (Krypsolis, Amgen).

Carfilzomib (Kyprolis), a second-generation proteasome inhibitor approved in 2012 for relapsed or refractory multiple myeloma RRMM [130], offers the advantage of a reduced peripheral neuropathy and has demonstrated effectiveness in patients with relapse after bortezomib therapy. However, drug resistance can occur, and, importantly, cardiovascular-related adverse events, first observed in the initial trials [131] and recently confirmed by a meta-analysis, raise particular concern [132].

1.7.1.3 Ixazomib (Ninlaro, Takeda).

In late 2015, ixazomib (Ninlaro; MLN9708), another boronic acid-derivative and inhibitor of the beta-5 chymotrypsin-like (CT-L) proteasome subunit activity, is the most recently approved PI, to be uses in combination with lenalidomide and dexamethasone in MM patients who had previously received one or more unsuccessful therapy [133].

Ixazomib toxicity profile is similar to that of bortezomib, although ixazomib appears to be associated with reduced incidence of peripheral neuropathy, possibly because of its greater selectivity for the CT-L subunit. However, severe thrombocytopenia and gastrointestinal adverse events have been reported [134].

1.7.2 Monoclonal Antibodies

In 2015, two monoclonal antibodies were approved for the treatment of RRMM: *elotuzumab* and *daratumumab* [105, 135, 136].

Elotuzumab is a monoclonal IgG-κ antibody directed against SLAMF7 (signaling lymphocytic activation molecule F7), a cell surface receptor involved in natural killer cell

activation, highly expressed on human plasma cells and corresponding myeloma cells [137].

Daratumumab (DARZALEX®) is a monoclonal IgG-κ antibody that binds to CD38, a transmembrane protein found on the surface of myeloma cells and responsible for cellular adhesion and ectoenzymatic activity [138].

Both elotuzumab and daratumumab act through recruitment of the immune system to enhance cellular cytotoxicity directed against myeloma cells [139, 140]. They are generally well tolerated when used as monotherapy and show a generally manageable tolerability profile in combination therapy [141]. Infusion-related reactions (IRRs) represent the most common adverse events like a high rate of neutropenia, thrombocytopenia and anemia [142, 143].

1.7.2.1 CD38 as immunotherapeutic target in multiple myeloma

CD38, a type II transmembrane glycoprotein, was discovered in 1980 by E.L Reinherz and S. Schlossman [144] and plays a role in regulation of migration, receptor-mediated adhesion by interaction with CD31 or hyaluronic acid, and signaling events [145]. Furthermore, CD38 also has ectoenzymatic activity and is involved in the generation of nucleotide metabolites, which play a role in the control of intracellular calcium stores [144]. Under normal conditions, CD38 is expressed at relatively low levels on myeloid and lymphoid cells and in some non-hematopoietic tissues [146, 147]. In contrast, plasma cells and multiple myeloma cells have high levels of CD38 expression, which makes CD38 an interesting target for therapeutic antibodies targeting cell surface molecules in MM [148].

Actually, daratumumab (fully human; Janssen Pharmaceuticals) is the first CD38-targeting antibody, which is approved as single agent and in combination with several standards of care in MM [148]. CD38 antibodies are not only evaluated in relapsed/refractory MM, but also in patients with newly diagnosed MM [144].

CD38 antibodies kill tumor cells via Fc-dependent immune effector mechanisms including complement-dependent cytotoxicity (CDC), antibody-dependent cell-mediated cytotoxicity (ADCC), antibody-dependent cellular phagocytosis (ADCP), and apoptosis upon secondary cross-linking [145].

Although, immunotherapy with CD38-targeting antibodies is an attractive approach because of a favorable toxicity profile and high activity of CD38 antibodies alone or in combination with standards of care for MM, there is substantial heterogeneity in quality and duration of response among patients [145]. Differences in frequency or activity of effector cells, as well as mechanisms of primary and/or acquired resistance including tumor-related factors, or reduced cell surface expression levels of the target antigen and high levels of complement inhibitors (CD55 and CD59), may contribute to differences in outcome of MM patients to monoclonal immunotherapy [145].

Noteworthy is a rapid decrease in CD38 expression levels on the MM cell surface during daratumumab-treatment generating a mechanism of resistance which hamper clinical practice. [149]. It is an early event, which also occurs on non-depleted MM cells and on non-malignant cells already observed after the first infusion, causing a status of acquired resistance which is a transient phenomenon, because CD38 levels are restored to baseline levels on the MM cells more or less 6 months after the last daratumumab infusion [144]. Furthermore, soluble CD38 may neutralize CD38-targeting antibodies and thereby have an impact on pharmacokinetic profile and response [150].

The prominent efficacy of the addition of daratumumab to lenalidomide and dexamethasone (DRd) or the addition to bortezomib and dexamethasone (DVd) was proven for patients with relapsed or refractory multiple myeloma (RRMM) [151].

Clinical data were obtained from the POLLUX (Phase3 Study Comparing daratumumab + lenalidomide + dexamethasone DRd Versus Rd in Subjects with Relapsed or Refractory Multiple Myeloma [RRMM]) and CASTOR (Phase3 Study Comparing DVd Versus Vd in Subjects with RRMM) trials [151].

Up to now, although relapsed or refractory MM (RRMM) remains incurable, patient survival was prolonged significantly due to novel regimens recently approved by the US Food and Drug Administration [151]. In virtue of the outstanding survival outcomes, 3 triplet regimens, anchored with these novel agents plus traditional regimens are now recommended for RRMM in clinical practice guidelines as standard therapies [152]. According to the latest guidelines, except for elderly or frail patients, almost all patients with RRMM who had received at least 1 or 1 to 3 prior therapies were recommended for the triplet regimens [152].

1.7.3 Immunomodulating Agents (IMiDs)

IMiDs (thalidomide, lenalidomide, pomalidomide) enhance the immune system cells that identify and attack cancer cells. They bind to cereblon and activate cereblon E3 ligase complex activity, resulting in the rapid ubiquitination and degradation of two specific B cell transcription factors: family zinc finger proteins Ikaros (IKZF 1) and Aiolos (IKZF3). IMiDs may cause direct cytotoxicity by inducing free radical mediated DNA damage. They also have antiangiogenic, immunomodulatory, and tumor necrosis factor alpha inhibitory properties [139].

The use of IMiDs in the treatment of MM stems from the "marked and durable responses" of thalidomide in a phase II study of 84 RRMM patients, eventually leading, in 2006, to its approval by the FDA for the disease when combined with dexamethasone. That same year also saw the approval of lenalidomide, a close derivative of thalidomide, for its use in RRMM, always in combination with dexamethasone. In 2015, the use of lenalidomide was extended to patients with newly diagnosed MM [117].

Pomalidomide, a third member of this IMiD group, received approval in 2015 for use in RRMM patients, whose disease had relapsed after > 2 previous treatments, including lenalidomide/bortezomib [117]. Other compounds have demonstrated sufficient efficacy in preclinical models, to warrant success in humans. Among these, avadomide (CC-122) [153], which is under investigation in a phase I study of patients with advanced solid tumors and non-Hodgkin lymphoma and MM, and CC-220 [154], currently tested in combination with dexamethasone in a phase I study in RRMM.

1.7.4 Alkylating Agents

The alkylating agent, able to induce irreversible DNA damage and apoptosis in myeloma cells, often combined with corticosteroids, remained the standard therapy for MM until the introduction of bortezomib and the IMiDs thalidomide and lenalidomide early in the 21st century. Recently, interest has been renewed in the discovery of new alkylating agents for MM treatment. Most of this attention has focused on bendamustine, currently licensed in Europe for MM. The National Cancer Institute's ClinicalTrials.gov website listed 34 studies involving bendamustine in various combinations for myeloma patients, although none of these investigations has progressed beyond phase II [155].

Tinostamustine, a fusion molecule that combines the molecular features of bendamustine and the HDAC inhibitor vorinostat, was reported to display good activity in preclinical studies of myeloma patient cells. This agent now is in a phase I trial of patients with lymphoma and myeloma previously shown to be refractory to treatment [117]. Melflufen or melphalan-flufenamide showed a clinical benefit rate of 62% MM patients, although hematologic toxicity was common [117, 156].

PT-112, a platinum-based compound under development, is the subject of three clinical trials, including a phase I/II dose-determining study in RRMM patients [117].

1.7.5 Histone deacetylase inhibitors (DACIs)

Histone deacetylases (HDACs) remove acetyl groups from lysine residues of, not only core histones, but also of non-histone proteins, such as tubulin, p53, NF-kB, STAT3, and HSP90, leading to faulty gene expression and aberrant cellular signaling [117]. Recently, Imai et al [157] reviewed the mechanisms of action of HDAC inhibitors in several hematologic cancers, including MM. HDAC inhibition, especially combined with proteasome inhibition, results in synergistic blockade of disposal of several pro-apoptotic proteins, altering the balance between pro- and anti-apoptotic proteins to favor cytotoxicity. Although HDAC inhibitors have demonstrated anti-myeloma activity as single agents in preclinical studies, their use in RRMM clinical trials generally has been disappointing [117], prompting their evaluation in combination with other drugs, mostly proteasome inhibitors. The pan-HDAC inhibitors panobinostat and vorinostat, which target more than one class of HDAC, have been the most widely studied in this context and used, in combination with bortezomib and dexamethasone, in clinical trials [158].

Panobinostat is associated with a warning regarding the drug increased risk of potentially fatal cardiac toxicity (ischemia, arrhythmias, ST-segment depression, and T-wave abnormalities) and severe diarrhea [159].

Vorinostat and belinostat (other pan-HDAC inhibitors, approved by the FDA for T-cell lymphomas), did not reveal a statistically significant therapeutic benefit in myeloma-based clinical trials. Thus, they are no longer considered valuable candidates for further investigations in MM [160].

1.7.6 HSP inhibitors

The heat shock proteins (HSPs) are a large group of highly conserved ATP-dependent molecular chaperones best known for their critical role in support of proper protein folding. Several evidences link the upregulation of HSPs with development of several different cancers, including MM [161]. Moreover, activation of the heat shock response is believed to be a major mechanism by which myeloma cells develop resistance to bortezomib [117]. However, the major HSP inhibitors developed as potential anticancer agents, primarily targeting the ATP-binding region of HSP90, showed modest clinical benefits and were often accompanied by unacceptable toxicity [117, 161]. Among the HSP90 inhibitors included in MM trials, usually in combination with bortezomib and/or a corticosteroid, the geldanamycin derivatives, tanespimycin, retaspimycin and luminespib have been employed. Only one trial reached phase III for MM before the drug sponsor (Bristol-Myers Squibb) reportedly terminated all further development [117].

HSF1 (heat shock transcription factor 1), an important regulator of the heat shock response in myeloma cells [162] has also been proposed as a potential target in MM. Although a number of HSF1 inhibitors have been the subject of preclinical studies of

MM, all have been lacking in specificity, and none has been advanced to clinical studies of patients [117].

1.7.7. Other therapeutic approaches and perspectives

Currently, a series of others small molecules have taken their place in the armamentarium of clinically beneficial anti-myeloma drugs, such as Poly(ADP-ribose) Polymerase Inhibitors [163], MDM2- Inhibitors [164], Kinesin Spindle Protein-Inhibitors (KPS) [165], exportin and Kinase-Inhibitors [166] and Apoptosis Inducers (like Bcl-2, IAP, and Mcl-1 Inhibitors) [167].

The clinical studies for these new molecules are still ongoing. However, a few side effects have already been reported for some of them. Filanesib, among the commonly used KPS molecules, exhibits thrombocytopenia, anemia, neutropenia, and fatigue [168].

The phase I trial of oral veliparib, the first PARP-inhibitor tested against MM [169] and bortezomib for pretreated RRMM patients indicated that the combination is well-tolerated with evidence of significant anti-myeloma activity reported [170]. However, a 2017 report from the drug sponsor (AbbVie) which failed to meet the primary endpoints in 2 phase III trials of veliparib in non-small-cell lung cancer and triple-negative breast cancer, has cast a shadow over the future viability of this PARP inhibitor for these and other cancers, including MM [117].

1.8 Folic acid-conjugated mesoporous silica-based nanosystem as a vehicle for targeted therapy in MM: the FOL-MSN-BTZ prototype.

Despite the great progress made in the management of MM during the last 20 years, the search for a cure has remained elusive. In fact, although, in most cases, these therapeutic advances have been able to switch from a rapidly fatal outcome of the disease to a chronic condition, this optimism has been often mitigated by disease recurrence, since resistance is commonly observed even after a successful response to therapy. Therefore, the development of novel therapeutic options aimed not only at extending patients' survival, but also at improving their quality of life are still needed.

In this context, the highly innovative multifunctional mesoporous silica nanoparticles (MSNs) technology might represent a potential drug delivery platform to be exploited in the treatment of multiple myeloma.

It is important to underline that this represents the first application of MSNs as DDS for the treatment of myeloma. Nor MSNs have ever been used to treat any other kind of cancer before.

So far, tumor-targeting inorganic (silica) nanoparticles have only been employed in an early phase I study (NCT02106598) as promising cancer-imaging probes that might serve as intraoperative visualization tools for an accurate and specific identification of lymph node metastases utilizing image-guided operative sentinel lymph node (SLN) mapping approaches [171, 172].

The MSU-type mesoporous silica functionalized with folic acid (FOL) and loaded with the proteasome inhibitor BTZ (referred as FOL-MSN-BTZ (EP 2001514B1), used in this study have been developed by NanoSiliCal Devices Srl, an innovative SME and spin-off

of the University of Calabria, where I spent the first 18 months of internship during my doctoral course.

These nanoparticles were synthetized modifying an interfacial synthesis procedure carried out at room temperature (RT), introducing cyclohexane as the organic phase in which the silicon source tetraethoxysilane (TEOS) is dissolved. This was aimed to limit mesoporous silica particles size, an essential parameter in drug targeting applications. The as-synthetized materials were functionalized on the external surface with the targeting ligand folic acid (see section 1.3) by amide bond formation, while the inner pore surface hosts the drug BTZ by means of a pH-sensitive bond.

More details and complete authoritative reviews may be found in the following manuscripts L. Pasqua et al. [173, 174], C. Morelli et al. [19] and patent (granted in EU and several other countries worldwide, including USA, Canada, Australia, China and Russia) *EP 2001514B1* "*Preparation of micro or nano-systems based on inorganic oxides with controlled porosity for carrying biologically active or activable substances*" (owned by NanoSiliCal Devices).

Figure 4 shows the Transmission Electron Microscopy (TEM) micrographs (panel a and c) of MSN-FOL material that exhibits a porous texture in adherence with materials of the MSU family, while Scanning Electron Microscopy (SEM) images (panels b and d) show that this synthesis procedure yields nanoscaled particles without a regular morphology appearing as aggregates of up to 500 nm.

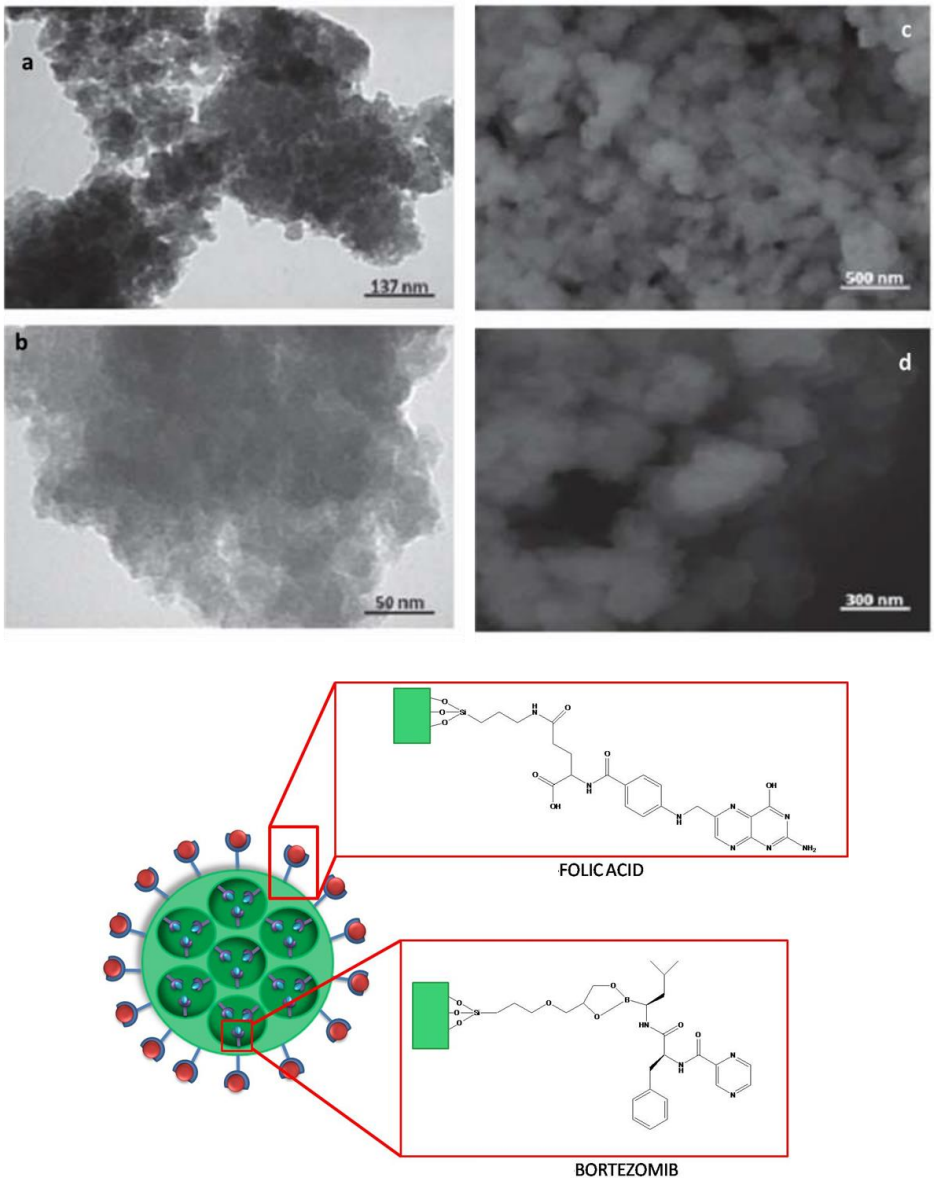

***Figure 4**: TEM (a, c) and SEM (b, d) micrograph of FOL-MSN. A representative scheme of FOL-MSN-BTZ prototype developed by NanoSiliCal Devices is given (lower panel).*

Such a conceived device should preferentially deliver the drug to FOL-expressing target tissues, preserving the cargo from premature leakage and metabolism thus avoiding unwanted side effects (Fig. 5).

In fact, the described pH-tunable system is expected to work efficiently at the low pH of tumor microenvironment, since the enhanced glycolytic rate of cancer cells causes an increase of intracellular lactic acid, which, in turn, contributes to lower the pH.

Summing up, we expect that the as conceived DDS could work as schematically illustrated in Fig 5.

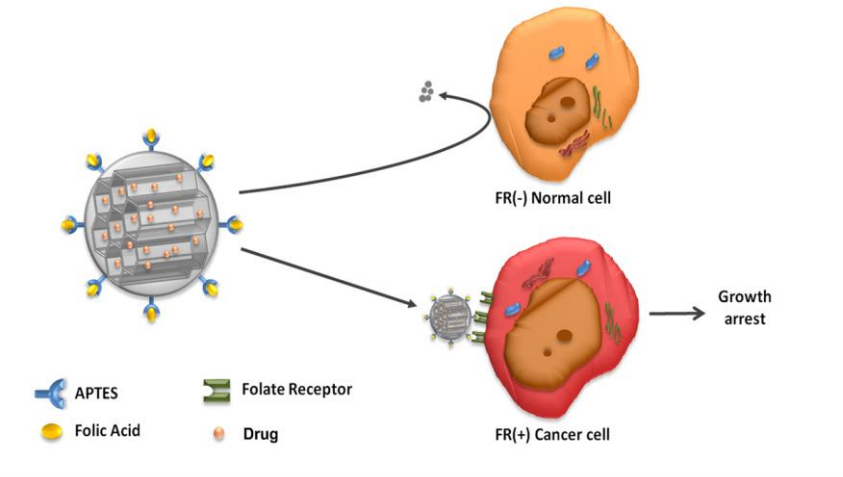

Figure 5*: Representation of mechanism of action of FOL-MSN-BTZ developed by NanoSiliCal Device.*

Furthermore, it is very important to emphasize that, due to their unique framework, MSNs offer a bifunctional surface, internal and external, making them a highly versatile tool, able to host even multiple target molecules on the same particle.

AIM OF THE STUDY

The goal of my PhD research project was to evaluate *in vitro* and *in vivo* the behavior and the effectiveness of the above described FOL-MSN-BTZ, as a multimodal nanovehicle for targeted drug delivery in MM.

MSNs cellular uptake as well as biocompatibility and efficacy of FOL-MSN-BTZ and vehicle alone (MSN-FOL) were first investigated on tumor and normal cell models, expressing or not FR, respectively. In fact, since a previous report by Morelli C. *et al.* [19] showed that the FOL grafted MSNs (MSN-FOL), tested here as controls, do not enter cells unless opportunely functionalized, and that a highly specific, receptor mediated, cellular internalization of MSN-FOL occurs exclusively in FR expressing cells [175] a behavior as that depicted in Figure 4 was expected.

Concomitant metabolic analyses in cells treated with FOL-MSN-BTZ or BTZ alone or MSN-FOL were performed to assess if different metabolic pathways are affected in response to each treatment.

In the last part of project, we validate the *in vitro* results and to evaluate MSNs efficacy but also potential toxicity, a xenograft mice model deriving from implanted MM cell line overexpressing FRβ (RPMI-8226), was developed, giving crucial information that are mandatory to plan the future use of this strategy in a clinical setting.

Finally, as a future perspective, we're developing a new prototype for BTZ delivery towards CD-38 overexpressing MM cells, since this antigen has become one of the main attractive targets for MM due to its high surface density on plasmacells membranes which led to the development of anti-CD38 monoclonal antibodies (mAbs) [149, 176], as above described (see section 1.7.2.1).

Preliminary data obtained on this new prototype will be discussed in the last section (2.8) of "*Results and discussion*."

2 RESULTS AND DISCUSSION

2.1 MSNs uptake selectively occurs in FR expressing tumor cells, affecting their viability

The effect of MSNs on cell proliferation was evaluated on different FR+ and FR- cell lines (Fig. 6-A) [19] including the human FRα-/FRβ+ MM cells lines, RPMI-8226 and U266B-1, being BTZ the treatment of choice for this type of cancer.

First of all, three different synthetic products of FOL-MSN-BTZ, bearing increasing amounts of FOL on the external surface (FOL content: 2880 < 2930 < 2938), were tested. These samples were obtained by gradually increasing folic acid amounts in the synthesis mixtures, as well as prolonging the reaction times. An approximate estimation of FOL content was obtained by means of Thermal Gravimetric Analysis, TGA, which revealed 2.6% (samples 2880), 3.3% (sample 2931) and 4.1% (sample 2938). Interestingly, the specificity towards FR+ cells increased proportionally to the increase of the content of FOL on MSNs. Therefore, while 2880 (low FOL) did not show any relevant selectivity for FR+ RPMI-8226 compared to FR- normal BJhTERT cells and exerted similar toxicities on both cell lines, the 2930 product (medium FOL) and 2938 product (high FOL) gradually showed increased selectivity towards FR+ RPMI-8226 cells. In particular, 2938 did not show any significant toxicity on FR- BJhTERT cells (Fig. 6-B). Furthermore, the vehicle alone (MSN-FOL: samples 2981/2931/2939) was always well tolerated, showing no evident toxicity on both normal and cancer cells.

Probably, the saturation of external surface of MSNs with folic acid should allow preserve the drug binding to the inner pores from extracellular pH fluctuations, keeping it stable during its way towards to target cell. This means that folic acid concentration affects MSNs selectivity, since the increasing of FOL amount make the vehicle more selective.

Then, selected particles grafted with the higher amount of folic acid (products 2938 for FOL-MSN-BTZ and 2939, i.e. the corresponding MSN-FOL,) were tested in proliferation assays (Fig. 7) on different FR+ (A-C) and FR- (D-F) cell lines and in all the following experiments, due to their high cell-specificity.

The choice of testing FOL-MSN-BTZ also in non-MM cell models was made just in order to verify the selectivity of our FOL-targeted prototype towards any kind of FR-expressing cells (e.g. HeLa) but not towards FR negative cells (e.g. BJhTERT, 3T3L1, HEK293). Strikingly, FOL-MSN-BTZ was able to induce death or inhibit proliferation in all FR+ tumor cells, but not in FR- normal cells, while free BTZ resulted toxic for all cell lines tested, independently on their FR expression.

These results fit very well with our TEM observations on RPMI-8226 and BJhTERT cells treated with FOL-MSN-BTZ (2938), which showed how MSNs uptake occurs in FR+ RPMI-8226 only and not in FR- BJhTERT cells, where they remain confined in the intercellular spaces (Fig. 8-A). Immunogold labelling experiments on RPMI confirmed that the recognition of MSN-FOL depends on FR, as it clearly shows Fig. 8-B, where the two representative images nicely depict the whole FR-mediated endocytic process, from the FR recognition at the cell membrane (left panel) to the sequestration in FR-immunopositive intracellular vesicles.

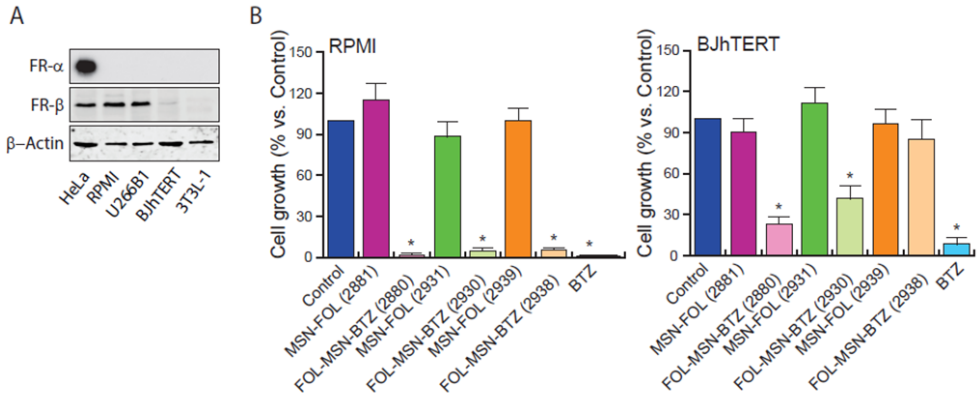

Figure 6: (A) *Protein expression of FR-α and FR-β in different cell lines. 50 µg of non-denatured proteins (for FR-α detection) and denatured proteins (for FR-β detection) from total lysates were loaded and subjected to WB analysis. B-actin was used as loading control.* ***(B)*** *Normal FR- BJhTERT cells and cancerous FR+ RPMI cells were left untreated or treated for 1h with MSN-FOL or FOL-MSN-BTZ deriving from different synthesis whose folic acid content is gradually increased (2881/2880<2931/2930 <2939/2938), comparing to the 1 hour of free BTZ treatment. Viability was determined after 3 days. Representative images of three independent experiments are shown. * $p \leq 0.05$ vs control.*

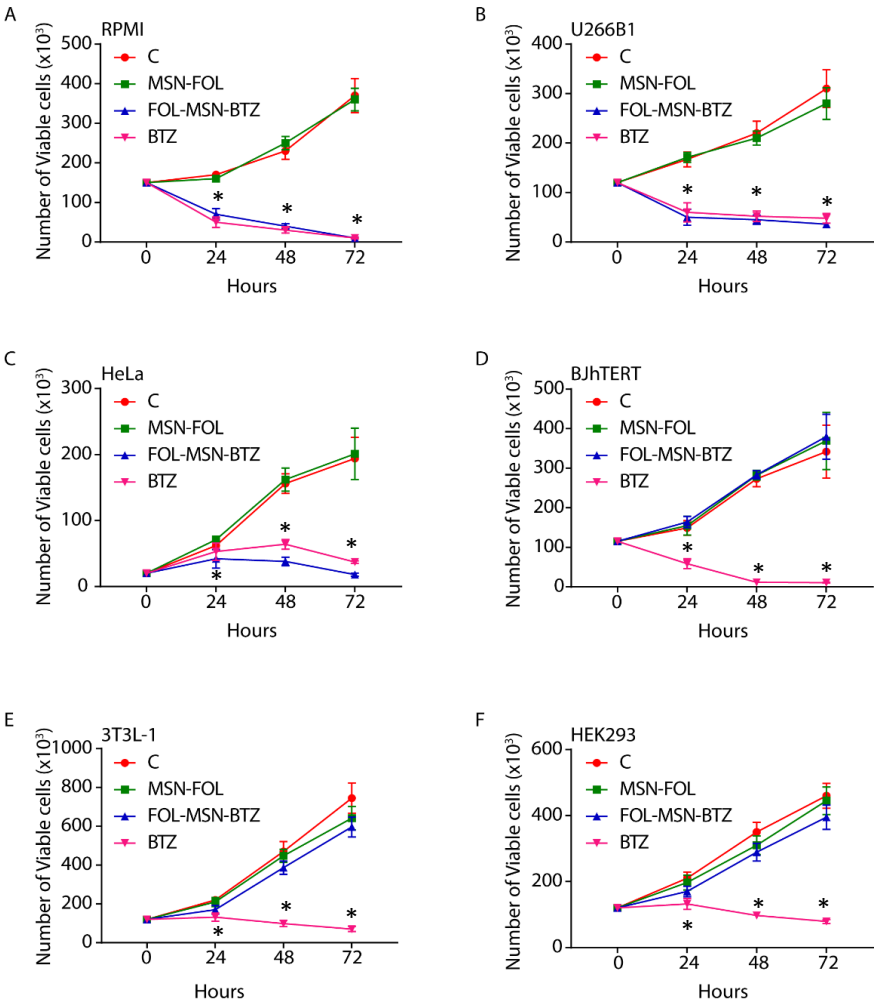

Figure 7: *FOL-MSN-BTZ induces death in FR+ cancer cells (A-C) but not in FR- normal cells (D-F). Cells were treated for 1h with FOL-MSN-BTZ (2938) or left untreated (C=control). MSN-FOL (2939) was used as negative control and the free drug BTZ as positive control. Cell viability has been evaluated after 24, 48 and 72h after treatment. Values represent the mean of three triplicate independent experiments. (*) $p < 0.05$ vs control.*

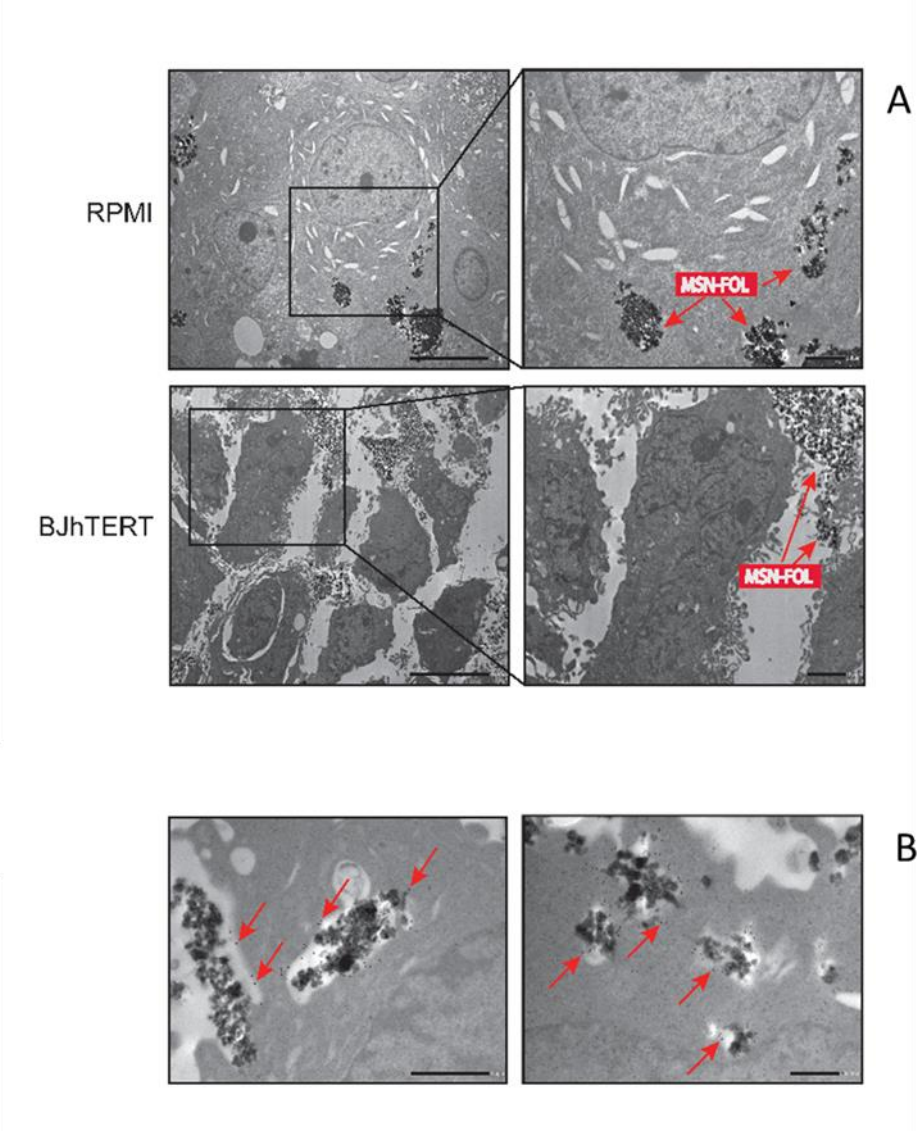

***Figure 8**: (A) TEM investigation on cancerous RPMI and normal BJhTERT cells after 1h treatment with FOL-MSN-BTZ (2938). Nanoparticles (arrows) enter FR+ RPMI only and not enter FR- BJhTERT cells. Scale bars 10 μm, x1200 magnification (left panels); scale bars 2 μm, x3000 magnification (right panels). (B) Colloidal-gold immunocytochemistry for FR (black dots indicated by arrows) in RPMI cells exposed to MSN-FOL for 1h. Scale bars 1 μm, x12.000 magnification (left panel); scale bars 500 nm, x15.000 magnification (right panel).*

2.2 Drug loaded MSNs selectively kill multiple myeloma cells but not normal cells: comparison with the free drug.

BTZ anticancer activity occurs through multiple mechanisms. Proteasome inhibition increases the levels of pro-apoptotic proteins and decreases several anti-apoptotic proteins, triggering both the intrinsic (mitochondrial Cyt c release and Cas-9 activation) and the extrinsic (Fas/Cas-8-dependent) apoptotic pathways in malignant cells [128]. Moreover, recent evidences report that the main mechanism of BTZ-induced cell death involves the accumulation of misfolded and functional proteins (including pro-apoptotic factors), normally degraded by the proteasome, and of reactive oxygen species (ROS) in the endoplasmic reticulum (ER), leading to ER stress and DNA damage induced apoptosis [108, 128].

Therefore, in order to assess if MSN-bound BTZ and BTZ trigger the same apoptosis pathways, cell death analysis was conducted on MM and normal cells. Indeed, (Fig. 9) shows that both FOL-MSN-BTZ and free BTZ lead to comparable apoptotic rates in FR+ MM RPMI treated cells (Fig. 9, upper panels), while negligible apoptosis was detected in FR- normal BJhTERT cells exposed to FOL-MSN-BTZ, confirming the striking specificity of MSN-bound BTZ towards tumor cells if compared to free BTZ (Fig. 9, lower panels). TEM observations gave similar results.

In Fig. 10 (upper panels), the red arrows indicate apoptotic cells (characterized by intact plasma membrane and condensed cytoplasm and chromatin) in RPMI treated with both FOL-MSN-BTZ and free BTZ. Accordingly, the molecular profile, showing the cleavage of caspases and PARP-1 (Fig. 11-A), an endogenous substrate of activated Cas-3 [177], as well as the Cyt c translocation from the mitochondria to the cytoplasm (Fig. 11-C), confirms the concomitant activation of the extrinsic (Cas-8 dependent) and the intrinsic

(Cas-9 dependent) apoptosis pathway observed in BTZ treated MM cells [178], also in FOL-MSN-BTZ treated cells. As expected, FOL-MSN-BTZ did not cause any injury to FR- BJhTERT cells, while BTZ seems to trigger a partanathos process, characterized by biochemical events of rapid activation of PARP-1, synthesis and accumulation of PAR polymer, mitochondrial depolarization, nuclear AIF translocation (which occurs early) and, perhaps at the late stage, caspase activation, although caspase activation is not obligatory (Fig.11-B, lower panels) [179]. However, the molecular analysis of BTZ treated samples did not reveal any of the classical apoptotic features (Fig. 11-B,D) while the absence of active (cleaved) caspases, a cleaved PARP-1, an up-regulated Receptor-Interacting Protein 1 (RIP1) kinase and DNA fragmentation (Fig.11-A) are consistent with a necroptosis signaling [180] or with the PARP-mediated programmed necrosis (parthanatos) [181, 182].

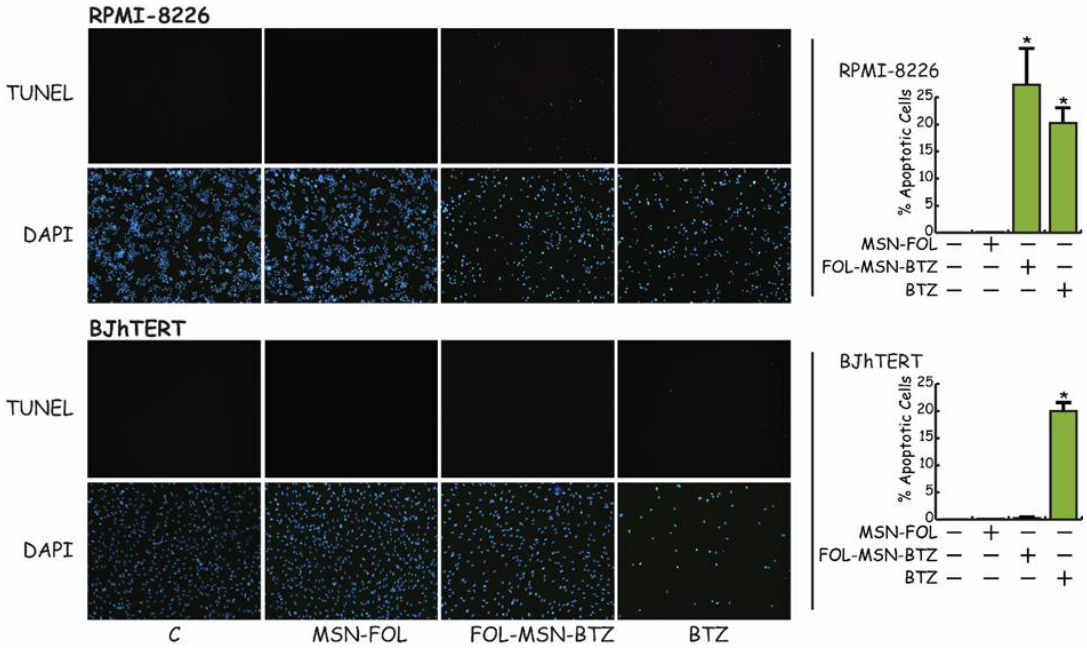

Figure 9: *BTZ is not toxic to normal cells when bound to targeted MSNs. RPMI and BJhTERT were treated or not (control) with MSN-FOL (2939), FOL-MSN-BTZ (2938) and free BTZ for 1h and processed for TUNEL assay after 36h. Nuclei were counterstained with DAPI. Cells were photographed at 10x magnification, and apoptotic cells from triplicate experiments were counted using Image J software (see graphs on the right). (*) $p < 0.05$ vs control.*

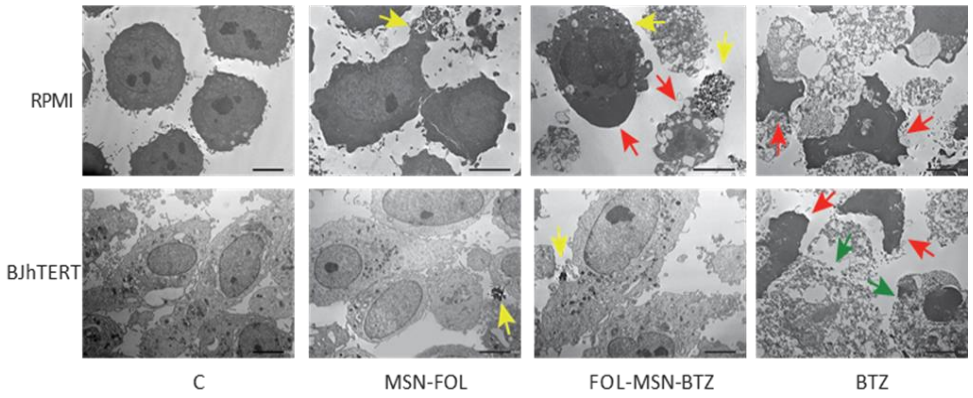

Figure 10: *A duplicate set of cells was processed for TEM analysis (see Materials and Methods). Red arrows: apoptotic cells; green arrows: parthanatotic cells; yellow arrows: MSNs. Scale bars 5 μm, x 2000 magnification.*

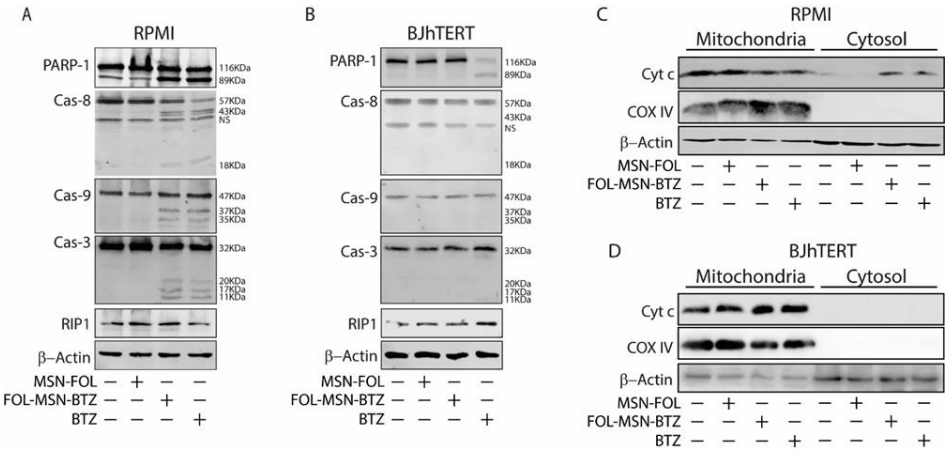

Figure 11: *A third set of both cell lines were treated as in (A) and (B) and total proteins (C and D) or, for cytochrome C localization, cytosolic and mitochondrial fractions (E and F) were extracted and subjected to WB analysis to assess the expression of the indicated apoptotic markers. β-Actin was used as loading control; COX IV: mitochondrial marker to assess fractionation quality. NS: Non-Specific bands.*

2.3 Effects of MSN-FOL vs FOL-MSN-BTZ on the cellular energetic pathways and mitochondrial function.

Energy pathways are highly sensitive to exposure to toxic agents, affecting several intracellular biochemical processes (glycolysis, Krebs cycle, electron transport and OXPHOS), resulting in the abnormal production of ATP and the release of heat and chemical byproducts into the extracellular environment [183]. In unfavorable conditions cancer cells can shift their metabolism dynamically between glycolysis and oxidative phosphorylation, rapidly adapting to the modifications occurring in their environment to survive, showing a kind of "metabolic flexibility" [184].

In order to characterize the metabolic effects of MSNs treatment and to obtain a detailed biochemical identification of tissue damage, FR+ and FR- cell lines were treated with equal amounts of MSN-FOL and FOL-MSN-BTZ, as described in *Materials and Methods*. Thus, the effects of MSN-FOL and FOL-MSN-BTZ on glycolysis and mitochondrial respiration were respectively detected through real-time measurements in Extracellular Acidification Rate (ECAR) and in Oxygen Consumption Rate (OCR), by the Seahorse Extracellular Flux (XFe96) Analyzer that, simultaneously, evaluates the two major energy producing cellular pathways.

Our results show that in FR+ RPMI-8226 cancer cells, FOL-MSN-BTZ significantly reduce both mitochondrial respiration and glycolytic metabolism as it occurs in free BTZ treated samples (Fig. 12 A-D).

The significant reduction of the key parameters of cellular respiration, (i.e. basal respiration, maximal respiration and spare respiratory capacity) induced by both free BTZ and FOL-MSN-BTZ (Fig. 12-B), confirms that BTZ exerts its cytotoxicity through a mitochondrial dysfunction [128, 185]. The obtained OCR trend is very similar to that

reported in literature for multiple myeloma cells revealing a trend that might be peculiar of this kind of cells [186, 187].

At the same time, MSN-bound BTZ and BTZ treatment promote an overall lowering of glycolytic flux with a significant reduction in glycolysis process.

The impairment in glycolysis and the OXPHOS-driven respiratory deficit, fit well with the apoptotic phenotype triggered by MSN-loaded BTZ and BTZ in FR+ RPMI cancer cells (see *section 2.2*). Collectively, these results describe the metabolic phenotype of BTZ-induced apoptotic cells and that underpins BIPN, since the latter is characterized by a number of physiologic alterations of mitochondria (like membrane potential and membrane transition pore alterations) leading to mitochondrial dysfunction [185].

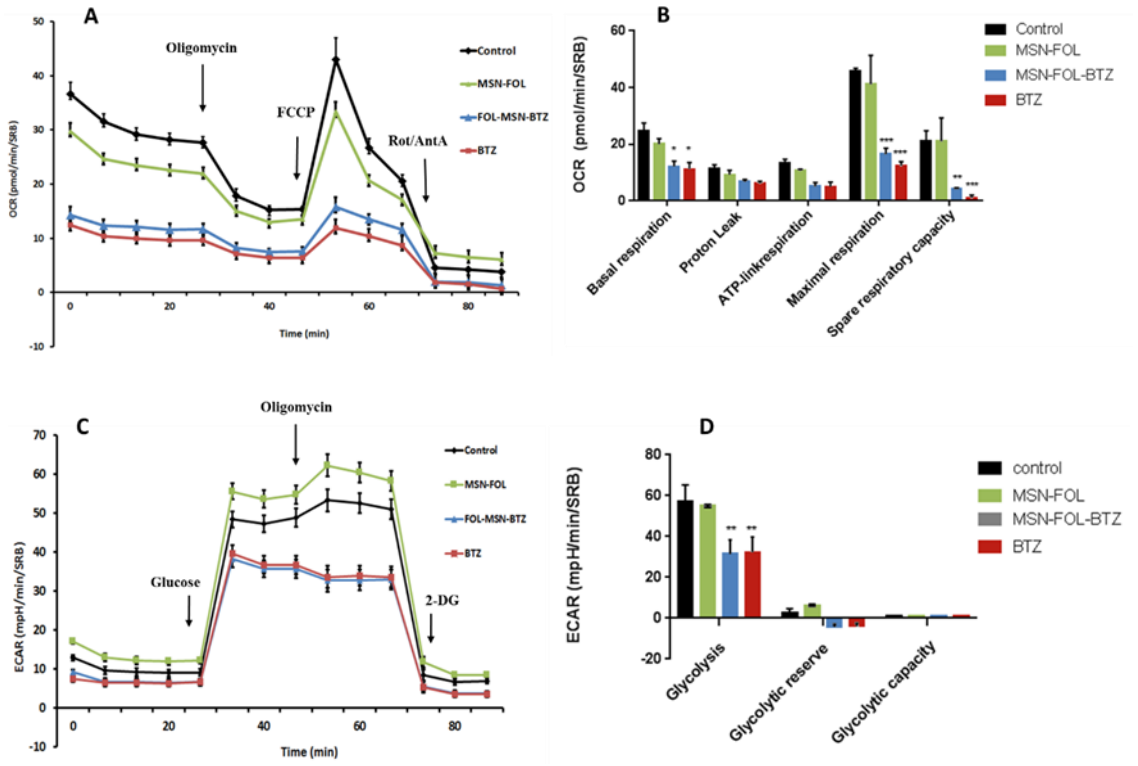

Figure 12: *The metabolic profile of RPMI-8226 cancer cell, treated for 1h with FOL-MSN-BTZ, MSN-FOL and BTZ (as positive control) or left untreated (Control), was assessed 18h after MSNs treatment using the Seahorse XF-e96 analyzer. (A) Representative tracing of mitochondrial respiration flux; specific perturbations were serially injected at 30 min (oligomycine), 50 min (FCCP) and 70 min (mix of rotenone and antimycin A) (B). Graphic representation of the basal respiration, maximal respiration, and spare*

respiratory capacity (right panel); modulators were serially injected at 30 min (glucose), 50 min (oligomycin) and 70 min (2-DG). (C) A schematic tracing of metabolic flux and a graphic representation of Glycolysis, Glycolytic reserve and Glycolytic capacity (D). Data shown are the mean ± SEM of 3 independent experiments performed in sixtuplicate and normalized by protein content (SRB). (*) p < 0.05; (**) p < 0.01; (***) p < 0.001 vs control (ANOVA TEST).

Conversely, in FR- normal BJhTERT cells (Fig. 13 A-D), only the free drug significantly abolishes mitochondrial respiration, affecting the basal respiration, ATP-link respiration, maximal respiration and the spare respiratory capacity. Surprisingly, FOL-MSN and FOL-MSN-BTZ seem to favor cell respiration increasing the maximal respiration and spare respiratory capacity respect to the control (Fig. 13-B).

It is important to underline that, in normal cells, mitotoxicity disappears when BTZ is loaded into MSNs. Indeed, the shooting down of the main parameters of mitochondrial respiration triggered by free BTZ are avoided when it is bound to MSNs.

ECAR flux (Fig. 13-C) suggests that the cells tend to shift to a more glycolytic phenotype, but no significant variations in glycolytic pathway parameters were detected after 18h of treatment with tested samples (Fig. 13-D). Noteworthy, in both cell lines, FOL-MSN alone did not show any significant effect on both processes, confirming that the vehicle itself does not affect cell metabolism.

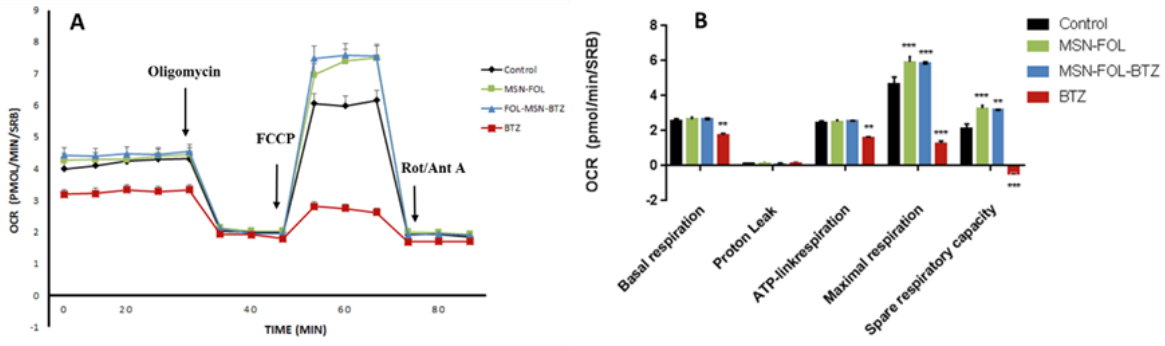

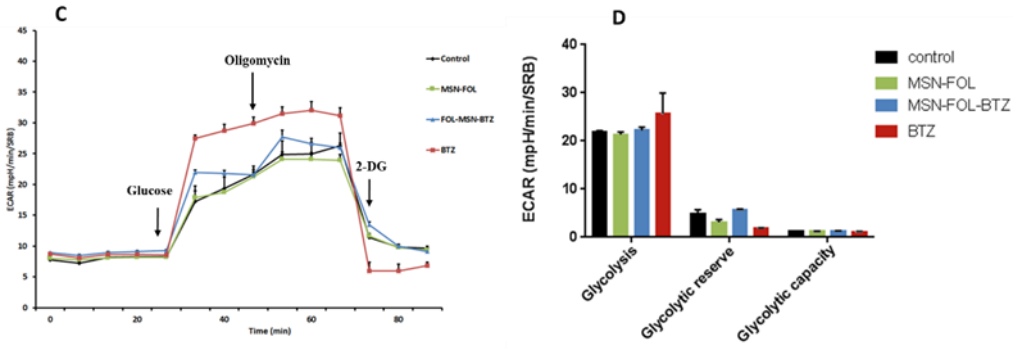

***Figure 13**: The metabolic profile of BJhTERT normal cells treated for 1h with FOL-MSN-BTZ, MSN-FOL and BTZ (as positive control) or left untreated (Control), was assessed 18h after MSNs treatment using the Seahorse XF-e96 analyzer. The modulators were serially injected at 30 min (oligomycine), 50 min (FCCP) and 70 min (mix of rotenone and antimycin A) for OCR measurement; glucose (30 min), oligomycin (50min) and 2-DG (70 min) for ECAR measurement. (A) Representative tracing of mitochondrial respiration flux and representative graph of basal respiration, proton leak, maximal respiration, ATP levels and spare respiratory capacity(B). A schematic tracing of glycolytic flux (Cl), and graphic representation of glycolytic parameters (Dl). Data shown are the mean ± SEM of 3 independent experiments performed in sixtuplicate and normalized by protein content (SRB). (*) $p < 0.05$; (**) $p < 0.01$; (***) $p < 0.001$ vs control (ANOVA).*

2.4 Reactive Oxygen Species (ROS) impact on anti-tumor activity of BTZ

As above mentioned, proteasome inhibition causes the accumulation of unfolded proteins, which trigger endoplasmic reticulum (ER) stress. The unresolved BTZ-induced ER stress has been shown to cause cell death via multiple pathways including overproduction of reactive oxygen species (ROS), becoming the major mediator of the cytotoxicity of BTZ [188].

Moreover, it is well known that a significant contribute to cellular ROS levels is provided by cell energy metabolism, since superoxide anion (O2·) represent the main byproduct of cellular respiration, generated by the incomplete reduction of O2 in the electron transport chain (ETC) [189]. An impairment of cellular respiration, concomitant with the mitochondrial accumulation of ubiquitinated proteins, occurs after proteasome inhibition, and this metabolic alteration is responsible for an increase in mitochondrial ROS production at ETC level [190].

ROS produced as a byproduct of protein folding contribute only partially to the generation of oxidative stress during ER stress [191]. Systems involved in calcium homeostasis make up another important component of ROS generation. Thus, oxidative stress can be mediated by Ca^{2+} leakage from the ER into the cytosol [188, 192]. Ca^{2+} leakage from the ER also results in cytochrome c release from the mitochondria impairing the electron transport system and resulting in altered mitochondrial membrane potential, and as result, production of ROS (Fig. 14). Therefore, calcium dysregulation and ROS production synergically take part in the BTZ-induced apoptosis cascade and are involved in degeneration mechanisms of primary sensory neurons and intraepidermal nerve fibers that are responsible of BTZ-associated chronic peripheral neuropathy [128].

In this context, a ROS detection assay was performed in order to assess if the MSN-loaded BTZ exerts a stronger or comparable impact on their production, respect to the free drug, in tumor cells. In the same time, it was important to understand whether the MSNs themselves affect cellular oxidative stress or not.

The analysis, performed on MM and normal cells, show that both FOL-MSN-BTZ and free BTZ lead to a comparable ROS production rate in FR+ RPMI-8226 treated cells, while marked ROS species induction in FR- normal BJhTERT cells was detected only under treatment with free BTZ, confirming the striking specificity of MSN-bound BTZ towards tumor cells and the safety of mesoporous silica vehicle. In fact, MSN-FOL does not trigger ROS production in any of the two cell lines tested (Fig. 14).

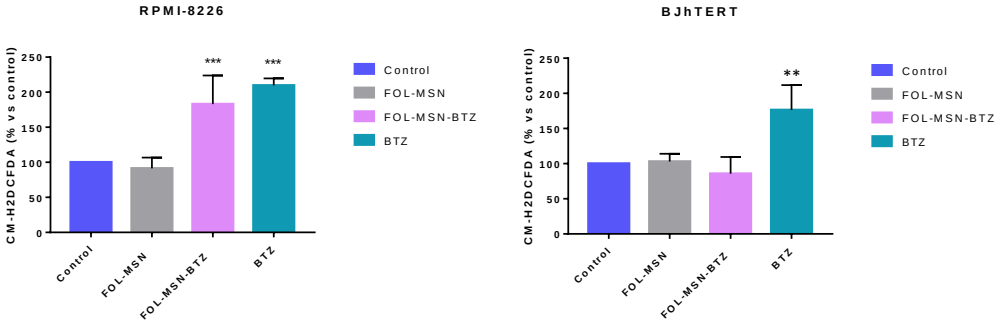

Figure 14: *Intracellular ROS levels revealed in FR+ RPMI-8226 cancer cells and FR- BJhTERT normal cells after treatment with MSN-FOL (negative control), FOL-MSN-BTZ and free BTZ (positive control). Untreated cells were used as negative control. Values represent the mean of three triplicate independent experiments. Data are shown as probe fluorescence normalized on viable cells number and expressed as percentage vs negative control. ***P < 0.001, **P < 0.01 vs control (t test).*

These results corroborate the evidences assuming the ROS involvement in the initiation of BTZ-associated apoptotic signaling, since an increase in generation of ROS induces cytochrome c release from mitochondria with consequent caspases activation [193, 194].

2.5 In vivo behaviour of MSN-based nano-DDS for target therapy: an intriguing debate in nanomedicine field.

The *in vivo* behavior of MSN-based nano-DDSs is drawing increasing attention for MSNs clinical application perspectives and has become a current hot topic in MSNs biosafety research. The adjuvant effect of MSNs still requires deeper investigation and understanding before their use in a clinical setting.

According to literature, silica-based nanostructures have acceptable biocompatibility to utilize in biomedical applications: silica materials, classified by FDA as "Generally Recognized as Safe", is used as a food-additive and in cosmetics [195]. In general, silica particles are degraded into water-soluble orthosilicic acid (Si(OH)4) which is also

absorbed by humans to form silica as a trace element. Moreover, MSNs with a diameter of 50-300nm are generally not toxic at concentrations below 100 μg/ml [4, 37, 196].

Our *in vitro* results already confirmed that MSNs (vehicle alone) are not toxic against the various cell lines tested, while, in *vivo*, MSNs exhibit lower hemolytic effect compared to nonporous silica, due to the lower density of silanol groups on their surface by the existence of pores [103].

Indeed, the major pathway of toxicity associated with silica is due to its surface chemistry (silanol groups) which can interact with the membrane components leading to the lysis of the cells and consequently leaking of the cellular components [20, 197].

Nonetheless, evaluation of safety and toxicity of MSNs is an important issue that needs to be deepened at using MSNs in clinical applications.

Surface properties of MSNs have a great impact on the biodistribution and biocompatibility of MSNs. For an instance, modification of the surface features through functionalization with PEG helps the MSNs to escape from being degraded by liver, spleen and lung tissues due to the longer circulation time of PEG-MSNs [198].

Cong *et al.*, reported the impact of pore size, shape and surface features of silica nanoparticles on the cellular toxicity [199].

The morphology of MSNs influences the biocompatibility, biodistribution, and clearance, as well as the shape, affecting cellular uptake, has been a major recent research concern [76, 103].

Any change in the micelle formation leads to a change in particles morphology. The large aspect ratio of MSNs can result in a more extended circulation time and therefore, different biocompatibility [200]. The degradation of orally administered MSNs depends on the shape and biological environment [2].

Controversy has arisen regarding the impact of particle size on the biocompatibility of MSNs. Particle size can manipulate biological factors such as *in vivo* distribution, blood-circulation time, and clearance [199]. With intravenous delivery, MSNs were found to be mainly distributed in the liver and spleen, with a minority of them in the lung, and a few in the kidney and heart. A longer blood circulation lifetime was observed for particles with smaller size [201].

Size of the nanoparticles also has a profound influence on the biodistribution and excretion of MSNs [20]. An increase in particle size led to an increase in its accumulation in the liver and spleen following intravenous administration. As well as the excretion of MSNs from urine increased by the elevation of particle size may affect the degradation rate and therefore biocompatibility [201].

Finally, despite the reported toxic effects of silica nanoparticles (SiNPs) on the immune system, the MSNs remain the safest choice among the various existing SiNPs as drug delivery tool [202], as it was reported for MSNs with extra-large pores (XL-MSNs; 30 nm pores) used *in vivo* for the delivery of macrophage-polarizing cytokines [203].

Therefore, once the uptake and cytotoxic activity of MSNs were studied and characterized *in vitro*, in the last phase of my PhD project, the safety and efficacy of our patented FOL-MSN-BTZ prototype were also investigated in animal models.

2.6 Evaluation of MSN-FOL and FOL-MSN-BTZ Maximum Tolerated Dose (MTD).

The maximum tolerated dose (MTD) for MSN- FOL and FOL-MSN-BTZ has been evaluated in healthy mice to assess the most efficacious concentration of our prototype to be employed in the subsequent *in vivo* efficacy study.

To this aim, female Balb/c mice were administered intravenously by the caudal vein once a week for 5 weeks (1qwx5) with MSN-FOL and FOL-MSN-BTZ at increasing concentrations corresponding to doses 1, 1.5, 2 and 3mg/kg of free BTZ. The MTD study showed an outstanding tolerability of MSN-FOL at all tested doses, throughout the treatment period (Fig. 15). In fact, MSN-FOL did not induce any significant reduction in body weight, nor other signs of general toxicity were observed in treated animals compared to controls.

Moreover, mice well tolerated MSN-FOL-BTZ administration at the doses of 1, 1.5 and 2 mg/kg, but did not tolerate the highest dose (3 mg/kg). For ethical reasons, the animals treated with the highest dose were sacrificed after the first administration.

For all the three tested concentration (1-1,5 and 2 mg/kg) there is not significant fluctuation in body weight in treated animals, compared to those untreated. Since MSN-FOL was tolerated up to concentration of 3mg/kg, we can conclude that the toxicity of FOL-MSN-BTZ 3 mg/kg is due to the activity of BTZ itself and not to the nature of the vehicle (MSN-FOL) (Fig. 15), confirming the *in vitro* data regarding the safety and biocompatibility on our vehicle.

This result leads to the first important conclusion: animals can tolerate a double dose of BTZ (2mg/kg) when the drug is delivered through the MSNs platform, if compared to the 1mg/kg of the free drug, which causes mice death (data not shown). This observation could fulfil one of the key aims of a good DDS, i.e. the improvement of therapeutic efficacy, by delivering the drug towards a specific tissue (e.g. the tumor site).

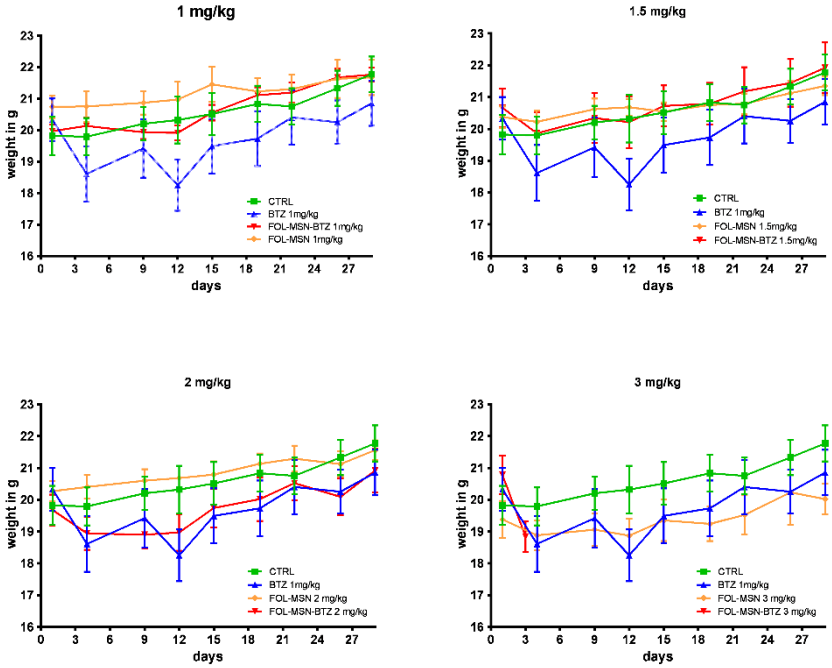

Figure 15: *Body weight gains of mice treated with increasing doses of MSN-FOL and FOL-MSN-BTZ and with 1mg/Kg free BTZ. Nanoparticles were administered intravenously once a week for 5 weeks. The results are expressed as mean ± SD and were statistically analyzed using the analysis of variance (ANOVA) and the Tukey-Kramer post-test (significance level set at $p<0.05$).*

2.6.1 Hematochemical evaluation

After 48h from the last administration, 5 mice/group were sacrificed and blood analyses for the hematochemical (Fig.15) and haematological parameters (Fig.16) have been performed, in order to investigate specific effects on hematologic components and evaluate the integrity of the main organs involved in body detoxification following MSNs treatment. The hepatic transaminases, alanine transaminase (ALT) or glutamate-pyruvate transaminase (GPT) and aspartate transaminase (AST) or glutamate-oxaloacetate transaminase (GOT) as predictors of liver injury were measured. The creatinine and urea measurement have been carried out to assess renal function, since, as previously reported, MSNs, once in the bloodstream, is rapidly converted by hydrolysis into water-soluble silicic acid (Si(OH)4), which, in turn, is safely excreted through the urines [11].

The FOL-MSN-BTZ 2mg/kg treated mice only reported a slight renal toxicity with a significant decrease in urea concentration compared to the untreated animals, likely due to BTZ rather than silica, since the FOL-MSN, at higher tested concentration (2mg/kg and 3mg/kg), conversely, seems to positively affect the renal activity. However, since the same parameters could not be determined in the urines, at present we cannot rule out the exact role of FOL-MSN-BTZ and the vehicle alone (MSN-FOL) on the renal function.

MSN-FOL-BTZ 2 mg/kg treated mice also showed a mild hepatic toxicity (increase in GPT/ALT concentration) compared to FOL-MSN 2mg/kg and FOL-MSN 3mg/kg treated mice, but not compared to control mice (untreated). This toxicity, although mild, could be referred to detoxification function of liver that filter xenobiotic materials, in this case the MSN-bond BTZ, since the vehicle alone did not affect hepatic function at any concentration tested (Fig. 16). Finally, FOL-MSN-BTZ 2mg/kg did not significantly alter GOT/AST values.

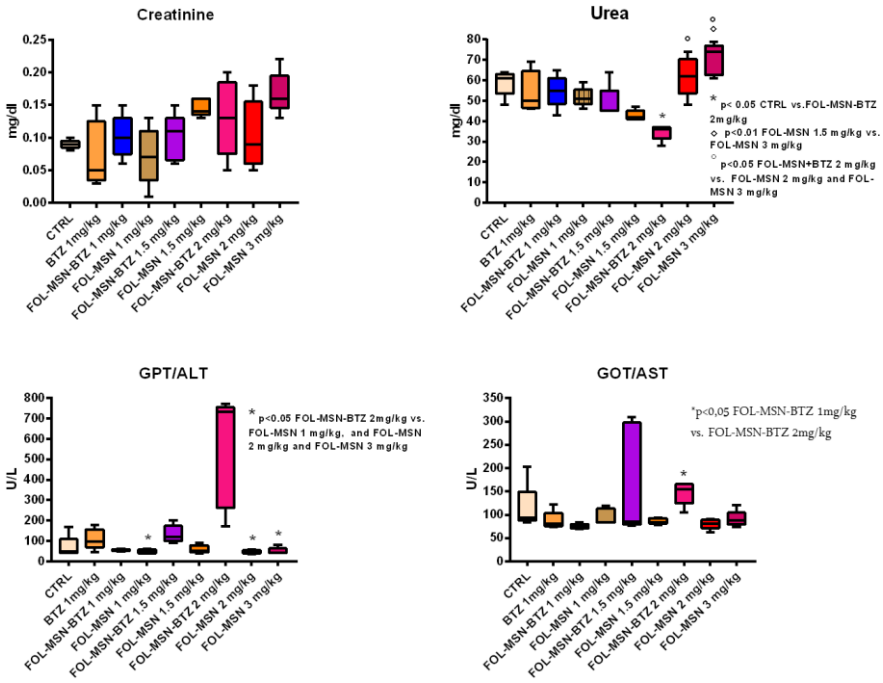

***Figure 16**: Assessment of hepatic and renal biochemical parameters at the end of treatment. ALT= Alanine transaminase or GPT= glutamate-pyruvate transaminase, AST= Aspartate transaminase or GOT=*

glutamate-oxaloacetate transaminase. The results were statistically analyzed using the analysis of variance (ANOVA) and the non-parametric Kruskal-Wallis statistic, Graphpad Prism (significance level set at $p<0.05$).

2.6.2 Hematological evaluation

No statistically significant differences were noticed between treated and not treated animals in haematological parameters, such as red blood cells (RBC), white blood cells (WBC), platelets (Plt), serum content of haemoglobin (Hgb) and haematocrit (Hct) (Fig. 17). The significant increase of mean corpuscular volume (MCV) was revealed in FOL-MSN-BTZ 2mg/kg treated mice respect to FOL-MSN 1mg/kg treated mice, thus these data are not comparable.

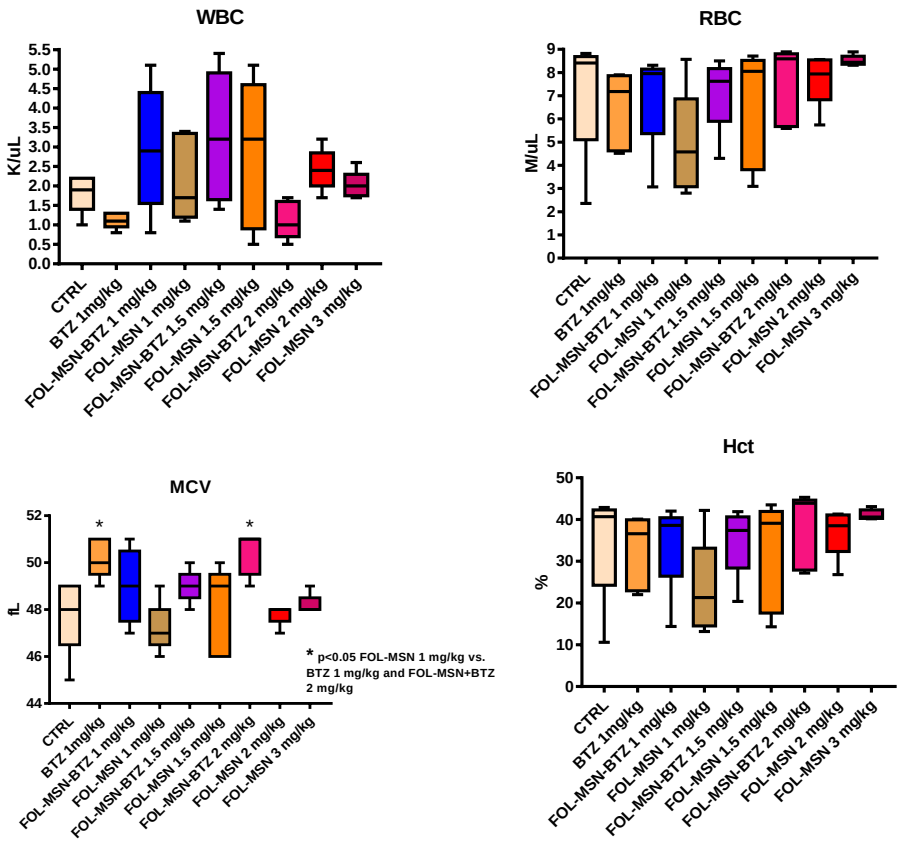

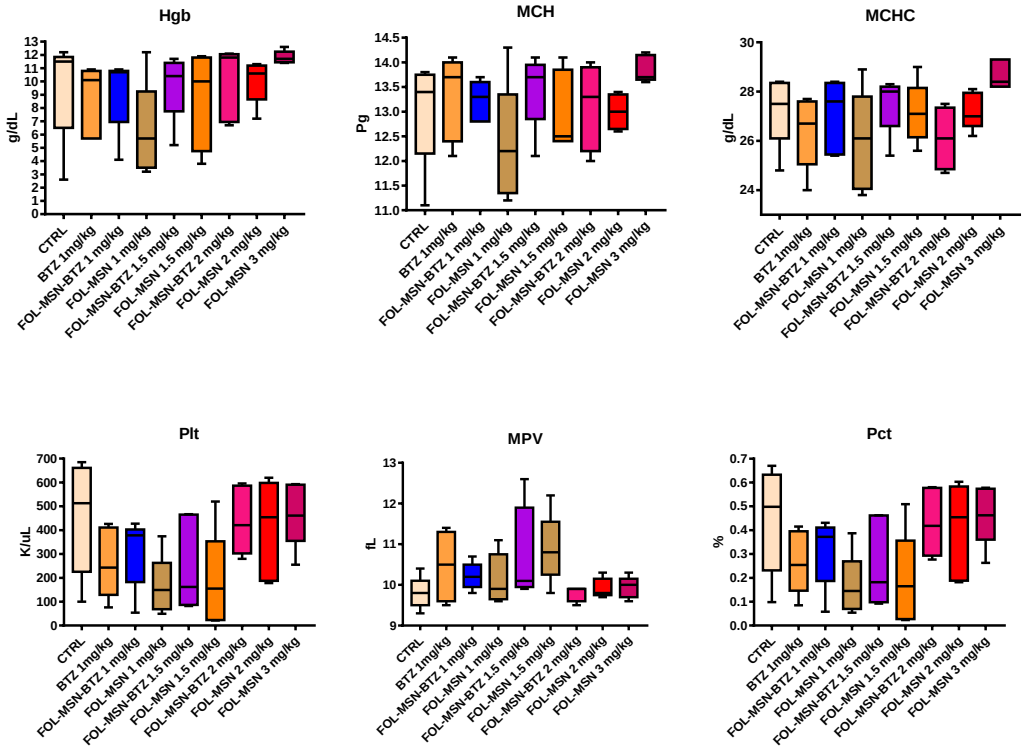

Figure 17*: Hematological parameters at the end of treatment. WBC: white blood cells, RBC: red blood cells, HGB: hemoglobin, MCV: mean corpuscular volume, HCT: hematocrit, HGB: hemoglobin, MCH: mean corpuscular hemoglobin, MCHC: mean cell hemoglobin concentration, PLT: platelets, MPV: mean platelet volume, PCT: plateletcrit. The results were statistically analyzed using the analysis of variance (ANOVA) and the non-parametric Kruskal-Wallis statistic, Graphpad Prism (significance level set at p<0.05).*

Similarly, we observe alterations ($p<0.05$) in the lymphocytes and granulocytes content in mice treated with FOL-MSN-BTZ 2 mg/kg, showing a decrease in lymphocytes and an increase in granulocytes counts compared to MSN-FOL 1mg/kg treated animals (Fig.

18), confirming that these observed fluctuations are independent from the vehicle, but depend on the drug.

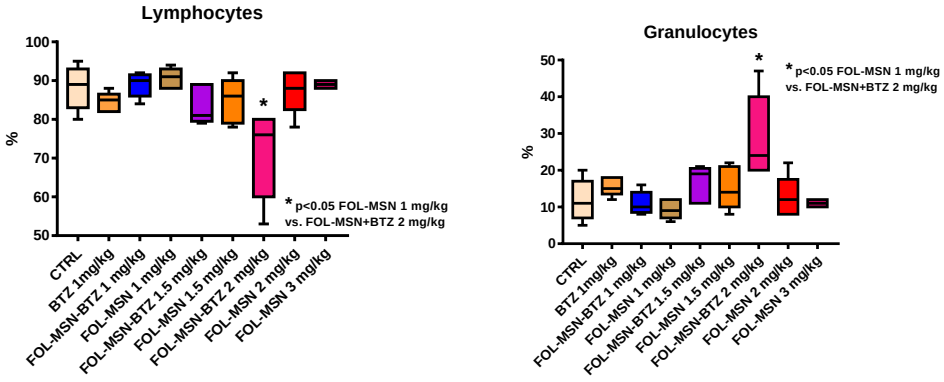

***Figure 18**: Hematological parameters at the end of treatment. The results were statistically analyzed using the analysis of variance (ANOVA) and the non-parametric Kruskal-Wallis statistic, Graphpad Prism (significance level set at $p<0.05$).*

The reduction of lymphocytes could presumably be due to a basal expression of FR on their surface, which could be recognized by the FOL function grafted onto the MSN surface. Granulocytes increase could be related to the activation of an anti-inflammatory response raised by a higher BTZ concentration (compared to BTZ 1mg/kg), but definitively not by MSN-FOL at any concentration tested, confirming, once again, the safety of our silica-based vehicle.

2.6.3 Histological examinations

After 48h from the last administration 3 mice/group were sacrificed and the main target organs were collected for histological examinations. All the mice treated with BTZ 1mg/kg or MSN-FOL-BTZ 2mg/kg showed spleen hypoplasia and reduced cellularity with slight dilation of blood sinusoids in sternum bone marrow. Similarly, animals treated with control MSN-FOL 2mg/kg showed a mild spleen hypoplasia, probably due to the

expression of FR β-isoform in this tissue [204]. Interestingly, no evident histopathological alterations were noticed in kidneys and liver, in any group of treated mice, including the FOL-MSN-BTZ 2mg/kg group (data not shown).

2.7 *In vivo* anticancer efficacy of FOL-MSN-BTZ

The aim of this experiment was to study the efficacy and the toxicity of silica nanoparticles loaded with bortezomib (BTZ) on tumor (MM) bearing mice. A RPMI 8226 MM cells-derived xenograft mice model was developed as described in *Materials and Methods*.

MSN-FOL and FOL-MSN-BTZ at 2 mg/kg were administered intravenously once a week for 5 weeks (1qwx5). Based on a previous MTD study (data not show), BTZ was used at 1mg/kg.

Animals well tolerated the treatment and no significant body weight loss was observed during the first 3 weeks of treatment. From the fourth week, FOL-MSN-BTZ treated animals showed a mild, although significant, weight loss, respect to the controls ($p<0.01$ vs Tumor and $p<0.05$ vs Tumor+MSN-FOL), likely due to the drug carried by the vehicle since the body weight of MSN-FOL treated animals resulted unaffected. A similar

reduction in body weight was induced by free BTZ (1mg/kg) compared to MSN-FOL and/or Tumor, always starting from the 4th week of treatment (Fig.19).

All together, these data demonstrate that the animals did well tolerate the treatments.

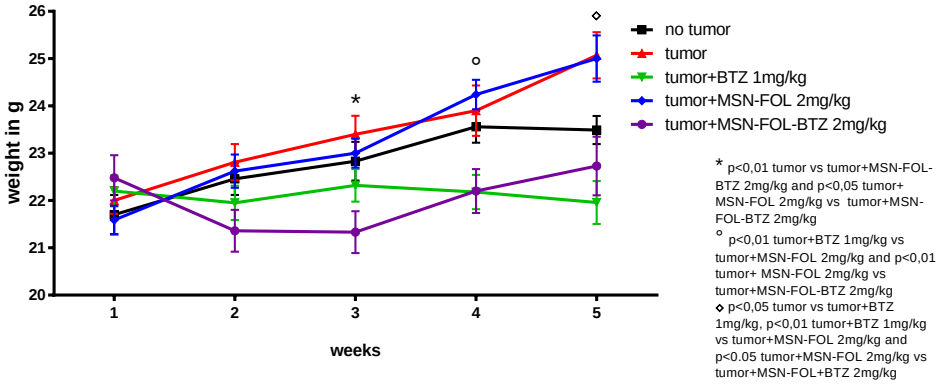

Figure 19*: Body weight gains of female mice treated with MSN-FOL-BTZ, MSN-FOL in the dose of 2mg/Kg or BTZ in the dose of 1mg/Kg. Nanoparticles were administered intravenously once a week for 5 weeks. The tumor volume was subtracted from the total body weight of tumor-bearing mice. Results are expressed as mean ± SD. Animals were sacrificed when tumor volume exceed about the 10% of body weight. The results were statistically analyzed using the analysis of variance (ANOVA) and the Tukey-Kramer post-test (significance level set at p<0.05).*

It is very important to notice, especially from a statistical point of view, that the majority of tumor not treated animals and MSN-FOL 2mg/kg treated mice were sacrificed before the end of the treatment period (table 4).

***Table 4**: Summary of mice sacrifice during xenograft experiment. BTZ, MSN-FOL and MSN-FOL-BTZ were all administered intravenously 10 ml/kg (the administered volume of drugs depends on each animal weight) once a week for 5 weeks (1qwx5).*

Treatment groups	# mouse	Sacrifice reason	Administrations				
			1	2	3	4	5
Untreated Tumor	6						X
	9	ulcerated tumor			X		
	10						X
	11	tumor volume exceed 10% of body weight			X		
	12	tumor volume exceed 10% of body weight		X			
	13	tumor volume exceed 10% of body weight			X		
	14	ulcerated tumor			X		
	15	tumor volume exceed 10% of body weight		X			
	16	tumor volume exceed 10% of body weight			X		
	17						X
	49	tumor volume exceed 10% of body weight			X		
Tumor + BTZ 1mg/Kg	18						X
	19						X
	20						X
	21						X
	22						X
	23	tumor volume exceed 10% of body weight				X	
	24	ulcerated tumor				X	
	25						X
	26						X
	27	tumor volume exceed 10% of body weight		X			
Tumor + MSN-FOL 2 mg/kg	28						X
	29						X
	30	tumor volume exceed 10% of body weight				X	
	31						X
	32	tumor volume exceed 10% of body weight				X	

	33						X
	34	ulcerated tumor			X		
	35	ulcerated tumor		X			
	36	ulcerated tumor				X	
	37						X
Tumor + MSN-FOL-BTZ 2 mg/kg	**38**						X
	39						X
	40						X
	41	ulcerated tumor				X	
	42						X
	43						X
	44						X
	45						X
	47						X

Most of the mice (72%) of the untreated tumor group were sacrificed after the third administration because tumor volume exceeded 10% of body weight or for the presence of ulceration of the tissue surrounding the tumor mass. Only 3 (out of 11) animals survived until the last administration. Interestingly, only 5 of the 10 animals of the group treated with MSN-FOL have been scarified for ulceration or excessive tumor growth, suggesting that the vehicle alone itself affects tumor volume, most likely for its preferential accumulation into FR+ tumor.

2.7.1 Tumor volume

Figure 20 shows a reduction in tumor volume growth in MSN-FOL treated animals with respect to control animals with untreated tumor. This intrinsic antitumor effect of MSN vehicle alone on tumor mass could be, supposedly, referred to both FOL targeted MSNs accumulation at the FR+ tumor site and to the EPR effect [205]. Another possibility could

be the beneficial effect of folic acid on fostering the immune system response [206]. However, all these hypotheses need to be further investigated. To this aim, the recovery of boron and silicon from explanted tissues (tumor, liver, kidney, lung, uterus, brain, spleen and sternum) by means of element analysis is ongoing in our laboratory. Results from this analysis will definitively give relevant information about the pharmacokinetic behavior of our MSNs. As expected from previous data, mice treated with free BTZ (1mg/kg) showed only a very slight increase of tumor volume during the whole experiment, confirming the anti-neoplastic effect of the drug. Surprisingly MSN-FOL-BTZ 2mg/kg treatment stopped the tumor growth immediately after the first administration (Fig.20). Importantly, just ~10% (only 1 mouse out of 9) of this group was sacrificed right before the end of the experimental period because of an excess growth in tumor volume (more of the 10% of body weight), condition that occurred, even earlier, in the 30% (3 out of 10) of the mice belonging to the free BTZ treated group (Table 4). Noteworthy, tumor mass was not more measurable (almost complete regression) at the end of the experiment in one mice of the FOL-MSN-BTZ treated group.

All these data strongly show the efficacy of our delivery system if compared to the free BTZ (1mg/Kg) (Fig. 20).

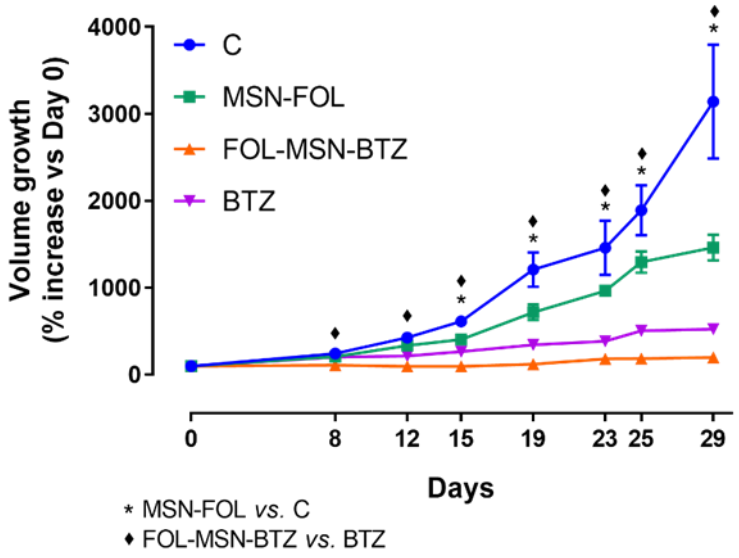

Figure 20: *Tumor growth percentage of female mice treated with BTZ in the dose of 1mg/Kg or FOL-MSN-BTZ and MSN-FOL in the dose of 2mg/Kg. Animals were sacrificed when tumor volume exceed about the 10% of body weight. Results are expressed as mean ± SD. The percentage was evaluated through the ratio between the tumor volume at each time point and the tumor volume at Time 0, for each group. The results were statistically analyzed using the analysis of variance (ANOVA) and the Tukey-Kramer post-test (significance level set at $p<0.05$).*

2.7.2 Hematochemical evaluation

After 48h from the last administration, mice were sacrificed and blood was collected and analyzed for the evaluation of the hematochemical parameters. Tumor bearing mice treated with free BTZ 1mg/kg or with FOL-MSN-BTZ 2mg/kg, showed hepatic toxicity (GPT/ALT increase) compared to tumor not treated animals and mice without tumor. Noteworthy, tumor-bearing mice treated with MSN-FOL 2mg/kg did not show any significant GPT/ALT increase compared to tumor bearing control animals (Fig. 21), indicating that hepatic toxicity is due to BTZ.

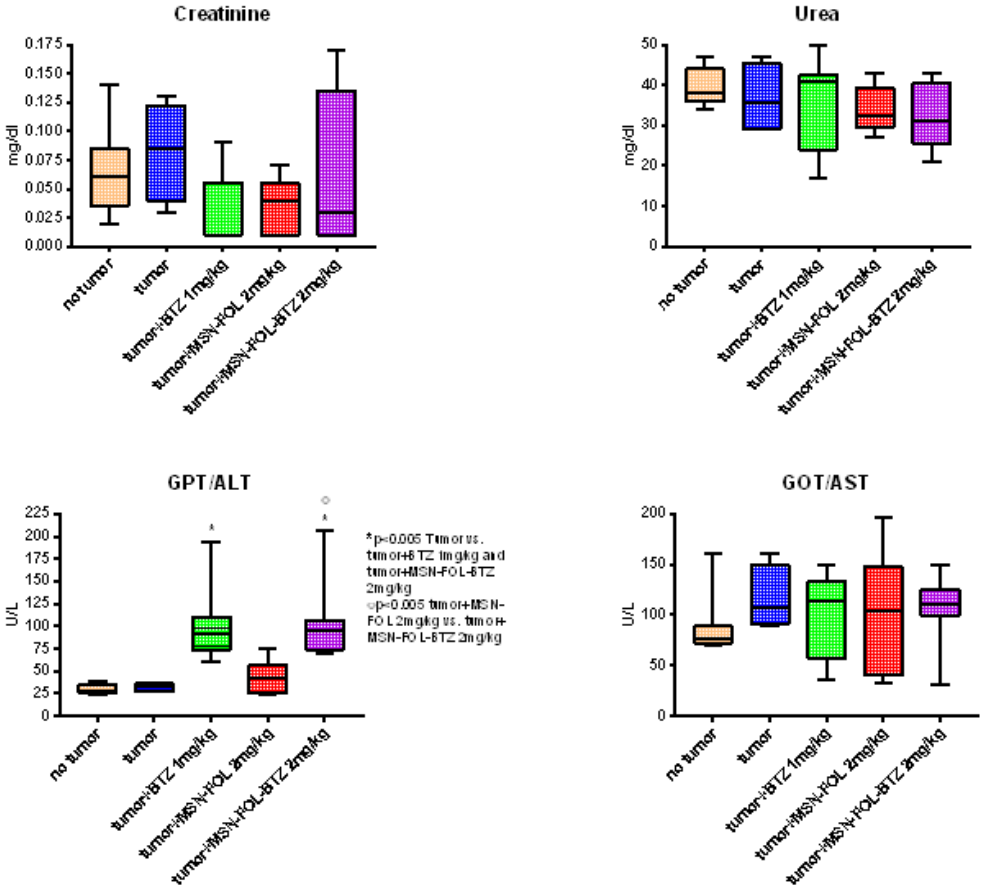

Figure 21*: Assessment of hepatic and renal biochemical parameters at the end of treatment. ALT= Alanine transaminase or GPT= glutamate-pyruvate transaminase, AST= Aspartate transaminase or GOT= glutamate-oxaloacetate transaminase. The results were statistically analyzed using the analysis of variance (ANOVA) and the non-parametric Kruskal-Wallis statistic, Graphpad Prism (significance level set at $p<0.05$).*

2.7.3 Hematological evaluation

After 48h from the last administration, also hematological parameters, such as RBC, WBC, Plt, Hgb serum content and Hct were determined. No statistic significant differences were noticed between treated and not treated animals in all the parameters analyzed (Fig. 22), confirming that the animals well tolerated the treatments.

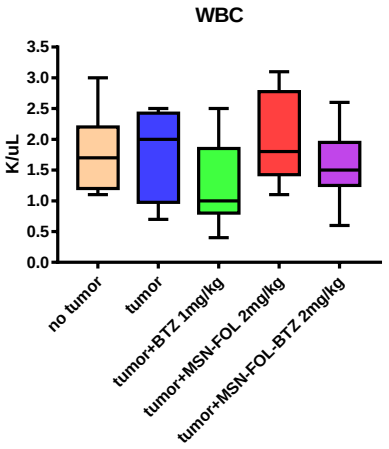
WBC
K/uL
3.5
3.0
2.5
2.0
1.5
1.0
0.5
0.0
no tumor
tumor
tumor+BTZ 1mg/kg
tumor+MSN-FOL 2mg/kg
tumor+MSN-FOL-BTZ 2mg/kg

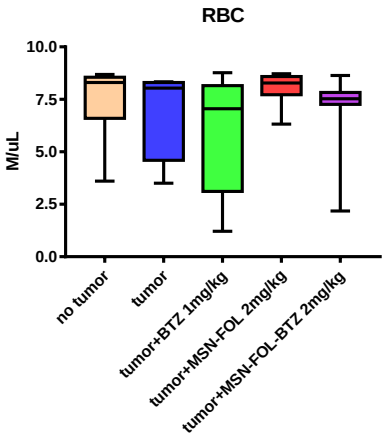
RBC
M/uL
10.0
7.5
5.0
2.5
0.0
no tumor
tumor
tumor+BTZ 1mg/kg
tumor+MSN-FOL 2mg/kg
tumor+MSN-FOL-BTZ 2mg/kg

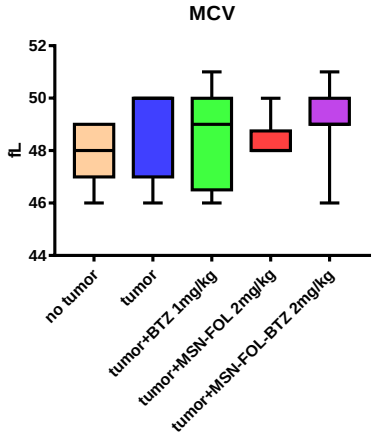
MCV
fL
52
50
48
46
44
no tumor
tumor
tumor+BTZ 1mg/kg
tumor+MSN-FOL 2mg/kg
tumor+MSN-FOL-BTZ 2mg/kg

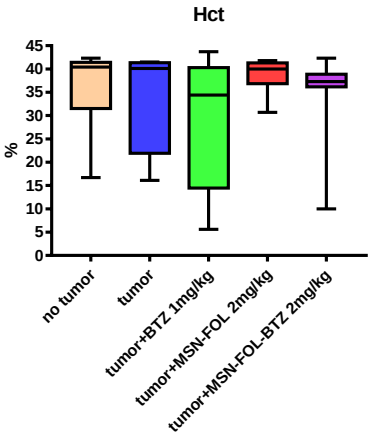
Hct
%
45
40
35
30
25
20
15
10
5
0
no tumor
tumor
tumor+BTZ 1mg/kg
tumor+MSN-FOL 2mg/kg
tumor+MSN-FOL-BTZ 2mg/kg

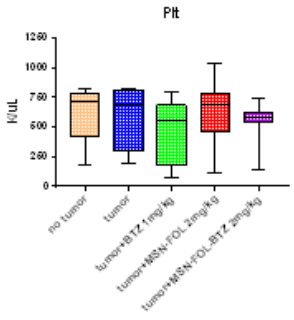
Plt
K/uL
1260
1000
760
500
250
0
no tumor
tumor
tumor+BTZ 1mg/kg
tumor+MSN-FOL 2mg/kg
tumor+MSN-FOL-BTZ 2mg/kg

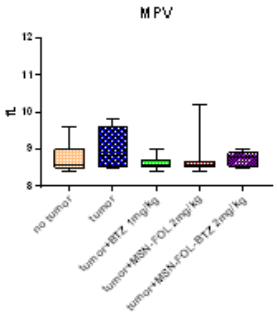
MPV
fL
12
11
10
9
8
no tumor
tumor
tumor+BTZ 1mg/kg
tumor+MSN-FOL 2mg/kg
tumor+MSN-FOL-BTZ 2mg/kg

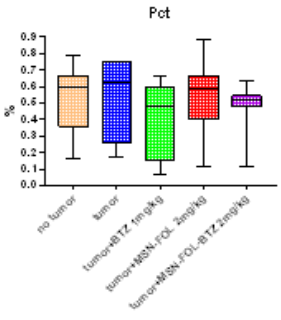
Pct
%
0.9
0.8
0.7
0.6
0.5
0.4
0.3
0.2
0.1
0.0
no tumor
tumor
tumor+BTZ 1mg/kg
tumor+MSN-FOL 2mg/kg
tumor+MSN-FOL-BTZ 2mg/kg

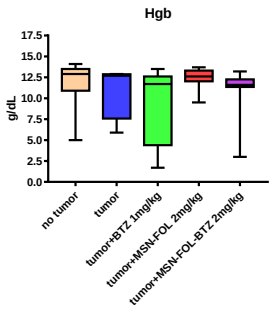
Hgb
g/dL
17.5
15.0
12.5
10.0
7.5
5.0
2.5
0.0
no tumor
tumor
tumor+BTZ 1mg/kg
tumor+MSN-FOL 2mg/kg
tumor+MSN-FOL-BTZ 2mg/kg

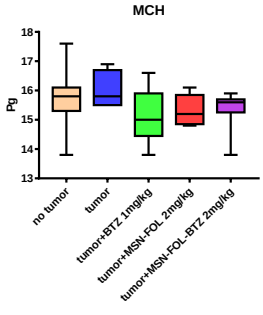
MCH
Pg
18
17
16
15
14
13
no tumor
tumor
tumor+BTZ 1mg/kg
tumor+MSN-FOL 2mg/kg
tumor+MSN-FOL-BTZ 2mg/kg

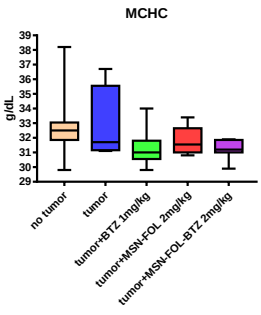
MCHC
g/dL
39
38
37
36
35
34
33
32
31
30
29
no tumor
tumor
tumor+BTZ 1mg/kg
tumor+MSN-FOL 2mg/kg
tumor+MSN-FOL-BTZ 2mg/kg

Figure 22: *Hematological parameters at the end of treatment. WBC: white blood cells, RBC: red blood cells, MCV: mean corpuscular volume, HCT: hematocrit, HGB: hemoglobin, MCH: mean corpuscular hemoglobin MCHC: mean cell hemoglobin concentration, PLT: platelets, MPV: mean platelet volume, PCT: plateletcrit. The results were statistically analyzed using the analysis of variance (ANOVA) and the non-parametric Kruskal-Wallis statistic, Graphpad Prism (significance level set at p<0.05).*

Also lymphocytes and granulocytes were analyzed and tumor bearing mice treated with MSN-FOL-BTZ 2 mg/kg showed alterations (p<0.01) in lymphocytes and granulocytes counts compared to mice with tumor not treated animals (Fig. 23).

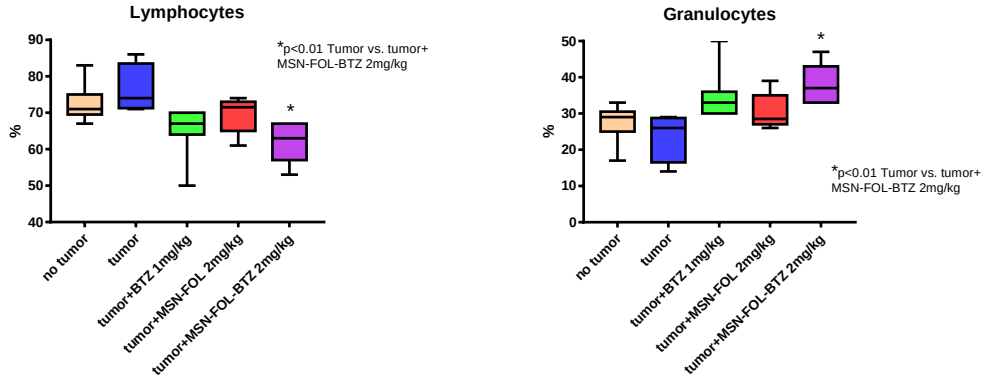

Figure 23*: Hematological parameters at the end of treatment. The results were statistically analyzed using the analysis of variance (ANOVA) and the non-parametric Kruskal-Wallis statistic, Graphpad Prism (significance level set at p<0.05).*

These data do not confirm those obtained from the MTD experiment. (Fig. 18), where no alterations have been observed. Therefore, the reduction of lymphocytes in the efficacy study could, likely, be explained by the immunosuppressive state of animals used for this experiment, being Severe Combined Immuno-Deficient (SCID) mice, that make them much more sensitive to any treatment.

2.7.4 Histological examinations

After 48h from the last administration 2/3 mice/group were sacrificed and spleen and sternum collected for histological examinations. Only the tumor-bearing mice treated with BTZ 1mg/kg showed mild hypoplasia in bone marrow, while no pathological

alterations were noticed in the spleen. Animals from all the other experimental groups, including FOL-MSN-BTZ, did not show any pathological alterations (data not shown).

2.7.5 Neurophysiological examinations

Caudal nerve sensory action potential (SAP) amplitude and digital nerve SAP amplitude were evaluated 24h after the last drug administration. Tumor bearing mice treated with FOL-MSN-BTZ 2mg/kg showed a significant decrease compared to Tumor+BTZ 1mg/kg ($p<0.01$) in caudal nerve SAP amplitude. A significant increase in digital nerve SAP amplitude was detected in Tumor+MSN-FOL-BTZ 2mg/kg with respect to Tumor+BTZ 1mg/kg ($p<0.01$). The caudal nerve sensory velocity was reduced under treatment with FOL-MSN-BTZ 2mg/kg compared to untreated group and Tumor+BTZ (Fig. 24).

The results obtained from the *in vivo* experimentation, regarding the effect of FOL-MSN-BTZ on peripheral neuropathy, suggest that our nanovehicle affects the functionality of mice neuronal cells.

This is not surprising since FR-α is expressed in the nervous system, being the vitamin folic acid a crucial environmental factor for its development [205], starting from the early fetal stages of the formation of the presumptive spinal cord and brain to the maturation and maintenance of the nervous system during infancy and childhood [206]. Indeed, an increased folic acid intake during pregnancy to reduce the risk of neural tube defects (NTDs) is suggested [207, 208].

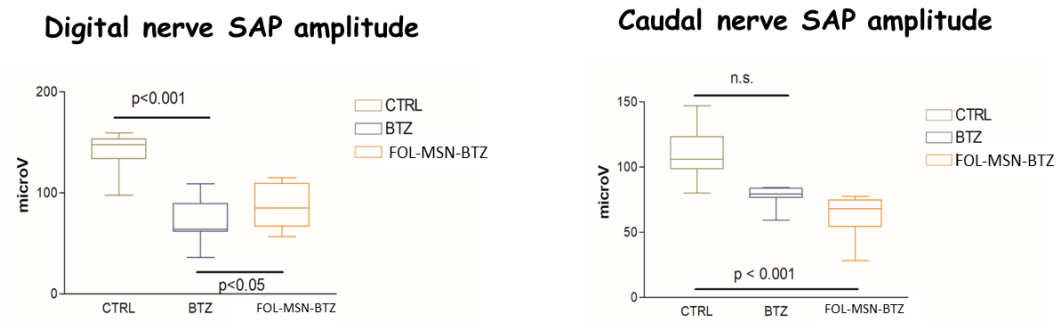

***Figure 24**: The graph reports the values of caudal and digital NCV and caudal amplitude recorded in control and treated mice after 48h from the last treatment. The results were statistically analyzed using the analysis of variance (ANOVA) and the non-parametric Kruskal-Wallis statistic, Graphpad Prism (significance level set at p<0.05).*

2.8 CD38L-MSN-BTZ: a new prototype to overcome the BTZ-induced peripheral neuropathy.

In this context, we are already working to develop a new, more selective, MSN-based prototype bearing BTZ and grafted, on the external surface, with a peptide able to recognize CD-38, a marker overexpressed on MM cells [207], referred as CD38L-MSN-BTZ. We embraced the suggestion of Professor Paul Richardson, the "father" of Bortezomib and also member of the Advisory board of NanoSiliCal Devices, to consider CD38 as a therapeutic target for MM.

The preliminary data obtained by this prototype are extremely exciting.

In fact, the so engineered system maintains the high selectivity of the FOL-MSN-BTZ prototype towards CD38+ RPMI-8226 MM cells, and showing no toxicity on normal BJhTERT cells, which express very low levels of CD38, as evidenced by western blot analysis (Fig. 25). Immunogold labelling experiments on RPMI confirmed that the recognition of CD38L-MSN depends on CD-38 as it clearly shows Fig. 26, where two representative images nicely depict the whole CD38-mediated endocytic process, from

the CD38 recognition at the cell membrane to the sequestration in CD38-immunopositive intracellular vesicles.

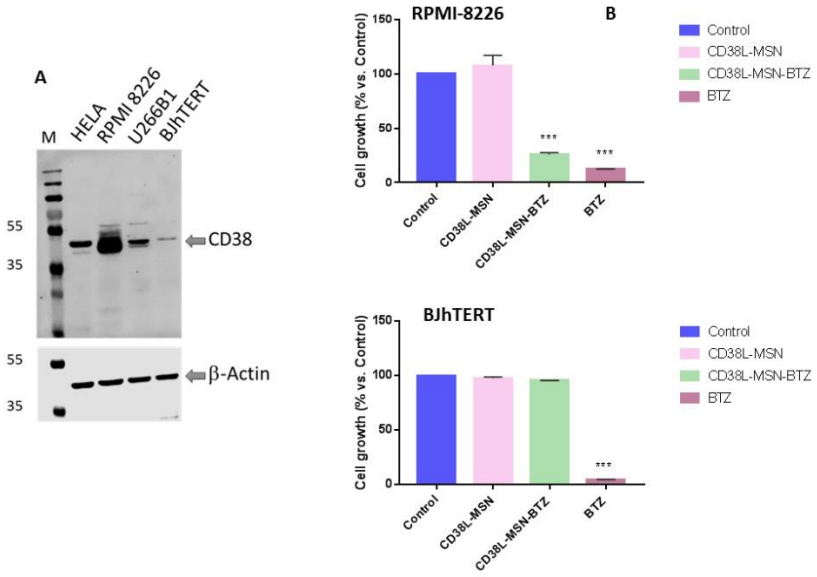

Figure 25*: (A) Protein expression of CD-38 in different cell lines. 30μ of denatured proteins from total lysates were loaded and subjected to WB analysis. β-actin was used as loading control. (B) Normal BJhTERT cells and cancerous CD38+ RPMI cells were left untreated or treated for 1h with MSN-CD38L, CD38L-MSN-BTZ, or free BTZ. Viability was determined after 3 days. Representative images of three independent experiments are shown. *** p ≤ 0.001 vs control (ANOVA).*

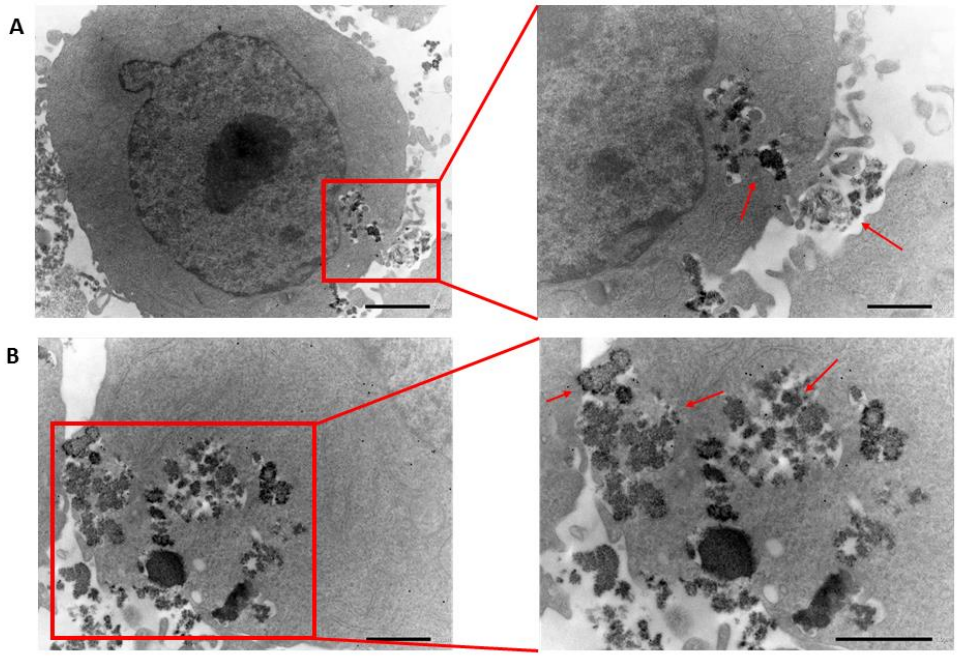

***Figure 26**: Colloidal-gold immunocytochemistry for CD-38 (black dots indicated by red arrows) in RPMI cells exposed to CD38-MSN for 2h. (**A**) Scale bars 2µm, x 4.000 magnification (left panel); scale bare 1µm, x 8000 magnification (right panel). (**B**) scale bars 1µm, x8000 magnification (left panel); scale bare 1µm x 12k (right panel).*

As mentioned in 1.7.2.1 section, under normal conditions, CD38 is expressed at relatively low levels on myeloid and lymphoid cells and in some non-hematopoietic tissues. In contrast, normal plasma cells and MM cells do express high levels of CD38 expression [144].

It is worth mentioning that CD-38 is also highly expressed in the two most studied immunosuppressive cell subsets that can be induced by MM cells: regulatory T-cells (Tregs) and B-cells (Bregs) [208]. Several reports showed increased frequencies of these cells in peripheral blood of MM patients [209, 210].

Tregs can be naturally occurring (generated in the thymus) or induced from effector T-cells and are biologically important for maintaining peripheral tolerance and limiting auto-immune disease [211]. However, they can also suppress anticancer immune

responses through several mechanisms [212]. MM cells were shown to induce Tregs from conventional T-cells *ex vivo* [213].

In line with the idea of MM-induced Treg expansion and active immune suppression, it has been found that lower Treg numbers in bone marrow and peripheral blood are associated with long-term survival in MM patients [214]. Furthermore, recent reports show an increased CD38 expression on Tregs as compared with conventional T-cells [210].

In addition, regulatory Bregs, identified by the $CD38^{high}$ cell surface phenotype, were shown to be capable of suppressing anti-MM cell antibody-dependent cellular cytotoxicity (ADCC) by NK cells [215].

Thereby, targeting CD38 on MM cells could gain in selectivity and effectiveness, allowing to overcome the limits of FR receptor as a target and, on the other hand, blocking Tregs/Bregs-induced immune suppression in MM and restoring the immune effector function against multiple myeloma.

Based on its expression profile, the CD-38 targeting could affect immunity system of treated patients inducing a hypothetical state of immunosuppression that could be counteracted coupling the administration of immunomodulatory agents as adjuvants of targeted therapy, among those reported for treatment in MM (see paragraph 1.7.3) or glucocorticoids such as dexamethasone to reinforce the inflammatory response. For instance, dexamethasone is contemplated among the standard of care regiments in MM, in combination with daratumumab and/or BTZ [152], as already discussed (see 1.7.2.1 section).

Furthermore, peptide-conjugate materials could elicit immunogenic response and exhibit instability because of enzymatic degradation due to soluble enzymes present in the blood

and membrane-bound enzymes and to a broad variety of peptidases [216, 217]. Several agents have been incorporated, including small sugars (e.g. trehalose) and polysaccharides (e.g. dextrans), to enhance the stability of protein and peptide based biopharmaceuticals [216]. Chemical modification with hydrophilic polymers has been described as a useful strategy to improve stability of so conceived therapeutic constructs, which can reduce clearance and promote circulating half-life to an attractive range. PEGylation is one such strategy that involves covalent attachment of a FDA approved polymer, polyethylene glycol (PEG) to a primary amino (-NH2) or sulfhydryl (-SH) groups of proteins or peptides [216]. PEG chains of molecular weight ranging from 5–40 kDa have shown to improve biological activity of therapeutic proteins or peptides and reduce immune responses to a larger extent [216]. Nonetheless, the PEGylation could hamper targeting action, thus representing a remote solution today [218].

An alternative strategy consists in replacing natural amino acids with non-natural analogues (N-methylation, D-amino acids, β-amino acids) in sites susceptible to enzymatic cleavage [219]. These replacements decrease the substrate recognition and binding affinity of proteolytic enzymes and increase stability. Cyclization of the peptide [220] is another interesting approach that we might take into account for future system optimization.

In addition to the CD38, a broad of new molecules that can be used to target disease-causing plasma cells in MM has been identified. The gene expression profiles analysis in bone marrow myeloma cells, via RNA-sequencing technology, has screened genes that are active in plasma cells [147]. Among these, CD138, a surface molecule highly expressed on MM cells which play a pivotal role in the development and/or proliferation of plasma cells; PDL-1 (programmed cell death protein ligand-1) expressed on MM cells

allowing for immune evasion [221]; CD74 also is strongly expressed in myeloma cells compared to healthy cells and has a role in the oncogenic process of cell proliferation and survival [147].

Finally, chimeric antigen receptor (CAR) engineered T cells targeting B cell maturation antigen (BCMA), CD138 and light chains are in active development for therapy of RRMM. CD19- targeted CAR T cells in conjunction with autologous stem cell transplantation (ASCT) also showed activity in RRMM [222], being CD19 a surface glycoprotein that is expressed from the earliest stages of B cell development until plasma cell terminal differentiation, when its expression is lost [147].

However, CD38 is a suitable target for therapy in MM patients due to its expression profile in the bone marrow (BM) microenvironment. MM cells expressed CD38 at high levels and, among the cells of the BM microenvironment it has been demonstrated that natural killer (NK), T cells, and monocyte express CD38 with different levels of expression. Growing evidence indicate that the efficacy of anti-CD38 mAbs is depending, at least in part, to the CD38 density of expression by MM cells and those of the immune-microenvironment [146]. The possibility to modulate CD38, increasing its expression by MM cells, could be the pre-requisite to potentiate the efficacy of anti-CD38 mAbs [176]. However, as reported in 1.7.2.1 section, the anti-CD38 mAbs may modulate the CD38 expression on the surface of MM cells by its internalization or capping, leading to an antibody resistance phenomenon which is of critical relevance in clinical practice [146]. Will the grafting of a CD38L to the external surface of our BTZ bearing MSNs be able to circumvent this resistance mechanisms? What we would expect is that MSNs unique framework will cope with the aim of protecting the bound peptide(s) from unwanted

plasma and tissue degradation, fulfilling a so craved requirement that will definitively seal MSNs outstanding reliability as a targeted drug delivery system.

Conclusion

Altogether, our results clearly identify, for the first time, a MSN-based nanodevice able to deliver BTZ to MM cells in a receptor-specific manner. In fact, a highly specific, FR mediated, endocytosis of MSNs bearing the folic acid function has been reported exclusively in MM FR-overexpressing cells. Once inside, the tumor-associated acidic environment triggers the release of BTZ, inducing apoptosis and impairing glycolysis and OXPHOS-driven mitochondrial respiration, also nourished by a strong ROS production. The lack of internalization of MSN-FOL and FOL-MSN-BTZ in FR- normal cells confirms that the folic acid function is the mediator of the cellular uptake process.

Importantly we demonstrated the biocompatibility and safety of the vehicle itself. In fact, MSN-FOL did not show any sign of toxicity both *in vitro* and *in vivo*. While free BTZ killed all cell lines tested regardless their FR expression, by inducing metabolic impairments, the binding to MSNs vehicle was able to abolish BTZ-induced toxicity in healthy cells.

These data were reinforced by *in vivo* experiments, which, first of all, confirmed the biocompatibility of mesoporous silica-based vehicles and, at the same time, demonstrated a gain of selectivity and therapeutic efficacy of BTZ when it is carried by MSN-FOL towards FR+ MM cells-derived tumors in mice models.

Overall, these data suggest that FOL-MSN-BTZ represents a great opportunity for targeted therapy of multiple myeloma, being able to be internalized, in a highly specific way, exclusively by FR over-expressing tumor cells. The as conceived DDS seems to preserve healthy cells and, in turn, is hoped to enable more effective and targeted treatment, resulting in improved outcomes for patients.

The next step will be to design a MSN-based device, which will not only be as efficacious as the FOL-MSN-BTZ prototype, but able it will also be able to abolish the BTZ-induced peripheral neuropathy. In this perspective, a new prototype, engineered for CD38 recognition, is already at an advanced stage of development.

Definitely, this study gave crucial information that are mandatory to plan the future use of this strategy in a clinical setting for MM therapy, paving the way for a future exploitation of our MSNs technology, not only in the oncological, but potentially in any other therapeutic field where a targeted and personalized approach would be the preferable treatment option.

3 MATERIALS AND METHODS

3.1 Chemicals and reagents.

Dulbecco's Modified Eagle's Medium (DMEM), RPMI 1640 (1x) Medium, Minimum Essential Media (MEM), L-Glutamine, penicillin/streptomycin (pen/strep), MEM Non-Essential Amino Acids Solution (100x), Fetal Bovine Serum (FBS) and phosphate-buffered saline (PBS) were from Gibco™ (Life Technologies, Monza MB, Italy). Trypsin-EDTA solution 10x, protease inhibitors (cOmplete™ ULTRA Tablets, cat#5892970001), Digitonin **(**D141)**,** formaldehyde, NP-40 and Bortezomib by MERCK/Sigma-Aldrich (Milan, Italy). Bortezomib was dissolved, for all the treatments, in ethanol at the final concentration 1mg/ml.

3.2 Cell cultures and treatments.

Human MM RPMI-8226 (RPMI) were purchased from ATCC where they were authenticated. Cells were stored according to supplier's instructions, and used within 6 months after frozen aliquots resuscitations. Normal foreskin fibroblast BJhTERT cells were kindly provided by Michael Lisanti, University of Salford, Manchester (UK). Cells were purchased from ATCC and transferred to our laboratory at passage n=3 and handled as above described. RPMI were cultured in RPMI-1640 medium, while BJhTERT in DMEM supplemented with 10% FBS, 100IU ml^{-1} pen/strep and 0,2 mM L-Glutamine. Mycoplasma negativity was tested monthly (PlasmoTest, Invivogen, Aurogene, Rome IT). For cells treatments, a ratio of 1 μg MSNs /10^5 cells are selected on the basis of titration experiments. Free BTZ was added as positive control in amounts corresponding to the percentage of BTZ carried by FOL-MSN-BTZ.

3.3 Cell proliferation assays.

MSNs effect on cell proliferation was assessed by trypan blue exclusion assay. Cells were seeded in triplicates for each condition, synchronized in serum free media (SFM) for 24h and then treated for 1h with MSNs 1 μg/10^5 cells. Cells were then switched to fresh growing medium plus 1% FBS and counted after 72h. Cell viability was determined by Countess® II Automated Cell Counter (Invitrogen, Life Technology), according to supplier's instructions.

3.4 TUNEL assay.

Apoptotic cells were determined by enzymatic labeling of DNA strand breaks using a Dead End Fluorometric TUNEL System (Promega, Milan, Italy) according to the manufacturer's instructions, in order to detect the DNA fragmentation, a hallmark of apoptosis. Briefly, $3x10^5$ cells were seeded on coverslips (poly-L-lysine-coated slides were used for RPMI cells to allow cells attachment) and treated as described for proliferation assays. After 36h, coverslips were mounted on slides using Fluoromount mounting medium (MERCK/Sigma-Aldrich) and observed under a fluorescence microscope (Olympus BX51, Olympus Italia, Milan, Italy). DAPI was used to counterstain the nuclei. Apoptotic cells were photographed at 10x magnification, using ViewFinder™ 7.4.3 Software, through an Olympus camera system dp50 and then counted by Image J software (NIH, Maryland, USA).

3.5 Transmission electron microscopy (TEM) and electron immunocytochemistry.

For conventional TEM analysis and electron immunocytochemistry, cells were treated as described for growth experiments and harvested either right after 1h MSNs treatment (to detect MSNs uptake) or after 36h following the 1h exposure to MSNs (to individuate cell death and/or cell injury in treated cells). All samples have been routinely fixed, dehydrated, and resin embedded using heat polymerization. Indirect immunolabeling has been performed on ultrathin sections (60 nm) collected on Formvar carbon-coated nickel grids. Grids with sections were floated on drops of 1% bovine serum albumin (BSA) in PBS containing 0.02-M glycine at room temperature for 30min to reduce nonspecific binding. Sections were then incubated with a rabbit polyclonal antibody against FR-β, cat#PA5-45768 (1:10) (Invitrogen, ThermoFisher) in PBS 0.1% BSA at 4°C overnight. The grids were then washed in four drops of PBS for a total of 15 min, transferred to 50μL drops of secondary antibody conjugated to 10-nm gold particles for 1 h at room temperature. After immunolabeling, the sections were rinsed with PBS and distilled water. Control staining to demonstrate the specificity of the immunolabeling was carried out with the same steps as above, but the primary antibody was replaced by PBS. All the observations were performed under an electron microscope operating at 80 kV (Jeol JEM -1400 Plus (Jeol Ltd., Tokyo, Japan).

3.6 Western blotting (WB) assay.

Protein expression of FRs, Casp-2/8/9, PARP-1, RIP-1, Cyt C, COX IV and β-actin, were assessed by Western blotting (WB) using cytosol and mitochondrial protein lysates from different cell lines. Cells were plated in growing medium and, after treatment with MSNs, lysed with cytosolic buffer containing 50 mmol/liter HEPES (pH 7.5), 150 mmol/liter NaCl, 1% Triton X-100, 1.5 mmol/liter MgCl2, 10 mmol/liter EGTA (pH 7.5), 10% glycerol, and inhibitors (0.1 mmol/liter Na3VO4, 1% phenylmethylsulfonyl fluoride, and 20 mg/ml aprotinin) and mitochondrial buffer (see below). The protein content was determined using Bradford dye reagent (Bio-Rad, Milan, Italy). 50 µg (cytosolic extract) and 10µg (mitochondrial extract) of denatured proteins, and non-denatured for FRs detection, were run on an 11% and 13% polyacrylamide gel respectively and transferred to nitrocellulose membranes.

The proteins were detected with specific polyclonal (p) or monoclonal (m) antibodies (Abs), recognized by IRDye secondary Abs (LI-COR Corporate, Nebraska USA).

The following primary Abs were employed: anti-human FOLR1 (AF5646, R&D Systems Inc., USA); anti-human FOLR2 (PA545768, ThermoFisher Scientific); anti-caspase-3 (8G10, #9665), anti-caspase-8 (1C12, #9746), anti-caspase-9 (#9502S), anti-RIP-1 (#711689), anti-COX IV (3E11, #4850), anti-Cyt C (D18C7, #11940) all from Cell Signalling, The Netherlands, and anti-β-Actin (AC-15, A1978) and anti-PARP-1 (sc-7150) (all from Santa Cruz Biotechnology, Inc), Anti-CD38 [EPR4106] ab108403 (from Abcam, Milan, Italy). Images were acquired with the Odyssey FC Imaging System (LI-COR Corporate).

3.7 Mitochondrial protein extraction.

Mitochondrial fractions were isolated from the cells plated and left in growth medium for 24h, where they were treated 1h with MSNs. After 36h, the cells were washed, collected and centrifuged to remove medium. Then, cells were incubated with cytoplasmic buffer containing sucrose 1M, Hepes 1M, Kcl 1M, MgCl2 1M, EDTA 1M, EGTA 1M and inhibitors digitonin 10% and PMSF 200mM. After 10 minutes in ice, the suspension was centrifuged; 13000 rpm for 5' at 4°C, and the cytoplasmic fraction was collected. The intact mitochondria in the pellet were washed twice with PBS and incubated with mitochondrial buffer consisting of Tris-HCL pH7.4 1M, EDTA 1M, EGTA 1M, TRITON X-100 and inhibitors PMSF 200mM, aprotinin 2mg/ml and Na3VO4 0.2 M. The final centrifugation at 13000 rpm for 10 minutes at 4°C, has allowed to collect mitochondrial fraction. 10µg of denatured proteins, determined as reported above, were run on a

13% polyacrylamide gel and transferred to nitrocellulose membranes. The proteins were detected as above (see WB assay section).

3.8 Seahorse XFe96 metabolic profile analysis.

Extracellular acidification rates (ECAR) and real-time oxygen consumption rates (OCR) were determined using the Seahorse Extracellular Flux (XFe- 96) analyzer (Seahorse Bioscience, Agilent Technologies, United States). Briefly, 40,000 cells/well were seeded, in a final volume of 125 µl, into XFe-96 well cell culture plates for 24h. For non-adherent RPMI-8226 cells, the Seahorse microplate was coated with 50µg/ml Poly-L lysine (Sigma Aldrich) before the seeding to allow cells attachment.

Then, cells were washed in XF assay media, for ECAR, or XF assay media supplemented with 10mM glucose, 1mM Pyruvate, 2mM L-glutamine and adjusted at 7.4 pH, for OCR measurement. Cells were then maintained in 175 µL/well of XF assay media at 37°C, in a non-CO_2 incubator for 1 hour. During the incubation time, 5 µL of 80mM glucose, 9 µM oligomycin, and 1 M 2-deoxyglucose (for ECAR measurement) or 10µM oligomycin, 9 µM FCCP, 10 µM Rotenone, 10 µM antimycin A (for OCR measurement), were loaded in XF assay media into the injection ports in the XFe-96 sensor cartridge. Data set was analyzed by XFe-96 software after the measurements were normalized by protein content (Sulforhodamine B, SRB). All experiments were performed three times independently.

3.9 Sulforhodamine B (SRB)-based *in Vitro* Toxicology Assay Kit.

After Seahorse analysis, Cells were briefly washed, fixed, and stained with the dye SRB (Acid Red 52) (Sigma Aldrich). The incorporated dye was then released from the cells with a TRIS base solution. An increase or decrease in the number of cells (total biomass) results in a concomitant change in the amount of dye incorporated by the cells in the culture. The signal was detected spectrophotometrically, measuring absorbance at a wavelength of 565 nm.

3.10 Reactive Oxygen Species (ROS) Detection

Cells were plated and left in growth medium for 24h, where they were treated for 1h with MSNs. After 6h, the cells were washed, trypsinized and centrifuged to remove the growth medium. The pellet was

resuspended in PBS containing the probe (chloromethyl-2′,7′–dichlorofluorescein diacetate (CM-H_2DCFDA), Molecular Probe, Invitrogen) to provide a final working concentration of 5μM dye and put in CO_2-incubator at 37°C for 1h. After probe incubation, the cells were returned to growth medium and incubated at 37°C for 20 minutes.

The assay is based on the premise that the nonpolar, nonionic DCFHDA crosses cell membranes and is enzymatically hydrolyzed by intracellular esterases to non-fluorescent DCFH. In the presence of ROS, DCFH is rapidly oxidized to highly fluorescent 2',7'-dichlorofluorescein (DCF), detectable by a fluorescence microplate reader. The fluorescence intensity was detectable by a fluorescence microplate reader in an excitation/emission range of 492–495/517–527 nm using Synergy H1 Hybrid Multi-Mode Reader (BioTek's Hybrid Technology. Milan, Italy). Probe fluorescence in each sample was normalized on viable cells, counted by means of Countess® II Automated Cell Counter (Invitrogen, Life Technology), according to supplier's instructions.

3.11 Statistical analysis.

Statistical analysis was performed using Student t test and ANOVA. Data were analyzed using GraphPad Prism 4 (GraphPad Software, Inc., San Diego, CA) and reported as the mean ± SD of at least 3 independent experiments, each performed in triplicates. * $p \leq 0.05$ *vs* control.

3.12 Maximum tolerated Dose (MTD).

MTD was conducted on 10 groups of mice (6 mice/group) receiving MSN-FOL and FOL-MSN-BTZ at increasing concentrations, as fallowing:

1. No treated mouse (Controls)
2. Free BTZ (1 mg/Kg)
3. FOL- MSN-BTZ (1 mg/Kg)
4. FOL- MSN (1 mg/Kg)
5. FOL- MSN-BTZ (1,5 mg/Kg)
6. FOL- MSN (1,5 mg/Kg)
7. FOL- MSN-BTZ (2 mg/Kg)
8. FOL- MSN (2 mg/Kg)
9. FOL- MSN-BTZ (3 mg/Kg)

3.13 Drug preparation and administration.

BTZ was administered at final concentration of 1mg/kg, chosen based on previous results [128]. BTZ is contained in a glass vial and was added first with 5% EtOH. This solution was vortexed and heated in the bath at 37 °C until it becomes clear, then 5% tween80 was added and the solution was vortexed once again. Finally, physiological was added and the solution was well vortexed and sonicated by immersion until the compound is completely suspended.

BTZ, MSN-FOL and FOL-MSN-BTZ were all administered intravenously once a week for 5 weeks.

Mice received doses of administration of FOL-MSN-BTZ and FOL-MSN at the concentrations of 1, 1,5, 2 and 3 mg/kg. The MSNs suspension was obtained in physiological solution with magnetic stirrer for 13 minutes. The administered volume depended on each animal weight.

Equal amounts of physiological solution were injected in control mice, corresponding to the different volumes taken to reach the desired concentrations of MSNs in treated animals.

3.14 Hematological and hematochemical analysis.

After 48h from the last administration, 5 mice/group were sacrificed and blood analyzed for the hematochemical and hematological parameters trough Konelab i20 and DASIT diagnostic (ThermoFisher Scientific, Milan, Italy).

3.15 Histological examinations.

After 48h from the last administration 3 mice/group were sacrificed and the main target organs collected for histological examinations. Once excised, the target organs were washed with 0.1 M phosphate buffered saline (PBS, pH 7.4), fixed by immersion in 10% buffered formalin o/n at RT, embedded in paraffin (Embedding Center Leica EG1160, Leica Biosystem, Wetzlar, Germany), cross-sectioned at 3 μm thickness by a rotary microtome, mounted on slides, and stained by Hematoxylin and Eosin (HE). Finally, they were observed under a light microscope (Nikon Eclipse 50i, Melville, NY, USA). Representative images were captured with a digital camera (Nikon Digital Sight DS-2Mv).

3.16 Efficacy studies.

This study was conducted on five weeks old Female SCID mice (C.B-17/IcrHanHsd-Prkdcscid) were purchase from Envigo (Bresso, Italy). The animal was inoculated at 7 weeks old.

RPMI-8226 cancer cells were subcutaneously implanted in the left hip of animals ($10x10^6$ cells/animal in 200µl PBS) obtaining an attachment percentage of tumor cells about 70%. Before to start with the administrations, the tumor growth was monitored until it reached a volume corresponding to a weight between 200 and 500 mg size (about 30-40 days after tumor implantation). At that time mice were divided in 5 groups, randomized on tumor size. The animals were divided as following:

1. No Tumor (n=7)
2. Untreated Tumor (n=11)
3. Tumor + BTZ 1mg/Kg 1qwx5 (n=10)
4. Tumor + MSN-FOL 2 mg/kg 1qwx5 (n=10)
5. Tumor + FOL-MSN-BTZ 2 mg/kg 1qwx5 (n=9)

3.18 Drug preparation and administration.

BTZ, MSN-FOL and FOL-MSN-BTZ were all administered intravenously 10 ml/kg once a week for 5 weeks. BTZ solution was prepared as reported for MTD study. MSN-FOL 2 mg/Kg and MSN-FOL-BTZ 2 mg/Kg were contained in a glass vial and were suspended in physiological solution (18 mg in 6.2 ml of physiological solution for MSN-FOL-BTZ and 16 mg in 6.1 ml of physiological solution for MSN-FOL). Suspending the MSNs with magnetic stirrer for 13 minutes, a MSN concentration equal to 26.20 mg / kg was obtained. The desired volume has been take at half of the height of the liquid, without touching the bottom of the container, without waiting for the sample to settle.

3.19 Evaluation of tumor volume.

The growth of subcutaneous tumors was measured twice a week using a Vernier caliper. The length (L) and width (W) of the tumors was measured and their volumes were calculated using the formula (L x W2)/2.

3.20 Nerve conduction velocity.

The day after the last administration, neurophysiological recordings were performed in the caudal and digital nerves to determine peripheral sensory/motor nerve functional status, using an electromyography apparatus (Micromed Matrix Light, Mogliano Veneto-Treviso, Italy).

The caudal nerve conduction velocity (VDC) was evaluated by placing a couple of recording needle electrodes at the base of the tail and a couple of stimulating needle electrodes 3.5 cm distally to the recording points. Similarly, the digital nerve conduction velocity (NCV) was determined by placing the recording electrodes close to the ankle bone and the stimulating electrodes close to the fourth toe near the digital nerve, 1.3 cm distally to the recording points. Both the caudal VDCs and digital NCVs were calculated measuring the latency between the stimulus artefact and the onset of the first peak of the elicited response and the distance between the recording and the stimulating points.

The amplitude of the sensory potential was also measured. The intensity, duration and frequency of stimulation were set up in order to obtain optimal results. All the recordings were performed under standard conditions in a controlled temperature and the animals were under isofluorane anesthesia along the whole procedure.

3.21 Hematological and hematochemical analysis.

Hematological and hematochemical parameters were evaluated at the end of the treatment as described for MTD study.

3.22 Histopathological Analysis.

Animals were sacrificed when tumor volume exceed about the 10% of body weight. Histopathological analysis was conducted as described for MTD study. The antitumor effect was evaluated comparing the tumor size of mice treated with MSN-FOL-BTZ and with BTZ only with tumor untreated.

3.23 Animal care.

Animals used for MTD and efficacy studies were subjected to a physical examination (health check) shortly after arrival.

The care and husbandry of animals were in conformity with the institutional guidelines in compliance with national (D.L. n. 26/2014) and international laws and policies (EEC Council Directive 86/609, OJ L 358, 1, Dec.12, 1987; Guide for the Care and Use of Laboratory Animals, U.S. National Research Council, 1996).

3.24 Statistical evaluation.

The differences in body weight and tumor volume were statistically analyzed using a 2-step approach: a nonparametric One-way ANOVA test and the Tukey-Kramer post-test (significance level set at $p<0.05$). Nerve conduction studies and hematochemical/hematological parameters were statistically analyzed using a 2-step approach involving a nonparametric One-way ANOVA test, the Kruskall-Wallis and the post-test Dunn (significance level set at $p<0.05$).

REFERENCES

1. Piktel, E., et al., *Recent insights in nanotechnology-based drugs and formulations designed for effective anti-cancer therapy.* Journal of nanobiotechnology, 2016. **14**(1): p. 39.
2. Li, W.P., et al., *Formation of oligonucleotide-gated silica shell-coated Fe(3)O(4)-Au core-shell nanotrisoctahedra for magnetically targeted and near-infrared light-responsive theranostic platform.* J Am Chem Soc, 2014. **136**(28): p. 10062-75.
3. Zhou, Y., et al., *Mesoporous silica nanoparticles for drug and gene delivery.* Acta pharmaceutica sinica B, 2018. **8**(2): p. 165-177.
4. Pasqua, L., et al., *Mesoporous silica nanoparticles in cancer therapy: Relevance of the targeting function.* Mini reviews in medicinal chemistry, 2016. **16**(9): p. 743-753.
5. Chen, H., et al., *Stepwise-acid-active organic/inorganic hybrid drug delivery system for cancer therapy.* Colloids Surf B Biointerfaces, 2018. **167**: p. 407-414.
6. Mai, W.X. and H. Meng, *Mesoporous silica nanoparticles: a multifunctional nano therapeutic system.* Integrative Biology, 2012. **5**(1): p. 19-28.
7. Lee, J.E., et al., *Multifunctional mesoporous silica nanocomposite nanoparticles for theranostic applications.* Accounts of chemical research, 2011. **44**(10): p. 893-902.
8. Nakamura, T., et al., *Mesoporous silica nanoparticles for 19 F magnetic resonance imaging, fluorescence imaging, and drug delivery.* Chemical science, 2015. **6**(3): p. 1986-1990.
9. Slita, A., et al., *Characterization of modified mesoporous silica nanoparticles as vectors for siRNA delivery.* Asian journal of pharmaceutical sciences, 2018. **13**(6): p. 592-599.
10. Zhang, B., et al., *Biodegradable hybrid mesoporous silica nanoparticles for gene/chemo-synergetic therapy of breast cancer.* J Biomater Appl, 2019. **33**(10): p. 1382-1393.
11. Nigro, A., et al., *Dealing with skin and blood-brain barriers: The unconventional challenges of mesoporous silica nanoparticles.* Pharmaceutics, 2018. **10**(4): p. 250.
12. Narayan, R., et al., *Mesoporous silica nanoparticles: A comprehensive review on synthesis and recent advances.* Pharmaceutics, 2018. **10**(3): p. 118.
13. Llopis-Lorente, A., et al., *Stimulus-responsive nanomotors based on gated enzyme-powered Janus Au-mesoporous silica nanoparticles for enhanced cargo delivery.* Chem Commun (Camb), 2019. **55**(87): p. 13164-13167.
14. Hasanzadeh, M., et al., *Mesoporous (organo) silica decorated with magnetic nanoparticles as a reusable nanoadsorbent for arsenic removal from water samples.* Environ Technol, 2015. **36**(1-4): p. 36-44.
15. Moghal, J., et al., *High-performance, single-layer antireflective optical coatings comprising mesoporous silica nanoparticles.* ACS Appl Mater Interfaces, 2012. **4**(2): p. 854-9.
16. Keasberry, N.A., C.W. Yapp, and A. Idris, *Mesoporous Silica Nanoparticles as a Carrier Platform for Intracellular Delivery of Nucleic Acids.* Biochemistry (Mosc), 2017. **82**(6): p. 655-662.
17. Cha, W., et al., *Mesoporous Silica Nanoparticles as Carriers for Intracellular Delivery of Nucleic Acids and Subsequent Therapeutic Applications.* Molecules, 2017. **22**(5).
18. Sun, X., et al., *Folic Acid and PEI Modified Mesoporous Silica for Targeted Delivery of Curcumin.* Pharmaceutics, 2019. **11**(9).
19. Morelli, C., et al., *PEG-templated mesoporous silica nanoparticles exclusively target cancer cells.* Nanoscale, 2011. **3**(8): p. 3198-3207.
20. Jafari, S., et al., *Mesoporous silica nanoparticles for therapeutic/diagnostic applications.* Biomedicine & Pharmacotherapy, 2019. **109**: p. 1100-1111.

21. Durfee, P.N., et al., *Mesoporous Silica Nanoparticle-Supported Lipid Bilayers (Protocells) for Active Targeting and Delivery to Individual Leukemia Cells.* ACS Nano, 2016. **10**(9): p. 8325-45.
22. Zhou, S., et al., *Intracellular pH-responsive and rituximab-conjugated mesoporous silica nanoparticles for targeted drug delivery to lymphoma B cells.* J Exp Clin Cancer Res, 2017. **36**(1): p. 24.
23. Buhmann, R., et al., *Immunotherapy with FBTA05 (Bi20), a trifunctional bispecific anti-CD3 x anti-CD20 antibody and donor lymphocyte infusion (DLI) in relapsed or refractory B-cell lymphoma after allogeneic stem cell transplantation: study protocol of an investigator-driven, open-label, non-randomized, uncontrolled, dose-escalating Phase I/II-trial.* J Transl Med, 2013. **11**: p. 160.
24. Sanchez-Salcedo, S., et al., *Mesoporous core-shell silica nanoparticles with anti-fouling properties for ovarian cancer therapy.* Chemical Engineering Journal, 2018. **340**: p. 114-124.
25. Paris, J.L., et al., *Decidua-derived mesenchymal stem cells as carriers of mesoporous silica nanoparticles. In vitro and in vivo evaluation on mammary tumors.* Acta biomaterialia, 2016. **33**: p. 275-282.
26. Gao, Y., et al., *Tracking mesenchymal stem cell tumor-homing using fluorescent silica nanoparticles.* Journal of Materials Chemistry B, 2015. **3**(7): p. 1245-1253.
27. Lin, Y.-S. and C.L. Haynes, *Impacts of mesoporous silica nanoparticle size, pore ordering, and pore integrity on hemolytic activity.* Journal of the American Chemical Society, 2010. **132**(13): p. 4834-4842.
28. Benezra, M., et al., *Multimodal silica nanoparticles are effective cancer-targeted probes in a model of human melanoma.* The Journal of clinical investigation, 2011. **121**(7): p. 2768-2780.
29. Phillips, E., et al., *Clinical translation of an ultrasmall inorganic optical-PET imaging nanoparticle probe.* Science translational medicine, 2014. **6**(260): p. 260ra149-260ra149.
30. Tang, W., et al., *Emerging blood–brain-barrier-crossing nanotechnology for brain cancer theranostics.* Chemical Society Reviews, 2019.
31. Chen, L., X. Zhou, and C. He, *Mesoporous silica nanoparticles for tissue-engineering applications.* Wiley Interdiscip Rev Nanomed Nanobiotechnol, 2019. **11**(6): p. e1573.
32. Meynen, V., P. Cool, and E.F. Vansant, *Verified syntheses of mesoporous materials.* Microporous and mesoporous materials, 2009. **125**(3): p. 170-223.
33. Zhou, Y., et al., *Mesoporous silica nanoparticles for drug and gene delivery.* Acta Pharm Sin B, 2018. **8**(2): p. 165-177.
34. Yamamoto, E. and K. Kuroda, *Preparation and Controllability of Mesoporous Silica Nanoparticles.* Enzymes, 2018. **44**: p. 1-10.
35. She, X., et al., *Tailored Mesoporous Silica Nanoparticles for Controlled Drug Delivery: Platform Fabrication, Targeted Delivery, and Computational Design and Analysis.* Mini Rev Med Chem, 2018. **18**(11): p. 976-989.
36. Chen, Y., H. Chen, and J. Shi, *Drug delivery/imaging multifunctionality of mesoporous silica-based composite nanostructures.* Expert opinion on drug delivery, 2014. **11**(6): p. 917-930.
37. Watermann, A. and J. Brieger, *Mesoporous Silica Nanoparticles as Drug Delivery Vehicles in Cancer.* Nanomaterials (Basel), 2017. **7**(7).
38. Shen, J., et al., *Assessment of folate receptor-β expression in human neoplastic tissues.* Oncotarget, 2015. **6**(16): p. 14700.
39. Cheung, A., et al., *Targeting folate receptor alpha for cancer treatment.* Oncotarget, 2016. **7**(32): p. 52553.

40. Farran, B., et al., *Folate-targeted immunotherapies: Passive and active strategies for cancer.* Cytokine Growth Factor Rev, 2019. **45**: p. 45-52.
41. Li, N., et al., *The utility of folate receptor-positive circulating tumor cell in cancer diagnosis in the elderly population.* Cancer Manag Res, 2019. **11**: p. 4097-4107.
42. Ding, Z., et al., *Increase in folate receptor alpha expression in nonfunctional pituitary adenomas.* Turk Neurosurg, 2015. **25**(2): p. 298-304.
43. Assaraf, Y.G., C.P. Leamon, and J.A. Reddy, *The folate receptor as a rational therapeutic target for personalized cancer treatment.* Drug Resist Updat, 2014. **17**(4-6): p. 89-95.
44. Leone, J.P., et al., *Expression of high affinity folate receptor in breast cancer brain metastasis.* Oncotarget, 2015. **6**(30): p. 30327-33.
45. Poh, S., et al., *Selective liposome targeting of folate receptor positive immune cells in inflammatory diseases.* Nanomedicine, 2018. **14**(3): p. 1033-1043.
46. Heo, G.S., et al., *Folate Receptor alpha-Targeted (89)Zr-M9346A Immuno-PET for Image-Guided Intervention with Mirvetuximab Soravtansine in Triple-Negative Breast Cancer.* Mol Pharm, 2019. **16**(9): p. 3996-4006.
47. Kelemen, L.E., *The role of folate receptor α in cancer development, progression and treatment: cause, consequence or innocent bystander?* International journal of cancer, 2006. **119**(2): p. 243-250.
48. Shen, J., et al., *Assessment of folate receptor alpha and beta expression in selection of lung and pancreatic cancer patients for receptor targeted therapies.* Oncotarget, 2018. **9**(4): p. 4485.
49. Fernández, M., F. Javaid, and V. Chudasama, *Advances in targeting the folate receptor in the treatment/imaging of cancers.* Chemical science, 2018. **9**(4): p. 790-810.
50. Liu, X., et al., *A dual responsive targeted drug delivery system based on smart polymer coated mesoporous silica for laryngeal carcinoma treatment.* New Journal of Chemistry, 2014. **38**(10): p. 4830-4836.
51. Zhang, H., et al., *Dual Functional Mesoporous Silicon Nanoparticles Enhance the Radiosensitivity of VPA in Glioblastoma.* Transl Oncol, 2017. **10**(2): p. 229-240.
52. Frigerio, B., et al., *Folate receptors and transporters: biological role and diagnostic/therapeutic targets in cancer and other diseases*. 2019, BioMed Central.
53. Maldonado-Báez, L., C. Williamson, and J.G. Donaldson, *Clathrin-independent endocytosis: a cargo-centric view.* Experimental cell research, 2013. **319**(18): p. 2759-2769.
54. Doherty, G.J. and R. Lundmark, *GRAF1-dependent endocytosis*. 2009, Portland Press Ltd.
55. Clark, A.J. and M.E. Davis, *Increased brain uptake of targeted nanoparticles by adding an acid-cleavable linkage between transferrin and the nanoparticle core.* Proceedings of the National Academy of Sciences, 2015. **112**(40): p. 12486-12491.
56. Salzano, G., et al., *Transferrin-targeted nanoparticles containing zoledronic acid as a potential tool to inhibit glioblastoma growth.* Journal of biomedical nanotechnology, 2016. **12**(4): p. 811-830.
57. Genta, I., et al., *GE11 peptide as an active targeting agent in antitumor therapy: A minireview.* Pharmaceutics, 2018. **10**(1): p. 2.
58. Sabio, R.M., et al., *New insights towards mesoporous silica nanoparticles as a technological platform for chemotherapeutic drugs delivery.* Int J Pharm, 2019. **564**: p. 379-409.
59. Danhier, F., A. Le Breton, and V.r. Préat, *RGD-based strategies to target alpha (v) beta (3) integrin in cancer therapy and diagnosis.* Molecular pharmaceutics, 2012. **9**(11): p. 2961-2973.

60. Majumder, P., *Integrin-mediated delivery of drugs and nucleic acids for anti-angiogenic cancer therapy: current landscape and remaining challenges.* Bioengineering, 2018. **5**(4): p. 76.
61. Lupold, S.E., *Aptamers and apple pies: a mini-review of PSMA aptamers and lessons from Donald S. Coffey.* American journal of clinical and experimental urology, 2018. **6**(2): p. 78.
62. Singh, R. and D. Bandyopadhyay, *MUC1: a target molecule for cancer therapy.* Cancer biology & therapy, 2007. **6**(4): p. 481-486.
63. Li, Y. and P. Cozzi, *MUC1 is a promising therapeutic target for prostate cancer therapy.* Current cancer drug targets, 2007. **7**(3): p. 259-271.
64. Chen, C., et al., *The biology and role of CD44 in cancer progression: therapeutic implications.* Journal of hematology & oncology, 2018. **11**(1): p. 64.
65. Kim, J.H., et al., *Hyaluronic Acid-Based Nanomaterials for Cancer Therapy.* Polymers (Basel), 2018. **10**(10).
66. Doi, T., et al., *Safety, pharmacokinetics, and antitumour activity of trastuzumab deruxtecan (DS-8201), a HER2-targeting antibody-drug conjugate, in patients with advanced breast and gastric or gastro-oesophageal tumours: a phase 1 dose-escalation study.* Lancet Oncol, 2017. **18**(11): p. 1512-1522.
67. Zhuo, H., et al., *Efficient targeted tumor imaging and secreted endostatin gene delivery by anti-CD105 immunoliposomes.* J Exp Clin Cancer Res, 2018. **37**(1): p. 42.
68. Caltagirone, C., et al., *Silica-based nanoparticles: a versatile tool for the development of efficient imaging agents.* Chem Soc Rev, 2015. **44**(14): p. 4645-71.
69. Varshosaz, J., et al., *LHRH Targeted Chonderosomes of Mitomycin C In Breast Cancer: An In Vitro / In Vivo Study.* Anticancer Agents Med Chem, 2019.
70. Cheung, L.W., et al., *Targeting gonadotropin-releasing hormone receptor inhibits the early step of ovarian cancer metastasis by modulating tumor-mesothelial adhesion.* Mol Ther, 2013. **21**(1): p. 78-90.
71. Roy, J., et al., *Targeted Tubulysin B Hydrazide Conjugate for the Treatment of Luteinizing Hormone-Releasing Hormone Receptor-Positive Cancers.* Bioconjug Chem, 2018. **29**(7): p. 2208-2214.
72. Schally, A.V., N.L. Block, and F.G. Rick, *Discovery of LHRH and development of LHRH analogs for prostate cancer treatment.* Prostate, 2017. **77**(9): p. 1036-1054.
73. Hao, D., et al., *(99m)Tc-LHRH in tumor receptor imaging.* Oncol Lett, 2017. **14**(1): p. 569-578.
74. Sivarajakumar, R., et al., *Nanoparticles for the Treatment of Lung Cancers.* Journal of Young Pharmacists, 2018. **10**(3): p. 276-281.
75. Qiao, Y., et al., *Stimuli-responsive nanotherapeutics for precision drug delivery and cancer therapy.* Wiley Interdiscip Rev Nanomed Nanobiotechnol, 2019. **11**(1): p. e1527.
76. Liu, D., et al., *The Smart Drug Delivery System and Its Clinical Potential.* Theranostics, 2016. **6**(9): p. 1306-23.
77. Chen, H., et al., *Dual-pH-sensitive mesoporous silica nanoparticle-based drug delivery system for tumor-triggered intracellular drug release.* Journal of Materials Science, 2018. **53**(15): p. 10653-10665.
78. Cheng, C.A., et al., *Supramolecular Nanomachines as Stimuli-Responsive Gatekeepers on Mesoporous Silica Nanoparticles for Antibiotic and Cancer Drug Delivery.* Theranostics, 2019. **9**(11): p. 3341-3364.
79. Song, Y., et al., *Mesoporous silica nanoparticles for stimuli-responsive controlled drug delivery: advances, challenges, and outlook.* Int J Nanomedicine, 2017. **12**: p. 87-110.

80. Yu, G. and X. Chen, *Host-Guest Chemistry in Supramolecular Theranostics.* Theranostics, 2019. **9**(11): p. 3041-3074.
81. Chang, B., et al., *Thermo and pH dual responsive, polymer shell coated, magnetic mesoporous silica nanoparticles for controlled drug release.* Journal of Materials Chemistry, 2011. **21**(25): p. 9239.
82. Kim, K., et al., *Hyaluronic Acid-Coated Nanomedicine for Targeted Cancer Therapy.* Pharmaceutics, 2019. **11**(7).
83. Mas, N., et al., *Enzyme-responsive silica mesoporous supports capped with azopyridinium salts for controlled delivery applications.* Chemistry, 2013. **19**(4): p. 1346-56.
84. Tan, J., et al., *Aptamer-Functionalized Fluorescent Silica Nanoparticles for Highly Sensitive Detection of Leukemia Cells.* Nanoscale Res Lett, 2016. **11**(1): p. 298.
85. Li, R., et al., *Redox dual-stimuli responsive drug delivery systems for improving tumor-targeting ability and reducing adverse side effects.* Asian Journal of Pharmaceutical Sciences, 2019.
86. Bansal, A. and M.C. Simon, *Glutathione metabolism in cancer progression and treatment resistance.* J Cell Biol, 2018. **217**(7): p. 2291-2298.
87. Nunes, S.C. and J. Serpa, *Glutathione in Ovarian Cancer: A Double-Edged Sword.* Int J Mol Sci, 2018. **19**(7).
88. Men, W., et al., *Fabrication Of Dual pH/redox-Responsive Lipid-Polymer Hybrid Nanoparticles For Anticancer Drug Delivery And Controlled Release.* Int J Nanomedicine, 2019. **14**: p. 8001-8011.
89. Peng, W., et al., *Core-Shell Structure Design of Hollow Mesoporous Silica Nanospheres Based on Thermo-Sensitive PNIPAM and pH-Responsive Catechol-Fe(3+) Complex.* Polymers (Basel), 2019. **11**(11).
90. Baca, M., et al., *Physicochemical and photocatalytic characterization of mesoporous carbon/titanium dioxide spheres.* Diamond and Related Materials, 2019: p. 107551.
91. He, D.G.H., X.; Wang, K.; Cao, J.; Zhao, Y., *A Light-Responsive Reversible Molecule-Gated System Using Thymine-Modified Mesoporous Silica Nanoparticles.* Langmuir, 2012. **28** (8): p. 4003-4008.
92. Zhang, R., et al., *Versatile triggered release of multiple molecules from cyclodextrin-modified gold-gated mesoporous silica nanocontainers.* ACS Appl Mater Interfaces, 2014. **6**(13): p. 9932-6.
93. Wen, J., et al., *Diverse gatekeepers for mesoporous silica nanoparticle based drug delivery systems.* Chem Soc Rev, 2017. **46**(19): p. 6024-6045.
94. Shen, L., B. Li, and Y. Qiao, *Fe(3)O(4) Nanoparticles in Targeted Drug/Gene Delivery Systems.* Materials (Basel), 2018. **11**(2).
95. Raza, A., et al., *Endogenous and Exogenous Stimuli-Responsive Drug Delivery Systems for Programmed Site-Specific Release.* Molecules, 2019. **24**(6).
96. Zhou S, S.H., Liub B and Du X, , *Integration of simultaneous and cascade release of two drugs into smart single nanovehicles based on DNA-gated mesoporous silica nanoparticles.* Chem. Sci., 2014. **5**: p. 4424-4433.
97. Huang, D.M., et al., *Highly efficient cellular labeling of mesoporous nanoparticles in human mesenchymal stem cells: implication for stem cell tracking.* FASEB J, 2005. **19**(14): p. 2014-6.
98. Ekkapongpisit, M., et al., *Labeling and exocytosis of secretory compartments in RBL mastocytes by polystyrene and mesoporous silica nanoparticles.* Int J Nanomedicine, 2012. **7**: p. 1829-40.
99. Yan, Y., et al., *Particles on the move: intracellular trafficking and asymmetric mitotic partitioning of nanoporous polymer particles.* ACS Nano, 2013. **7**(6): p. 5558-67.

100. Fisichella, M., et al., *Uptake of functionalized mesoporous silica nanoparticles by human cancer cells.* J Nanosci Nanotechnol, 2010. **10**(4): p. 2314-24.
101. Slowing, II, et al., *Exocytosis of mesoporous silica nanoparticles from mammalian cells: from asymmetric cell-to-cell transfer to protein harvesting.* Small, 2011. **7**(11): p. 1526-32.
102. Yanes, R.E., et al., *Involvement of lysosomal exocytosis in the excretion of mesoporous silica nanoparticles and enhancement of the drug delivery effect by exocytosis inhibition.* Small, 2013. **9**(5): p. 697-704.
103. Li, H., et al., *Evaluation of biomimetically synthesized mesoporous silica nanoparticles as drug carriers: Structure, wettability, degradation, biocompatibility and brain distribution.* Mater Sci Eng C Mater Biol Appl, 2019. **94**: p. 453-464.
104. Paris, J.L., et al., *Tuning mesoporous silica dissolution in physiological environments: a review.* Journal of Materials Science, 2017. **52**(15): p. 8761-8771.
105. Rajkumar, S.V., *Multiple myeloma: Every year a new standard?* Hematol Oncol, 2019. **37 Suppl 1**: p. 62-65.
106. Mohan, M., A. Matin, and F.E. Davies, *Update on the optimal use of bortezomib in the treatment of multiple myeloma.* Cancer Manag Res, 2017. **9**: p. 51-63.
107. Goldschmidt, H., et al., *Navigating the treatment landscape in multiple myeloma: which combinations to use and when?* Ann Hematol, 2019. **98**(1): p. 1-18.
108. Fairfield, H., et al., *Multiple myeloma in the marrow: pathogenesis and treatments.* Ann N Y Acad Sci, 2016. **1364**: p. 32-51.
109. Masarwi, M., et al., *Multiple Myeloma and Fatty Acid Metabolism.* JBMR Plus, 2019. **3**(3): p. e10173.
110. Kawano, Y., et al., *Multiple Myeloma and the Immune Microenvironment.* Curr Cancer Drug Targets, 2017. **17**(9): p. 806-818.
111. Weaver, C.J. and J.D. Tariman, *Multiple Myeloma Genomics: A Systematic Review.* Semin Oncol Nurs, 2017. **33**(3): p. 237-253.
112. Lionetti, M. and A. Neri, *Utilizing next-generation sequencing in the management of multiple myeloma.* Expert Rev Mol Diagn, 2017. **17**(7): p. 653-663.
113. Hungria, V.T.M., et al., *New proteasome inhibitors in the treatment of multiple myeloma.* Hematol Transfus Cell Ther, 2019. **41**(1): p. 76-83.
114. Mhaskar, R. and B. Djulbegovic, *Bisphosphonates for Patients Diagnosed With Multiple Myeloma.* Jama, 2018. **320**(14): p. 1483-1484.
115. Kumar, S.K., et al., *Multiple myeloma.* Nat Rev Dis Primers, 2017. **3**: p. 17046.
116. Chim, C.S., et al., *Management of relapsed and refractory multiple myeloma: novel agents, antibodies, immunotherapies and beyond.* Leukemia, 2018. **32**(2): p. 252-262.
117. Abramson, H.N., *The Multiple Myeloma Drug Pipeline-2018: A Review of Small Molecules and Their Therapeutic Targets.* Clin Lymphoma Myeloma Leuk, 2018. **18**(9): p. 611-627.
118. Suraweera, A., K.J. O'Byrne, and D.J. Richard, *Combination therapy with histone deacetylase inhibitors (HDACi) for the treatment of cancer: achieving the full therapeutic potential of HDACi.* Frontiers in oncology, 2018. **8**: p. 92.
119. Landowski, T.H., et al., *Mitochondrial-mediated disregulation of Ca2+ is a critical determinant of Velcade (PS-341/bortezomib) cytotoxicity in myeloma cell lines.* Cancer Res, 2005. **65**(9): p. 3828-36.
120. Luczkowska, K., et al., *Pathophysiology of drug-induce peripheral neuropathy in patients with multiple myeloma.* J Physiol Pharmacol, 2018. **69**(2).
121. Meregalli, C., et al., *Bortezomib-induced peripheral neurotoxicity in human multiple myeloma-bearing mice.* J Biol Regul Homeost Agents, 2015. **29**(1): p. 115-24.

122. Carozzi, V., A. Canta, and A. Chiorazzi, *Chemotherapy-induced peripheral neuropathy: what do we know about mechanisms?* Neuroscience letters, 2015. **596**: p. 90-107.
123. Eldridge, S., L. Guo, and J. Hamre III, *A Comparative Review of Chemotherapy-Induced Peripheral Neuropathy in In Vivo and In Vitro Models.* Toxicologic pathology, 2020: p. 0192623319861937.
124. Luczkowska, K., et al., *Pathophysiology of drug-induce peripheral neuropathy in patients with multiple myeloma.* J. Physiol. Pharmacol, 2018. **69**(2): p. 165-172.
125. Alé, A., A.A. Argyriou, and J. Bruna, *Sphingolipid metabolism products: potential new players in the pathogenesis of bortezomib-induced neuropathic pain.* Annals of translational medicine, 2018. **6**(Suppl 1).
126. Meregalli, C., et al., *Evaluation of tubulin polymerization and chronic inhibition of proteasome as citotoxicity mechanisms in bortezomib-induced peripheral neuropathy.* Cell Cycle, 2014. **13**(4): p. 612-621.
127. Staff, N.P., et al., *Bortezomib alters microtubule polymerization and axonal transport in rat dorsal root ganglion neurons.* Neurotoxicology, 2013. **39**: p. 124-131.
128. Meregalli, C., *An Overview of Bortezomib-Induced Neurotoxicity.* Toxics, 2015. **3**(3): p. 294-303.
129. Sung, M.H., et al., *Dynamic effect of bortezomib on nuclear factor-kappaB activity and gene expression in tumor cells.* Mol Pharmacol, 2008. **74**(5): p. 1215-22.
130. Muchtar, E., M.A. Gertz, and H. Magen, *A practical review on carfilzomib in multiple myeloma.* Eur J Haematol, 2016. **96**(6): p. 564-77.
131. Mushtaq, A., et al., *Efficacy and toxicity profile of carfilzomib based regimens for treatment of multiple myeloma: A systematic review.* Crit Rev Oncol Hematol, 2018. **125**: p. 1-11.
132. Shah, C., et al., *Cardiotoxicity associated with carfilzomib: systematic review and meta-analysis.* Leuk Lymphoma, 2018. **59**(11): p. 2557-2569.
133. Richardson, P.G., et al., *New developments in the management of relapsed/refractory multiple myeloma - the role of ixazomib.* J Blood Med, 2017. **8**: p. 107-121.
134. Moreau, P., et al., *Oral Ixazomib, Lenalidomide, and Dexamethasone for Multiple Myeloma.* N Engl J Med, 2016. **374**(17): p. 1621-34.
135. Sherbenou, D.W., T.M. Mark, and P. Forsberg, *Monoclonal Antibodies in Multiple Myeloma: A New Wave of the Future.* Clin Lymphoma Myeloma Leuk, 2017. **17**(9): p. 545-554.
136. *<Monoclonal Ab in MM Richardson.pdf>.*
137. Palumbo, A. and P. Sonneveld, *Preclinical and clinical evaluation of elotuzumab, a SLAMF7-targeted humanized monoclonal antibody in development for multiple myeloma.* Expert Rev Hematol, 2015. **8**(4): p. 481-91.
138. Frerichs, K.A., et al., *CD38-targeting antibodies in multiple myeloma: mechanisms of action and clinical experience.* Expert Rev Clin Immunol, 2018. **14**(3): p. 197-206.
139. *Multiple myeloma: 2018 update on diagnosis, risk-stratification, and management.* Am J Hematol, 2018. **93**(8): p. 981-1114.
140. Zamagni, E., et al., *Anti-CD38 and anti-SLAMF7: the future of myeloma immunotherapy.* Expert Rev Hematol, 2018. **11**(5): p. 423-435.
141. Wang, Y., et al., *Elotuzumab for the treatment of multiple myeloma.* J Hematol Oncol, 2016. **9**(1): p. 55.
142. Blair, H.A., *Daratumumab: A Review in Relapsed and/or Refractory Multiple Myeloma.* Drugs, 2017. **77**(18): p. 2013-2024.
143. Dimopoulos, M.A., et al., *Daratumumab, lenalidomide, and dexamethasone for multiple myeloma.* New England Journal of Medicine, 2016. **375**(14): p. 1319-1331.

144. Van De Donk, N.W. and S.Z. Usmani, *CD38 antibodies in multiple myeloma: mechanisms of action and modes of resistance.* Frontiers in immunology, 2018. **9**: p. 2134.
145. Krejcik, J., et al., *Daratumumab depletes CD38+ immune regulatory cells, promotes T-cell expansion, and skews T-cell repertoire in multiple myeloma.* Blood, The Journal of the American Society of Hematology, 2016. **128**(3): p. 384-394.
146. Giuliani, N. and F. Malavasi, *The immunotherapy in multiple myeloma: honoring the past, studying the present, and trying to design the future.* Frontiers in immunology, 2019. **10**: p. 1945.
147. Sarıman, M., et al., *Investigation of Gene Expressions of Myeloma Cells in the Bone Marrow of Multiple Myeloma Patients by Transcriptome Analysis.* Balkan medical journal, 2019. **36**(1): p. 23.
148. Morandi, F., et al., *CD38: a target for immunotherapeutic approaches in multiple myeloma.* Frontiers in immunology, 2018. **9**: p. 2722.
149. Krejcik, J., et al., *Monocytes and Granulocytes Reduce CD38 Expression Levels on Myeloma Cells in Patients Treated with Daratumumab.* Clin Cancer Res, 2017. **23**(24): p. 7498-7511.
150. Nijhof, I., et al., *CD38 levels are associated with response and complement inhibitors contribute to resistance in myeloma patients treated with daratumumab.* Blood, 2016. **128**: p. 959-970.
151. Zhang, T.-t., et al., *Cost-effectiveness of daratumumab-based triplet therapies in patients with relapsed or refractory multiple myeloma.* Clinical therapeutics, 2018. **40**(7): p. 1122-1139.
152. Spencer, A., et al., *Daratumumab plus bortezomib and dexamethasone versus bortezomib and dexamethasone in relapsed or refractory multiple myeloma: updated analysis of CASTOR.* Haematologica, 2018. **103**(12): p. 2079-2087.
153. Bjorklund, C.C., et al., *CC-122 is a cereblon modulating agent that is active in lenalidomide-resistant and lenalidomide/dexamethasone-double-resistant multiple myeloma pre-clinical models*. 2016, Am Soc Hematology.
154. Matyskiela, M.E., et al., *A cereblon modulator (CC-220) with improved degradation of Ikaros and Aiolos.* Journal of medicinal chemistry, 2017. **61**(2): p. 535-542.
155. Dhakal, B., et al., *Phase I/II trial of bendamustine, ixazomib, and dexamethasone in relapsed/refractory multiple myeloma.* Blood Cancer J, 2019. **9**(8): p. 56.
156. Wickstrom, M., et al., *Melflufen - a peptidase-potentiated alkylating agent in clinical trials.* Oncotarget, 2017. **8**(39): p. 66641-66655.
157. Imai, Y., Y. Maru, and J. Tanaka, *Action mechanisms of histone deacetylase inhibitors in the treatment of hematological malignancies.* Cancer Sci, 2016. **107**(11): p. 1543-1549.
158. Harada, T., *[Role of HDAC isoforms and development of treatment of multiple myeloma using isoform-specific HDAC inhibitors].* Rinsho Ketsueki, 2019. **60**(9): p. 1265-1274.
159. Moore, D.C., J.R. Arnall, and R.D. Harvey, *Incidence and management of adverse events associated with panobinostat in the treatment of relapsed/refractory multiple myeloma.* J Oncol Pharm Pract, 2019. **25**(3): p. 613-622.
160. Puvvada, S.D., et al., *A phase II study of belinostat (PXD101) in relapsed and refractory aggressive B-cell lymphomas: SWOG S0520.* Leuk Lymphoma, 2016. **57**(10): p. 2359-69.
161. Gao, C., et al., *Inhibition of Heat Shock Protein 90 as a Novel Platform for the Treatment of Cancer.* Curr Pharm Des, 2019. **25**(8): p. 849-855.
162. Rossi, A., et al., *The proteasome inhibitor bortezomib is a potent inducer of zinc finger AN1-type domain 2a gene expression: role of heat shock factor 1 (HSF1)-heat shock factor 2 (HSF2) heterocomplexes.* J Biol Chem, 2014. **289**(18): p. 12705-15.

163. Xiong, T., et al., *PJ34, a poly(ADP-ribose) polymerase (PARP) inhibitor, reverses melphalan-resistance and inhibits repair of DNA double-strand breaks by targeting the FA/BRCA pathway in multidrug resistant multiple myeloma cell line RPMI8226/R.* Int J Oncol, 2015. **46**(1): p. 223-32.
164. Manier, S., et al., *Inhibiting the oncogenic translation program is an effective therapeutic strategy in multiple myeloma.* Sci Transl Med, 2017. **9**(389).
165. Nijhof, I.S., et al., *Current and New Therapeutic Strategies for Relapsed and Refractory Multiple Myeloma: An Update.* Drugs, 2018. **78**(1): p. 19-37.
166. Allegra, A., et al., *Selective Inhibitors of Nuclear Export in the Treatment of Hematologic Malignancies.* Clin Lymphoma Myeloma Leuk, 2019.
167. Tron, A.E., et al., *Discovery of Mcl-1-specific inhibitor AZD5991 and preclinical activity in multiple myeloma and acute myeloid leukemia.* Nat Commun, 2018. **9**(1): p. 5341.
168. D'Agostino, M., et al., *Novel investigational drugs active as single agents in multiple myeloma.* Expert Opin Investig Drugs, 2017. **26**(6): p. 699-711.
169. Soumerai, J.D., et al., *The PARP Inhibitor Veliparib Can Be Safely Added to Bendamustine and Rituximab and Has Preliminary Evidence of Activity in B-Cell Lymphoma.* Clin Cancer Res, 2017. **23**(15): p. 4119-4126.
170. Xu, A., A. Mazumder, and J.A. Borowiec, *Cell line-dependent synergy between the PARP inhibitor veliparib and the proteasome inhibitor bortezomib in the killing of myeloma cells*. 2015, Am Soc Hematology.
171. Bradbury, M.S., et al., *Intraoperative mapping of sentinel lymph node metastases using a clinically translated ultrasmall silica nanoparticle.* Wiley Interdisciplinary Reviews: Nanomedicine and Nanobiotechnology, 2016. **8**(4): p. 535-553.
172. Watermann, A. and J. Brieger, *Mesoporous silica nanoparticles as drug delivery vehicles in cancer.* Nanomaterials, 2017. **7**(7): p. 189.
173. Pasqua, L., et al., *Preparation of bifunctional hybrid mesoporous silica potentially useful for drug targeting.* Microporous and mesoporous materials, 2007. **103**(1-3): p. 166-173.
174. Pasqua, L., et al., *Engineered Stimuli-Responsive Nanoparticles for the Interaction With Biological Structures*, in *Chemistry of Silica and Zeolite-Based Materials*. 2019, Elsevier. p. 399-412.
175. Morelli, C., et al., *PEG-templated mesoporous silica nanoparticles exclusively target cancer cells.* Nanoscale, 2011. **3**(8): p. 3198-3207.
176. Costa, F., B. Dalla Palma, and N. Giuliani, *CD38 Expression by Myeloma Cells and Its Role in the Context of Bone Marrow Microenvironment: Modulation by Therapeutic Agents.* Cells, 2019. **8**(12): p. 1632.
177. Thornberry, N.A. and Y. Lazebnik, *Caspases: Enemies within.* Science, 1998. **281**(5381): p. 1312-1316.
178. Mitsiades, N., et al., *Molecular sequelae of proteasome inhibition in human multiple myeloma cells.* Proc Natl Acad Sci U S A, 2002. **99**(22): p. 14374-9.
179. Tang, D., et al., *The molecular machinery of regulated cell death.* Cell Research, 2019. **29**(5): p. 347-364.
180. Jouan-Lanhouet, S., et al., *TRAIL induces necroptosis involving RIPK1/RIPK3-dependent PARP-1 activation.* Cell Death Differ, 2012. **19**(12): p. 2003-14.
181. Sosna, J., et al., *TNF-induced necroptosis and PARP-1-mediated necrosis represent distinct routes to programmed necrotic cell death.* Cell Mol Life Sci, 2014. **71**(2): p. 331-48.
182. Moriwaki, K. and F.K. Chan, *Regulation of RIPK3- and RHIM-dependent Necroptosis by the Proteasome.* J Biol Chem, 2016. **291**(11): p. 5948-59.

183. Burns, J.S. and G. Manda, *Metabolic Pathways of the Warburg Effect in Health and Disease: Perspectives of Choice, Chain or Chance.* Int J Mol Sci, 2017. **18**(12).
184. Winer, L.S.P. and M. Wu, *Rapid analysis of glycolytic and oxidative substrate flux of cancer cells in a microplate.* PloS one, 2014. **9**(10): p. e109916.
185. Flatters, S., P.M. Dougherty, and L. Colvin, *Clinical and preclinical perspectives on chemotherapy-induced peripheral neuropathy (CIPN): a narrative review.* BJA: British Journal of Anaesthesia, 2017. **119**(4): p. 737-749.
186. Fan, S., et al., *PINK1-Dependent Mitophagy Regulates the Migration and Homing of Multiple Myeloma Cells via the MOB1B-Mediated Hippo-YAP/TAZ Pathway.* Advanced Science, 2020: p. 1900860.
187. Dalva-Aydemir, S., et al., *Targeting the metabolic plasticity of multiple myeloma with FDA-approved ritonavir and metformin.* Clinical Cancer Research, 2015. **21**(5): p. 1161-1171.
188. Lipchick, B.C., E.E. Fink, and M.A. Nikiforov, *Oxidative stress and proteasome inhibitors in multiple myeloma.* Pharmacological research, 2016. **105**: p. 210-215.
189. De Santis, M.C., et al., *Signaling pathways regulating redox balance in cancer metabolism.* Frontiers in oncology, 2018. **8**: p. 126.
190. Maharjan, S., et al., *Mitochondrial impairment triggers cytosolic oxidative stress and cell death following proteasome inhibition.* Scientific reports, 2014. **4**: p. 5896.
191. Chong, W.C., M.D. Shastri, and R. Eri, *Endoplasmic Reticulum Stress and Oxidative Stress: A Vicious Nexus Implicated in Bowel Disease Pathophysiology.* Int J Mol Sci, 2017. **18**(4).
192. Song, I., et al., *Mitochondrial modulation decreases the bortezomib-resistance in multiple myeloma cells.* International journal of cancer, 2013. **133**(6): p. 1357-1367.
193. Masaki, R., *Mechanism of action of bortezomib in multiple myeloma therapy.* International Journal of Myeloma, 2016. **6**: p. 1-6.
194. Song, I.-S., et al., *Combination treatment with 2-methoxyestradiol overcomes bortezomib resistance of multiple myeloma cells.* Experimental & molecular medicine, 2013. **45**(10): p. e50.
195. Health, U.D.o. and H. Services, *Food and Drug Administration CFR-Code of Federal Regulations Title 21*.
196. Croissant, J.G., Y. Fatieiev, and N.M. Khashab, *Degradability and Clearance of Silicon, Organosilica, Silsesquioxane, Silica Mixed Oxide, and Mesoporous Silica Nanoparticles.* Adv Mater, 2017. **29**(9).
197. Zhao, Y., et al., *Interaction of mesoporous silica nanoparticles with human red blood cell membranes: size and surface effects.* ACS Nano, 2011. **5**(2): p. 1366-75.
198. Yu, E., et al., *Improved controlled release of protein from expanded-pore mesoporous silica nanoparticles modified with co-functionalized poly(n-isopropylacrylamide) and poly(ethylene glycol) (PNIPAM-PEG).* Colloids Surf B Biointerfaces, 2017. **149**: p. 297-300.
199. Cong, V.T., et al., *Rod-shaped mesoporous silica nanoparticles for nanomedicine: recent progress and perspectives.* Expert Opin Drug Deliv, 2018. **15**(9): p. 881-892.
200. Shao, D., et al., *The shape effect of magnetic mesoporous silica nanoparticles on endocytosis, biocompatibility and biodistribution.* Acta Biomater, 2017. **49**: p. 531-540.
201. He, Q., et al., *In vivo biodistribution and urinary excretion of mesoporous silica nanoparticles: effects of particle size and PEGylation.* Small, 2011. **7**(2): p. 271-80.
202. Chen, L., et al., *The toxicity of silica nanoparticles to the immune system.* Nanomedicine, 2018. **13**(15): p. 1939-1962.
203. Kwon, D., et al., *Extra-Large Pore Mesoporous Silica Nanoparticles for Directing in Vivo M2 Macrophage Polarization by Delivering IL-4.* Nano Lett, 2017. **17**(5): p. 2747-2756.

204. Yi, Y.S., *Folate Receptor-Targeted Diagnostics and Therapeutics for Inflammatory Diseases.* Immune Netw, 2016. **16**(6): p. 337-343.
205. Maeda, H., et al., *Tumor vascular permeability and the EPR effect in macromolecular therapeutics: a review.* J Control Release, 2000. **65**(1-2): p. 271-84.
206. Samblas, M., J.A. Martinez, and F. Milagro, *Folic Acid Improves the Inflammatory Response in LPS-Activated THP-1 Macrophages.* Mediators Inflamm, 2018. **2018**: p. 1312626.
207. Moreno, L., et al., *The Mechanism of Action of the Anti-CD38 Monoclonal Antibody Isatuximab in Multiple Myeloma.* Clin Cancer Res, 2019. **25**(10): p. 3176-3187.
208. Franssen, L.E., et al., *Immunotherapy in myeloma: how far have we come?* Therapeutic advances in hematology, 2019. **10**: p. 2040620718822660.
209. Favaloro, J., et al., *Myeloma skews regulatory T and pro-inflammatory T helper 17 cell balance in favor of a suppressive state.* Leuk Lymphoma, 2014. **55**(5): p. 1090-8.
210. Feng, X., et al., *Targeting CD38 Suppresses Induction and Function of T Regulatory Cells to Mitigate Immunosuppression in Multiple Myeloma.* Clin Cancer Res, 2017. **23**(15): p. 4290-4300.
211. Penaloza-MacMaster, P., *CD8 T-cell regulation by T regulatory cells and the programmed cell death protein 1 pathway.* Immunology, 2017. **151**(2): p. 146-153.
212. Kumar, P., P. Bhattacharya, and B.S. Prabhakar, *A comprehensive review on the role of co-signaling receptors and Treg homeostasis in autoimmunity and tumor immunity.* J Autoimmun, 2018. **95**: p. 77-99.
213. Tai, Y.-T. and K.C. Anderson, *Targeting CD38 alleviates tumor-induced immunosuppression.* Oncotarget, 2017. **8**(68): p. 112166.
214. Ohue, Y. and H. Nishikawa, *Regulatory T (Treg) cells in cancer: Can Treg cells be a new therapeutic target?* Cancer Sci, 2019. **110**(7): p. 2080-2089.
215. Zhang, L., et al., *Regulatory B cell-myeloma cell interaction confers immunosuppression and promotes their survival in the bone marrow milieu.* Blood Cancer J, 2017. **7**(3): p. e547.
216. Mandal, A., et al., *Ocular delivery of proteins and peptides: Challenges and novel formulation approaches.* Advanced drug delivery reviews, 2018. **126**: p. 67-95.
217. Tesauro, D., et al., *Peptide-based drug-delivery systems in biotechnological applications: recent advances and perspectives.* Molecules, 2019. **24**(2): p. 351.
218. SEBAK, A.A., *LIMITATIONS OF PEGYLATED NANOCARRIERS: UNFAVOURABLE PHYSICOCHEMICAL PROPERTIES, BIODISTRIBUTION PATTERNS AND CELLULAR AND SUBCELLULAR FATES.* Int J App Pharm, 2018. **10**(5): p. 6-12.
219. Chatterjee, J., F. Rechenmacher, and H. Kessler, *N-methylation of peptides and proteins: an important element for modulating biological functions.* Angewandte Chemie International Edition, 2013. **52**(1): p. 254-269.
220. Slough, D.P., S.M. McHugh, and Y.S. Lin, *Understanding and designing head-to-tail cyclic peptides.* Biopolymers, 2018. **109**(10): p. e23113.
221. Tremblay, D., *Novel targets in multiple myeloma.* American Journal of Hematology/Oncology®, 2017. **12**(10).
222. Lin, Q., et al., *Recent updates on CAR T clinical trials for multiple myeloma.* Molecular cancer, 2019. **18**(1): p. 154.